A Novel Drug Delivery System: Adenosine-Loaded Chitosan Nanoparticles

by

Marla Jan Reid

Submitted in partial fulfilment of the requirements
for the degree of Master of Applied Science

at

Dalhousie University
Halifax, Nova Scotia
November 2013

DEDICATION PAGE

I dedicate this work to my parents, without none of this would have been possible. Thank you for your loving support and encouragement, and for always believing in me. This is for you.

TABLE OF CONTENTS

LIST OF TABLES

LIST OF FIGURES

ABSTRACT

Adenosine is currently limited in its application as a treatment for various cancers since intravenous infusion has not been successful due to enzymatic degradation. The protection of adenosine/ATP can be acheieved by a liposome drug delivery system. However, liposomes have low encapsulation efficiencies (4-16%). Entrapment/association of adenosine into chitosan nanoparticles offers a possible solution to this problem. A novel drug delivery system for adenosine has been developed and tested. The delivery system is fabricated from chitosan nanoparticles which are formed by ionotropic gelation. This design is aimed at improving entrapment/association efficiency and the bioavailability of the drug within the body by protecting it from degrading enzymes.

The size, zeta potential, morphology, entrapment efficiency, and *in vitro* drug release were investigated as a function of initial adenosine loading (16, 39, 56 % (w/w)). In the swollen state, the nanoparticle had an average size in the range of 425 to 515 nm and a positive zeta potential, as measured by dynamic light scattering. Particle size measured by transition electron microscopy varied in the range 135 to 183 nm. Average entrapment efficiency in the range of 72 to 78% was achieved depending on initial adenosine loading and an average association efficiency of 84%. Release studies show that more than 98% of the adenosine remained entrapped/associated with the chitosan nanoparticles for at least 120 hours in PBS (pH 7.4). In conclusion chitosan nanoparticles show great promise as a potential new delivery system where high entrapment can be achieved. However, further investigation is required in developing suitable release characteristics for the system.

LIST OF ABBREVIATIONS USED

A_1AR	Ligand-A1 adenosine receptor
$A_{2A}AR$	Ligand- A2A adenosine receptor
$A_{2B}AR$	Ligand- A2B adenosine receptor
A_3AR	Ligand- A3 adenosine receptor
Ad	Adenosine
AE	Association efficiency
ANOVA	Analysis of variance
ATP	Adenosine triphosphate
AV	Atrioventricular
CH	Chitosan
Da	Dalton
DA	Degree of acetylation
DLS	Dynamic light scattering
$DMSO_2$	Dimethyl Sulphone
EE	Entrapment efficiency
EPR	Enhanced permeation and retention effect
GI	Gastrointestinal
ICG	Indocyanine green
IGA	Immunoglobulin A
IV	Intravenous
KCl	Potassium chloride
Kcps	Kilocounts per second
KH_2PO_4	Monopotassium phosphate
LC	Loading capacity
MPS	Mononuclear phagocyte system
MWCO	Molecular weight cut off
$Na_2HPO_4 \bullet H_2O$	Sodium phosphate monobasic
NaOH	Sodium hydroxide

NF-κB	Nuclear factor kappa-light-chain-enhancer of activated B cells
NMR	Nuclear magnetic resonance
PBS	Phosphate buffered solution
PDI	Polydispersity index
PEG	Poly (ethylene glycol)
PGA	Poly (L-glutamic) acid
PLA	Polylactic acid
PLGA	Polylatic-glycolic acid
Ppm	Parts per million
PSTV	Paroxysmal supraventricular tachycardia
qNMR	Quantitative liquid nuclear magnetic resonance
RES	Reticuloendothelial system
ssNMR	Solid-state nuclear magnetic resonance
TEM	Transition electron microscope
TMC	N, N, N-trimethylchitosan chloride
TPP	Tripolyphosphate
UV	Ultraviolet
VEGF	Vascular endothelial growth factor
w/o	Water-in-oil
w/w	Weight per weight
WPW	Wolf Parkinson White Syndrome

ACKNOWLEDGMENTS

Foremost I would like to thank and acknowledge my supervisors Dr. Amyl Ghanem and Dr. Su-Ling Brooks for their guidance and knowledge they have provided throughout this project. To Dr. Paul Gratzer, thank you for sitting on my committee and your time and diligence of reviewing this dissertation. A great thank you to the staff in the PEAS department who helped and supported me: Ms. Diana Orsini, Ms. Paula.Mckenna, Mr. Ray Dube, Dr. Jan Healssig, Dr. Adam Donalson, and Dr. Pegg.

Furthermore, I would like to recognize and thank Dr. Ping Li of Scientific Imaging Suite (IRM) for aid in TEM characterization and the Centre for Water Resource Studies for use of their Zetasizer. As well, Dr. Ulrike Werner-Zwanziger and Dr. Mike Lumsden of the Nuclear Magnetic Resonance Research Resource (NMR^3) for solid-state and liquid-state NMR data acquisition and interpretation.

Lastly, I would like to extend my gratitude to the Department of Chemical Engineering, Faculty of Graduate Studies, and Natural Sciences and Engineering Research Council of Canada (NSERC) to without their funding this research would not be possible.

1.0 INTRODUCTION

The subject of this thesis is to design a drug delivery system for adenosine by entrapping the molecule into chitosan nanoparticle drug delivery system for the purpose of controlled released. Adenosine is currently limited in its application as a treatment for various cancers as it is rapidly degraded upon administration. Incorporation of adenosine into a carrier matrix can improve the bioavailability of the drug within the body by protecting it from degrading enzymes. The following introductory section outlines the rationale behind incorporating adenosine into a drug delivery system.

1.1 Adenosine

The use of adenosine/ adenosine triphosphate (ATP) for the treatment of tissue ischemia and various cancers has noticeable potential in pharmacology. However, other than treatment for paroxysmal supraventricular tachycardia (PSVT) the use of adenosine has been restricted as intravenous (IV) infusion has not been successful, largely due to enzymatic degradation of the adenosine by adenosine deaminase but also due to its highly-charged state (Eikvar and Kirkeboen, 1998). There has been some research done on the protection of adenosine/ATP by a liposome drug delivery system that could inhibit the enzyme degradation thereby improving its half-life in circulation (Arakawa et al., 1998; Chien, 2010; Hartner et al., 2009; Korb et al., 2008; Puisieux et al., 1994). A liposome drug delivery system could also facilitate cell uptake by masking its charge. Nonetheless, the leading limitations in using liposomes for adenosine drug delivery are their low encapsulation efficiency (4-16%), and reduced stability (Arakawa et al., 1998; Chien, 2010). Missing from the previous work is the use of nanoparticles as a carrier system for adenosine. Nanoparticles have the same benefits as liposomes in drug delivery but they have a longer shelf life, stability, and higher entrapment efficiency (Jong and Borm, 2008).

1.2 Brief History of Evolution of Controlled Drug Delivery

Controlled drug delivery arose in the mid-1960s when Folkman and coworkers presented a new method of constant rate drug therapy by incorporating a therapeutic agent in Silastic sealed tubing which was implanted in the body (Folkman et al., 1964). Folkman demonstrated that the rate of drug release decreased as tubing thickness increased, this was the first zero order

controlled drug delivery implant *in vivio* (Hoffman, 2008). Companies devoted to controlled drug delivery began to emerge in the 1960's and 1970's. One of these companies, Alza, developed the first commercial macroscopic rate-controlling membrane drug delivery system producing zero order release (Wright and Hoffman, 2012). Ocusert®, an ophthalmic insert, delivered pilocarpine in a controlled manner for one week from two transparent, rate controlling ethylene -vinyl acetate copolymer membranes (Patel et al., 2010). In 1986, Debiopharm introduced the first clinically approved microscopic sustained released biodegradable polymer depot drug delivery system. The PLGA microparticle delivered triptorelin (D-Trp-6 LHRH; Decapeptyl®) for the treatment of prostate cancer (Hoffman, 2008; Wright and Hoffman, 2012). Nanoscopic drug delivery systems began in the late 1970's and is still dynamic and progressing to clinically efficacious products today. Three key technologies have made nano-therapeutics successful: (1) PEGylation, the development of polyethylene glycol-conjugated drugs or drug carriers; (2) active targeting, this is accomplished by conjugating targeting moieties to the polymer carrier so it targets specific cells; and (3) passive targeting through enhanced permeation and retention effect (EPR), where nano drug carries are lured within tumors owing to the permeable vasculature of the developing tumor (Hoffman, 2008; Wright and Hoffman, 2012).

1.3 Controlled Drug Delivery

The objective of drug delivery is for the administered drug to remain within the therapeutic window for a specified length of time. This can sometimes be difficult to achieve with traditional drug delivery methods. Traditional drug delivery such as oral and injections prompt simple, fast-acting responses (Wang et al., 2005). These systems lack the ability and mechanism to administer the active agent in a constant manner as they are passive and rely on drug diffusion through pores or degradation of the carrier matrix (Zhang, 2009). This can lead to toxic levels of administration and reduce potencies as a result of degradation. However, controlled release technology delivers the drug at a specified rate and/or site for a predetermined time period determined by the needs of the patient and disease. At least one of the following requirements must be satisfied to be a controlled release drug delivery system 1) action of the drug must be prolonged at a fixed rate, 2) action of the drug must be localized by targeting a certain target cell type, and 3) the physiological and therapeutic needs of the body should determine the amount

and rate of drug release (Troy and Hauber, 2006). Controlled release technology can be used to administer the drug within the therapeutic window for a sustained period of time (Kalantzi et al., 2009). A controlled release system can protect the drug from degradation *in vivo* thus improving the half-life, a measure of the time required for the concentration of a substance in blood or plasma to change by one-half (Bryant and Knights, 2011). Furthermore, controlled release can increase bioavailability, the quantity of drug absorbed into the systemic circulation, and decrease the clearance rate, the time it takes the body to eliminate the drug (Danhier et al., 2012; Singh et al., 2010; benet and Zia-Amirhosseini, 1995). It is for these reasons that control release technology is one of the major areas being studied in drug delivery research.

Controlled release drug delivery can employ drug-encapsulating polymers, whether natural or synthetic. First the active agents is incorporated into the polymer, once it is administered it may release the active agent at constant rate over a period of time, ranging from days to months (Bhowmik et al., 2012). The drug can be incorporated into the polymer in such a way that the release depends on 1) their gradual diffusion from the polymeric matrix, 2) erosion of the matrix, 3) release from the surface of the matrix (Golan et al., 2011; Reynolds et al., 2010) or 4) a combination of methods. If the drug is covalently bonded to the polymer, the release may depend on the degradation of the polymer matrix where the bond is cleaved due to a chemical reaction (Liechty et al., 2010). Chitosan is a notable natural polymer for the delivery of therapeutic agents. By incorporating drug molecules in chitosan nanoparticles the clearance can be decreased and the circulation half-life of the drug extended (Kadam, et al. 2012).

1.3.1 Polymeric Drug Delivery

Synthetic carrier polymers are generally non-biocompatible, non-biodegradable and expensive whereas natural polymers are not (Mitra and Dey, 2011). Biodegradable polymers are receiving a lot of attention by researchers, as natural biological processes are able to degrade the materials within the body. These materials eliminate the need to remove the delivery system once the active agent has been released (Brannon-Peppa, 1997). Chitosan, a natural cationic polyaminosaccharide, is a significant material in the progression of drug delivery systems

because it is nontoxic, biocompatible, biodegradable, and has mucoadhesive properties (Agnihotri et al., 2004; Islam et al., 2012).

There are a number of potential benefits that could result from incorporating adenosine into a chitosan matrix. For example, it is hypothesized that the formulation of adenosine into chitosan nanoparticles would protect adenosine from physical and degradation barriers thus decrease the drug degradation upon administration thereby its increasing half-life and bioavailability, reducing frequent dosing at high levels, and finally increasing drug stability and circulation time in the blood. It is also hypothesized that adenosine would slowly diffuse from the adenosine-chitosan nanoparticles or be released from the surface, thereby improving its release characteristics. This has led to the present study, where a controlled release system for adenosine using chitosan nanoparticles has been investigated.

2.0 RESEARCH OBJECTIVES

The main aim of this research was to develop a drug delivery system for IV delivery of adenosine via enhanced chitosan polymer control. Adenosine is currently limited in its application in pharmacology as intravenous infusion has not been successful due to enzymatic degradation. It is hypothesized that the adenosine-chitosan complex will increase the half-life of the drug by decreasing drug degradation thus improving the stability of adenosine in the systemic circulation when administered intravenously. All of these objectives aspire to yield experimental data that can be used to improve the effectiveness of adenosine and other drugs with similar properties using a chitosan carrier matrix. The outcome of an optimally designed delivery system would have a major influence on the health and lives of numerous patients by reducing frequent high dosing of adenosine. The efficacy of adenosine is highly dependent on the speed of administration and the amount due to its short half-life. The specific objectives of this study were to:

2.1 Objective 1- Compare two methods (internal entrapment and adsorption) for incorporating adenosine into chitosan-TPP nanoparticles.

Adenosine will either be entrapped into the chitosan matrix during the ionotropic gelation process or adsorbed onto the surface of the chitosan matrix. Adenosine release rate from entrapped formulation is expected to be slow as it diffuses from the chitosan complex. Whereas no diffusion is expected for the release of adenosine from the adenosine surface adsorbed chitosan complex, the release rate will be reliant on the degree of bond degradation.

2.2 Objective 2- Characterize the size and morphology of the chitosan-TPP nanoparticles.

The size and characterization of the chitosan nanoparticles is important for IV delivery of adenosine therefore after nanoparticles formation, the size and morphology will be measured by dynamic light scattering and transmission electron microscopy. The diameter of the smallest blood capillary is roughly 4 μm therefore nanoparticles are ideal for IV administration (Tiyaboonchai, 2003). The adenosine-chitosan complex must be approximately 100 nm in diameter for prolonged circulation in the blood stream. Smaller sized particles have an extended

circulation time, particles greater than 100 nm are taken up by the reticuloendothelial system in the liver, spleen, lung, and bone marrow (Tiyaboonchai, 2003). It is also important to control the morphology of the nanoparticles in order to enhance the degree of internalization. Particles that are spherical in shape are more easily internalized than those that are rod or tubular shaped (Prokop, 2011). Nanoparticles with irregular surfaces promote protein adhesion or absorption (Kumar et al., 2013; Shi, 2009). Consequently, it is ideal to have smooth, spherical nanoparticles.

2.3 Objective 3- Determine the (i) adenosine loading and (ii) release characteristics of the drug-loaded chitosan-TPP nanoparticles.

In order to measure the release characteristics of the drug-loaded chitosan nanoparticles, the amount of adenosine loaded must first be quantified. Adenosine will be loaded into the chitosan nanoparticles during nanoparticle formation. Following formation of the adenosine loaded chitosan nanoparticles the amount of drug entrapped/associated will be measured. For the treatment of paroxysmal supraventricular tachycardia an overall dose of 6 mg for adults or 0.1 mg/kg for pediatric patients of adenosine is the present prescribed dosage for a 1 to 2 second rapid intravenous bolus (Haas et al., 1994; Wittwer and Muhr, 1997). The drug-loaded chitosan nanoparticle formulation should contain at least 6 mg of adenosine. In order to reduce frequent dosing the drug must be released at a constant rate from the chitosan complex for an extended period of time. By determining the release characteristics of adenosine from the chitosan complex one can maximize the adenosine-chitosan formulation to have a residence time close to 24 hours to decrease administration to a one per day dose by prolonging the release.

3.0 LITERATURE REVIEW

The purpose of this section is to present a review of the existing progress of the entrapment of nanoparticles for the purpose of controlled drug release. This overview will include chitosan and its properties that make it an ideal natural polymer for nanoparticle drug delivery such as degree of deacteylation, biodegradability, biocompatibility, and its derivatives. It will also look into the benefits of using nanoparticles and their fabrication methods, which include ionotropic gelation, emulsion cross-linking, coacervation, spray drying, and freeze drying. In addition, the literature review section will cover adenosine, its uses and mechanism of action.

3.1 Drug Delivery

Drug delivery systems aim to maintain a drug that has been administered within the therapeutic window for a determined period of time. This means the concentration of the drug must remain between the maximum blood level value (toxic level that could cause adverse effects) and a minimum value (where the drug is no longer active) (Winstanley et al., 2007).

Traditional drug delivery systems can have wide range fluctuations in serum concentrations. This is due to most of the drug being released not long after administration and causing the drug concentration to quickly elevate, peak and then decrease (Schafer-Korting, 2012). Figure 3.1 exemplifies the plasma concentration profile overtime for drugs when governed from rapid release dosage systems. The concentration rapidly increases, peaks to where there can be undesirable side effects, and then rapidly declines below the minimum therapeutic level where there can be insufficient treatment (Winstanley et al., 2007). Little time is spent within the therapeutic window consequently frequent repetitive dosing is essential to maintain concentrations within this limit. Control release drug delivery is able to regulate the drug release rate to eliminate under and over dosing and as well reducing frequent dosing to increase patient compliance (Schafer-Korting, 2012). The steady amount of drug released over time is also known as zero order release; the drug release process occurs at a constant rate and is independent of the concentration of the drug (Uchegbu and Schatzlein, 2006). Nonetheless, zero order release cannot be maintained as the concentration of drug approaches zero. As illustrated by Figure 3.1, with accurate dosing, zero order release can be maintained within the therapeutic

window. First there is an initial increase of drug concentration in plasma and then within time it reaches a constant concentration.

3.2 Types of Controlled Release Drug Delivery Systems

To produce a gradual release of drug, controlled release drug delivery systems depend on diffusion and osmotic pressure. During the diffusion process the drug diffuses through a polymer from an area of higher concentration to one of lower concentration (Isha et al., 2012). The drug entrapped within the polymer dissolves to form a saturated solution and then diffuses across the membrane at a constant rate. Zero order release persists as long as there is adequate drug inside the polymer to form a saturated solution to preserve the stationary concentration gradient through the membrane (Siepmann et al., 2012). The release rate will decay to zero once the concentration gradient decreases due to the dissolved drug concentration dwindling below saturation.

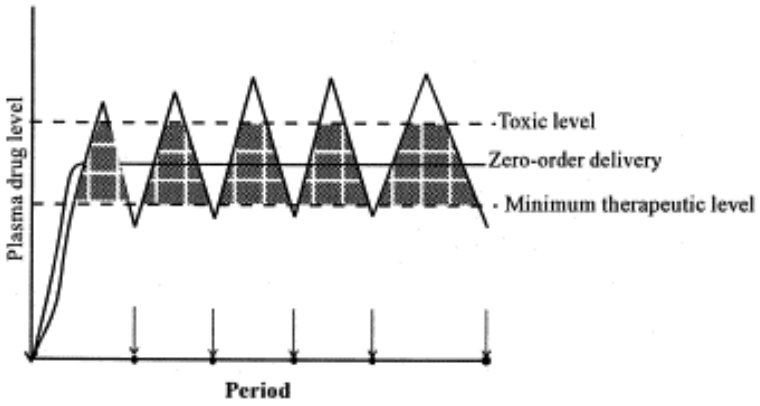

Figure 3.1: Controlled drug delivery versus immediate release. (Kumar, 2000)

Osmotic pumps have been designed to provide zero-order release by use of osmotic pressure. Osmotic systems are for the most part independent of pH and other physical factors as they operate on the principle of osmotic pressure (Shivanand and Devmurari, 2010). The elementary osmotic pump contains a rate controlling semi-permeable membrane surrounding the active agent. A small drilled orifice of significant size is comprised within the membrane through which the active agent is dispensed (Shivanand and Devmurari, 2010). Controlled release of the drug resides in the water permeation characteristics of the membrane. The drug dissolves as osmotic water flows though the semi-permeable membrane and transports it though the orifice

(Siepmann et al., 2012; Shivanand and Devmurari, 2010). If the pressure gradient between the core and external medium is upheld, zero order will continue (Siepmann et al., 2012). The elementary osmotic pump is an ideal system for delivering drugs that are comparatively water soluble. The push-pull osmotic pump is capable of delivering both poorly and extremely water soluble drugs at a constant rate (Shivanand and Devmurari, 2010). A small orifice is drilled within the semi-permeable membrane surrounding the drug similar to the elementary osmotic pump where the drug will be released. However differing from the elementary osmotic pump, a soluble polymer excipient layer is added underneath the active agent (Siepmann et al., 2012). The drug dissolves due to osmotic flow of water across the semi-permeable membrane. During this process the polymer excipient swells and pushes the dissolved drug through the orifice (Shivanand and Devmurari, 2010; Siepmann et al., 2012).

Another popular method of controlled release is to use a carrier particle for the delivery of therapeutic agents. Natural and synthetic degradable polymers are ideal carrier molecules (Uchegbu and Schatzlein, 2006). The drug can be incorporated into the polymer where the release depends on either their gradual diffusion from the polymeric matrix, erosion of the matrix, or release from the surface of the matrix (Siepmann et al., 2012). If the drug is covalently bonded to the polymer the release may depend on the erosion of the polymer matrix (Rabi et al., 2010). Chitosan is a notable natural polymer for the delivery of therapeutic agents.

3.3 Mechanism of Drug Release from Particulate Systems

The release mechanism of the drug depends on how the drug molecules are incorporated in the nanoparticles, either on the surface or entrapped inside the matrix as shown in Figure 3.2. Drugs that are adsorbed on the surface will dissolve suddenly when they come in contract with the release medium creating a burst effect of drug release (Dash et al., 2011; Wang et al., 2005). Drug release due to diffusion through a porous matrix begins when the matrix swells from water penetrating into the particulate system and the pores enlarge leading to greater swelling (Dash et al., 2011; Omidian and Park, 2008). If the matrix is very well cross-linked this enlargement may be retarded and subsequently slower diffusion can still take place. The drug will then start to diffuse from the swollen matrix. Thus this mechanism of drug release initiates slowly and proceeds rapidly over (Agnihotri, et al. 2004).

Biodegradable polymers remove the need to eliminate the delivery system after the active agent has been released as natural biological processes degrade the materials inside in the body (Brannon-Peppa, 1997). Drugs released from a biodegradable delivery system can result from a combination of drug diffusion and polymer erosion. There are two types of erosion that can occur to degradable polymers - bulk erosion and surface erosion. In bulk erosion the degradation of the polymer leads to considerable reduction in molecular weight and change in material properties as a function of time, the erosion rate declines as material is lost from the total polymer volume (Dumitriu and Popa, 2013; Tamada and Langer, 1993). Bulk erosion can result in unpredictable release profiles with burst effects owing to multiple channels of drug diffusing out of the polymeric system. Hence, matrices that experience bulk erosion should not be employed for drugs with limited therapeutic windows. In contrast, polymeric drug delivery systems that undergo surface erosion can achieve zero order release kinetics if release is by diffusion near the surface (Siepmann et al., 2012). The release rate from surface erosion, material lost from the polymers external surface, is proportional to the surface area of the drug delivery system (Brannon-Peppa, 1997; Tamada and Langer, 1993). Hydrolytic degradation degrades most biodegradable synthetic polymers into biologically acceptable monomer-like compounds. Whereas enzymatic degradation is the main process that degrades natural polymers into degradation products, for example, amino acids or sugars (Siepmann et al., 2012).

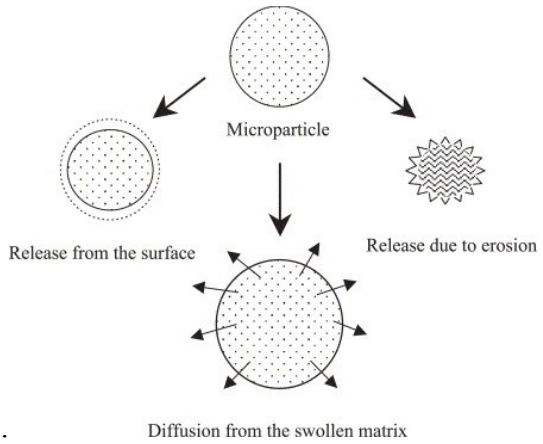

Figure 3.2: Mechanism of drug release of particulate systems (Agnihotri, et al. 2004)

Controlled release systems can also be modified to react to stimuli as a result of environmental signals. Stimuli-sensitive polymers can prompt changes in the volume of the polymer or size of the pores as a result to certain stimuli (Ulbricht, 2012). For example, different chemical or physical stimuli such as pH, temperature, enzymes, light, ultrasound, or ionic strength can initiate changes in the matrix structure that lead to drug release (Fleige et al., 2012; Hoffman, 2013). The presence of the amino groups on the chitosan molecule makes the biopolymer well suited for stimuli response. Changes in pH can cause the formulation to swell or de-swell. For example at a low pH chitosan can swell, while at a high pH chitosan appears to collapse. In an acidic environment protonation of the amino group of the chitosan occurs and the chains separate from the electrostatic repulsion. This movement amongst the chains causes chitosan to swell as water molecules penetrate (Buranachai et al., 2010)

3.4 Adenosine

Adenosine is a white crystalline powder that is soluble in water, its solubility increases when heated. Adenosine (Figure 3.3), a purine nucleoside, is a metabolite of the high-energy intracellular compound adenosine triphosphate (ATP) (Cohen and Downey, 2009). Adenosine has been termed 'retaliatory metabolite', a type of cell regulator (Newby, 1984). In other words adenosine's unique mechanism of formation signals both an imbalance between tissue oxygen demand and the supply of oxygen and it initiates responses to restore the balance such as vasodilatation and reduction of activities that utilize ATP (Shryock and Beladinelli, 1997). In various essential biochemical pathways, the intermediate metabolite of adenosine has been indicated to play a role in regulation of coronary and systemic vascular tone, platelet function and lipolysis in adipocytes (Manjunark and Pranavkumar, 2009). Binding to the common extracellular receptors subtypes, mainly A1, A2a, A2b, and A3, brings out the primary actions of adenosine.

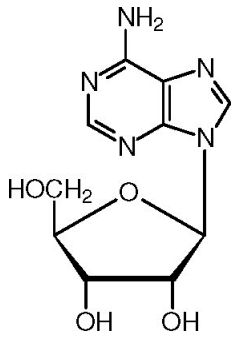

Figure 3.3: Chemical structure of adenosine ($C_{10}H_3N_5O_4$ and molecular weight of 267.24 g /mol)

Under normal conditions adenosine cannot penetrate cells through the plasma membrane due to it being a charged molecule. It is for this reason that no specific transport mechanisms exist and intravenous infusion has not produced consistent results (Chien, 2010). Adenosine is rapidly metabolized (enzyme degradation) and has a relatively short half-life (less than 10 seconds) limiting its efficacy (Lerman and Belardinelli, 1991). A carrier such as a drug delivery system could protect adenosine from enzyme degradation thereby improving its half-life in systemic circulation. Furthermore, protection of the adenosine through a drug delivery system could facilitate cell uptake by masking its charge.

3.4.1 Adenosine and Its Uses

Until recently adenosine was only used in specific disorders like paroxysmal supraventricular tachycardia (PSVT) and PSVT related to Wolff Parkinson White (WPW) syndrome. As a result of the safety (negligible or no impact on blood pressure) and efficacy (86-100 %) of adenosine it is often the first line of therapy for PSVT (Paul and Pfammatter, 1997). Adenosine briefly depresses the sinus node activity slowing conduction in the atrioventricular (AV) node which momentarily blocks the AV node (Paul and Pfammatter, 1997; Robins and Lyons, 2004). Regular sinus rhythm can be stored in patients with PSVT by this delay in the re-entry pathways through the AV node. Common effects associated with adenosine consist of facial flushing, dyspnea because of bolus doses into the ascending aorta, chest pain, and bronchoconstriction from inhalation (Paul and Pfammatter, 1997).

Currently there is increasing evidence that adenosine and ATP have remarkable potential in pharmacology, as adenosine receptors could be promising therapeutic targets for cancer therapy. New approaches have been studied over the last decade in treating cancer; one that shows great promise is founded on distinct targets that are expressed generally in tumor cells but not in healthy cells. Adenosine is an ideal candidate for this novel approach as it may serve as a biological marker and its receptors as a target for specific ligands leading to cell growth inhibition. Given that the level of adenosine receptors is up regulated in cancerous tissues but found to be low in normal tissue makes this a promising method (Fisher et al. 2009).

3.4.2 Adenosine Receptors and Cancer Therapy

The anti-tumor effect of A_1AR plays a role in averting the growth of glioblastomas (Fisher et al., 2009). The A_1AR has also been found to have pro-tumoral effects by increasing chemotaxis in cancers such as melanoma and contributing to tumor cell growth in breast cancer (Gessi et al., 2010).

A_{2A}AR has been shown to promote apoptosis of human A375 melanoma cells though activation by extracellular adenosine (Gessi et al., 2010). Additionally, A_{2A}AR facilitates angiogenesis by promoting endothelial cell proliferation, migration and synthesis of messages for growth factors such as vascular endothelial growth factor (VEGF) (Gessi et al., 2010). Activation of A_{2A}AR may also play a role in the inhibition of the immune response to tumors whereas the up regulation of the expression levels of angiogenic factors in microvascular endothelia cells by A_{2B}AR plays a role in the development of tumor growth (Fisher et al., 2009).

In normal cells the A_3AR agonist stimulates production of growth factors by initiation of the NF-κB signaling pathway and stimulates apoptosis and growth inhibition though deregulation of the NF-κB and the Wnt signaling pathways in tumor cells (Fisher et al., 2009; Fisher et al., 2002). The A_3AR are generally found expressed in the human lung and liver, low amounts are found in the brain, testes, and heart, and no A_3AR expressions are detected in the spleen or kidney (Sajjad and Firestein 1993). A_3AR ligands and agonist inhibit various tumor cell growths such as melanoma, colon or prostate carcinoma and lymphoma by means of targeting tumor cells that

have a higher expression of A_3AR than normal or adjacent cells that have a low expression of A_3AR (Fishman et al., 2002). Morello and coworkers (2007) have indicated that a high level of A_3AR was expressed primary in thyroid cancer tissues while normal tissues do not express A_3AR. Similar results have also been confirmed by Madi and coworkers (2004) showing that colon and breast carcinomas had high expression levels of A_3AR protein and mRNA than the neighboring normal tissues derived from healthy subjects. Hence, agonist and ligands of A3AR such as adenosine are a promising novel class of drugs for cancer therapy due to their distinctive features that target mainly malignant cells without damaging normal cells.

Table 3.1 below gives a summary of the all adenosine subtype receptors and their main function in either the growth or decrease in cancer cells for various types of cancer

.

Table 3.1: Summary of adenosine receptors and their role in cancer

Adenosine receptor type	Targeted cancer	Role of adenosine receptor
A_1AR	Breast carcinoma cells	Increases proliferation
	Glioblastoma carcinoma cells	Decreases proliferation
$A_{2A}AR$	Endothelial cells	Increases migration and VEGF
$A_{2B}AR$	Endothelial cells	Increases proliferation
A_3AR	Lymphoma cells, prostate carcinoma, colon carcinoma, and melanoma	Decreases Proliferation and increases apoptosis

3.5 Chitosan

Chitosan is obtained by alkaline N-deacetylation of chitin (Sailaja, et al. 2010). The structure of chitosan is shown in Figure 3.4. Chitin is the second-most abundant polysaccharide in nature and is the principle component of the exoskeletons from organisms such as crustaceans and also found in the cell wall of fungi (Dash et al., 2011). The term chitosan is not used to define a unique polymer but rather a family of copolymers with numerous molecular weights, viscosity, and degree of deacetylation (Illum, 1998). Chitosan is a copolymer containing of N-acetyl-glucosamine (A-unit) and glucosamine (D-unit) connected together by β(1-4) glycosidic bonds

as depicted in Figure 3.5 (Gan and Wang, 2007; Einbu, 2007). The amine and hydroxyl sites on each repeat unit allow for chemical modification of chitosan, providing a site for specific modification, crosslinking, or addition of peptides (Aranaz, et al. 2010). The chemical structure and biocompatibility of chitosan is similar to that of glycosaminoglycan, which is present in many extracellular matrices (Yeh and Lin, 2008).

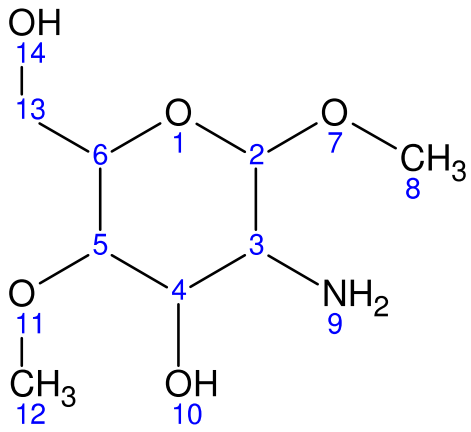

Figure 3.4: Chemical structure of chitosan poly (d-glucosamine) repeat units

The properties of chitosan and its ability to be modified using mild processing techniques make it a suitable material for drug delivery systems. A few of the properties of chitosan nanoparticles are that they nontoxic with highly biocompatible and biodegradable as chitosan is a natural polymer (Kumar, 2000). Chitosan nanoparticles also have the aptitude to improve bioavailability by promoting absorption, which prolongs contact time between substrates and cell membrane; their nanoparticle size enables the drug uptake through the cell membrane (Bowman and Leong, 2006; Tiyaboonchai, 2003). This allows active molecules to localize at their desired site of action. Chitosan is soluble in most organic acid solutions at pH levels below 6.5 and behaves as a linear polyelectrolyte. Chitosan in solution carries a high positive charge density, one charge per glucosamine unit (Kas, 1996). It has been demostrated that chitosan is stable in aqueous solution for several weeks (Aiba, 1989). Hence, chitosan can serve as an ideal material for many different applications in the biomedical field.

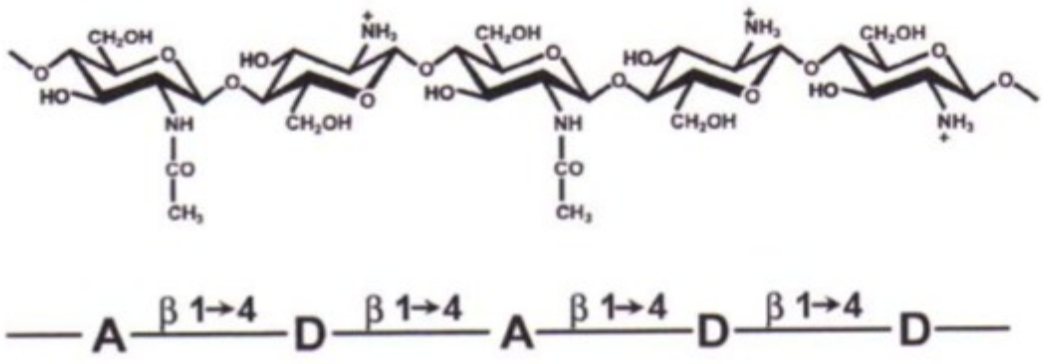

Figure 3.5: Chemical structure of a partially de-N-acetylated chitosan. (Einbu, 2007)

3.5.1 Chitosan Uses

Chitosan is utilized in numerous fields such as cosmetics, water and waste treatment, as well as for pharmaceutical and biomedical applications. Chitosan has several uses for biomedical purposes such as surgical dressings. Biagini and coworkers have established a N-carboxybutyl chitosan dressing for the treatment of plastic surgery donor sites to support ordered tissue regeneration (Biagini, et al. 1991). Substantial work has been published on chitosan and its use as a drug delivery system, in particular chitosan nanoparticles. Mitra and co-workers (2001) demonstrated that encapsulated dextran-doxorubicin chitosan nanoparticles exhibit passive drug delivery and increased survival rate when used as a chemotherapy agent for cancer. The therapeutic efficacy is correlated to the enhanced circulation time and its accumulation at tumor sites facilitated by the nanoparticles. Khatri and coworkers results indicate that chitosan nanoparticles are effective for nasal mucosal delivery of pDNA. The mucoadhesive system was capable of prompting systemic, mucosal and cellular immune responses (Khatri, et al., 2008). The study performed by De Campos and coworkers also successfully used chitosan as a drug delivery system by entrapping cyclosporine into chitosan nanoparticles. The drug was effectively delivered to the ocular mucosa where a therapeutic concentration in the external ocular tissues was achieved while circumventing cyclosporine concentrations in the inner ocular structures, blood, and plasma (De Campos et al., 2001).

It has been noted that chitosan increases absorption of compounds across the mucosal barrier (Islam et al., 2012). The mucoadhesivity of chitosan is one of the reasons it has been used for drug delivery systems and is the result of the electrostatic interaction from its cationic charge and the negative charge on the mucosal surfaces (He et al., 1998). The positive charge carried from chitosan is due to the availability of the free amino group whereas the negative charge of the mucin, an essential part of the mucosal barrier, in which it interact with is due to the ionization of sialic acid (Dhawan, et al. 2004). It has been demonstrated that chitosan (when pronated) affects cell permeability and enhances paracellular permeability of drugs across the mucosal epithelia by opening the intercellular tight junctions (Thanou, et al. 2001; Van der Lubben, et al. 2001). Chitosan causes reversible effects on epithelial morphology and temporarily alters gating properties of tight junctions (Dodane, et al. 1999). Mucoadhesive carrier systems are advantageous as they can protect the entrapped drug from the hostile environment within the gastrointestinal (GI) tract (Takeuchi, et al. 2005).

3.5.2 Degree of Deacetylation

Chitosan is either the fully or partially N-deacetylated derivative of chitin (Figure 3.6) with a usual degree of deacetylation of less than 0.5. The deacetylation process involves the release of acetyl groups from chitin to result in a cationic charge (Kalut, 2008). In other words it is the number of amino groups on the polymer chain that have had their acetyl functional groups chemically removed. The degree of deacetylation of chitosan can alter the cellular uptake properties of chitosan nanoparticles as well as the molecular structure (Huang et al., 2004). At higher degree of deacetylation, the molecule is more highly charged and chitosan has a prolonged conformation with a more flexible chain. Whereas, at a low degree of deacetylation, and a low charge, chitosan molecule becomes a more rod like or coiled shape (Illum, 1998; Errington et al., 1993). Cell adhesion and the way chitosan interacts with cells all depend on the degree of deacetylation. This is because an increase in the degree deacetylation can result in more interactions between chitosan and cells. This interaction is a result of the presence of free amino groups (Dash et al., 2011). For this reason, a lower degree of deacetylation leads to faster biodegradation rates and higher degree of deacetylation possess a slower degradation rate as well

as favoring cell adhesion resulting in improved uptake (Zhang and Neau, 2001; Riva et al., 2011).

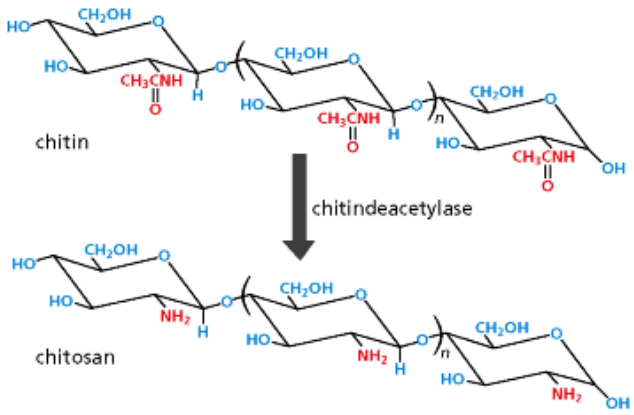

Figure 3.6: Chitosan, N-deacetylated derivative of chitin

3.5.3 Biodegradability of Chitosan

Biodegradation is the breakdown of a material assisted by a biological host after responding to the physio-chemical conditions within (Freitas, 2003). The metabolic fate of chitosan in the body greatly depends on its biodegradability (Dash et al., 2011). Lysozyme plays a major role in the biodegradation of chitosan and results in the products glucosamine and N-acetylglucosamine (Chellat et al., 2000; Kean and Thanou, 2009). The two products are further degraded by the glycoprotein synthetic pathway to carbon dioxide (Chan et al., 2007). The higher the cross-linking of chitosan, the slower biodegradation is, hence, biodegradation can be controlled through cross-linking (Yamamoto and Amaike, 1997). Biodegradation of chitosan in living organisms is also dependent on the degree of deacetylation and molecular weight. The higher degree of deacetylation and molecular weight results in slower degradation rate (Kean and Thanou, 2009; Zhang and Neau, 2001). The reason for this is that lysozymes disrupt regions of the chitosan molecular chain that comprise more than three N-acetyl-D-glucosamine units in sequence. Chitosan with a higher degree of deacetylation will be further stable since it will have more N-acetyl-D-glucosamine units in sequence (Mi et al., 2001).

3.5.4 Biocompatibility of Chitosan

Chitosan is a natural polymer and is considered highly biocompatible in many biomedical applications as it does not cause allergic reactions and rejection (Agnihotri et al., 2004). Although chitosan is not naturally found in the human body the monomers that make up chitosan, N-acetylglucosamine and glucosamine are. The whole polymer is structurally similar to hyaluronic acid that is located in connective, epithelial, and neural tissue (Narayan, 2009). Chitosan gradually degrades completely to products such as amino sugars that are entirely absorbed by the human body (Agnihotri et al., 2004). These degradation products are natural metabolites (Norouzi et al., 2012).

The antimicrobial activity of chitosan and its derivatives have attracted much attention as an agent against fungi, bacteria, and viruses. As well, industries have profited from applying chitosan's antimicrobial properties in food preservation and wound dressings (Kong et al., 2010). Further study of chitosan's mechanism of action is required to fully understand how it employs its antimicrobial activities. Still, it is thought that the cationic charge of chitosan (pKa= 6.3) due to the positively charged amino group of glucosamine interacts with negatively charged microbial cell membranes (Kong et al., 2010; Raafat et al., 2008). This interaction hinders important bacterial activities resulting in leakage of proteinaceous and other intracellular components (Kong et al., 2010; Raafat et al., 2008).

3.5.5 Modification of Chitosan and its Derivatives

The chemical structure of chitosan provides potential for alterations at the C-2 position. At this position the primary amine group can be functionalized by quarternization, to create a polymer for specific functions (Riva, et al. 2011). Modifications can also be made on one of the two-hydroxyl groups. In addition, chitosan properties can be improved by grafting functional groups without modifying the initial skeleton of chitosan to preserve its original properties (Riva, et al. 2011). Chitosan derivatives are ideal for gene therapy since quarternization improves the mucoadhesive properties of chitosan (Mourya, et al. 2008). N,N,N-trimethylchitosan chloride (TMC) is the most common quarternized chitosans used for gene therapy. Steroids or fatty acids can be grafted onto chitosan or glycol chitosan to create a drug delivery system that can either

actively or passively target anticancer drugs to tumors (Riva, et al. 2011). The polymer that results from the conjugation of a hydrophobic moiety to chitosan is able to self-assemble and encapsulates poorly soluble drugs (Riva, et al. 2011).

3.6 Nanoparticles

Nanoparticles are solid colloidal particles that are often composed of insoluble polymers and have a minimum of one dimension that is 100 nanometers or less in size (Christian et al., 2008; Gilmore et al., 2008). The properties of many materials change when formed into nanoparticles, therefore the surface chemistry of a nanoparticle is noticeably different from that of the original material (Christian et al., 2008). Due to their small size, nanoparticles are used in or being evaluated for use in, many fields and applications. Nanostructured materials are being used to construct alloys as hard as diamonds to make drill bits, armor plate, and jet engine parts (Dutta and Gupta, 2006). A fast emerging application of nanoparticles is in the biomedical (drug delivery) area to promote novel methods of diagnosis and treatment of human diseases.

Due to the wide ranging properties of nanoparticles they are now desirable for drug carrier systems. Nanoparticles can be engineered to slowly degrade, react to stimuli, control drug release from the matrix and be site-specific (Meena et al., 2011). To offer a more effective cure with fewer side effects nanoparticles can be manufactured with surface ligands, or modifications can be made to the surface design to allow for targeted drug delivery systems. This will allow the nanoparticle to bind to the site of interest such as a tumor or cell membrane (Provenzale and Silva, 2009). Nanoparticles are versatile as they can be administered through various routes such as oral, intravenous, ocular, rectal, intranasal, intramuscularly, and subcutaneously. The selection of the route of administration is determined by patient acceptability, properties of the drug, access to a diseased area, and efficiency in dealing with certain disease (Meena et al., 2011). The ultimate aim is to minimize drug degradation and loss, prevent harmful side effects and increase the availability of the drug at the disease site (Jin and Ye, 2008).

Nanoparticles have a higher surface area to volume ratio than larger particles. The higher surface area allows them to be more reactive to certain other molecules. As a result

nanoparticles possess a high carrier capacity allowing many drug molecules to be integrated in the particle matrix, this includes the ease of integration of both hydrophilic and hydrophobic substances (Gelperina et al., 2005). The small size of nanoparticles also allows them to be more readily taken up by the human body, cross biological membranes and enter cells, tissue and organs that larger size particles cannot (Meena et al., 2011). Desai and coworkers were able to demonstrate in their study that the diameter of the particle can notably affect the uptake in Caco-2-cell lines. Nanoparticles with a diameter of 100 nm had a 2.5 fold greater uptake than 1 μm microparticles, and 6 fold greater uptake than 10 μm microparticles (Desai et al., 1997). This means that nanoparticles have a reasonably greater intracellular uptake compared to microparticles.

3.6.1 Types of Nanoparticles Applied to Drug Delivery

Nanoparticles for drug delivery systems can be created using a diversity of materials including but not limited to polymers, liposomes, metals, and ceramics. Each material offers a distinctive characteristic that makes it advantageous for drug delivery as well as being biocompatible and biodegradable.

Dendrimers are created with different types of polymers such as poly (L-glutamic)acid (PGA) and poly(ethylene glycol) (PEG) by either convergent or divergent step growth (Jin and Ye, 2008). PGA and PEG are also known as synthetic polymers. Considering that dendrimers are hydrophilic, they can also be used as a coating agent for drug delivery (Jin and Ye, 2008). Biodegradable polymer nanoparticles for instance, polylactic acid (PLA) and polylatic-glycolic acid (PLGA), have drawn substantial attention seeing as they are biodegradable and do not accumulate in the body (Jin and Ye, 2008).

Liposomes, synthesised from cholesterol, are non-toxic phospholipids with a spherical shape (Yih and Al-Fandi, 2006). Until the liposome attaches to the outer membrane of the target cell the fatty layer protects the enclosed drug (Jin and Ye 2008). Liposomes are a harmless system that can circulate the blood stream for a long time. This makes them ideal for anticancer drugs in view of the fact that they can target the cancer cells without harming the normal cells (Yi and Al-

Fandi, 2006). The diameter of liposomes varies from 400 nm to 2.5 μm, due to this order of size they are rapidly cleared by the mononuclear phagocyte system (MPS) (Malam et al., 2009).

Metal nanoparticles have the facility to transport large drug dose as a result of their small size and large surface area (Yih and Al-Fandi, 2006). Gold nanoparticles are non-toxic and have little accumulation in the liver, spleen, and other organs (Jin and Ye, 2008).

Ceramic nanoparticles are porous inorganic systems that can be engineered with desirable size and porosity. Silica, titania, and alumina have been researched for cancer therapy (Yih and Al-fandi, 2006).

3.6.2 Biodistribution of Nanoparticles

Initially after intravenous injection the highest level of nanoparticles is found to be in the blood, which decreases over time because the particles migrate to the inner organs. Serum proteins that bind to the surface of nanoparticles contribute to the major loss of the injected dose from circulation - this is known as the reticuloendothelial system (RES) (Li and Huang, 2008). Chitosan nanoparticles are hydrophilic which helps them to escape removal by the RES. Chitosan is naturally degraded by the body either by lysozymes or other enzymes whereas other nanoparticles might accumulate inducing negative consequences (Wu et al., 2005; Dutta et al., 2004).

Nanoparticles depend on openings among the endothelium to pass through barriers, consequently tissue such as the liver, spleen, bone marrow, and tumors with permeable endothelial walls generally contribute to substantial uptake (Li and Huang, 2008). The increased rate of tumor uptake of nanoparticles is based on the properties of enhanced permeation and retention effect (EPR), nanoparticles are filtered out from the blood stream into the tumor site and subsequently accumulate at the site. Fast proliferation of endothelial cells and diminished amounts of pericytes yields anomalous tumor vasculatures and leaky walls. This results in large pores ranging from 100 nm to 600nm in diameter in the tumor vasculatures, compared to normal vessel pores of 5–10 nm (Wang et al., 2011; Yuan et al., 1995). These large junctions allow the

nanoparticles to pass into the tumor. Hence, the EPR effect is responsible for passive targeting to the tumor site for the nanoparticle delivery systems. (Saxena et al., 2006). Traditional chemotherapeutics affect both cancer cells and normal cells as they distribute through the body. The EPR effect allows nanoparticle chemotherapeutics to attain greater therapeutic efficacy and reduced toxicity because of increased intra-tumor drug concentrations and decreased normal-tissue concentrations (Wang et al., 2011). Yuan and coworkers found that tumor vessels were permeable to liposomes of up to 400 nm in diameter (2001). Moreover, nanoparticles are capable of increasing intracellular drug concentration owing to their ability to congregate in cells without being detected by P-glycoprotein a leading drug resistance mechanism (Cho et al., 2008).

Terentyuk and coworkers observed the biodistribution of gold nanoparticles after 24 hours of administration and found the maximum gold build-up in the liver and spleen. They concluded that distribution in the inner organs was size dependent, with larger ones collecting more such as the liver (Terentyuk et al., 2009). Saxena et al (2006) used both free indocyanine green (ICG) solution and poly (DL-lactic-co-glycolic) (PLGA) nanoparticle suspension for biodistribution studies. The free solution resulted in the highest levels of ICG in the liver showing that it is the major role of IGA removal from the blood circulation followed by the kidneys, spleen, heart and lungs. However, the nanoparticle formulation displayed a variation in biodistribution with the highest ICG levels in the liver followed by the spleen, heart and kidneys. (Saxena et al., 2006)

3.7 Methods of Preparation of Chitosan Particles

Many nanoparticle preparation techniques have been employed. The most widely developed methods for chitosan particulate systems are ioniotropic gelation, emulsion solvent diffusion, and coacervation. Other common methods include spray drying and freeze drying. Selection of any of the methods should take into account factors such as particle size requirement, chemical and thermal stability of the active agents, reproducibility of the release kinetic profiles, stability of the final product, and residual toxicity related with the final products (Agnihotri et al., 2004).

3.7.1 Ionotropic Gelation

Preparation of chitosan nanoparticles by ionotropic gelation has attracted much attention for drug delivery since it is a simple and mild method without the use of organic solvent or high shear force, decreasing the possible toxicity effect of reagents and other detrimental outcomes that come with chemically cross linking (Tiyaboonchai, 2003; Dash et al., 2011). Electrostatic interaction is founded on the contact of the cationic charge of the amine group of chitosan and negatively charge group of polyanion (Sailaja et al., 2010). Sodium tripolyphosphate (TPP), a polyanion, is the most popular ionic crosslinking agent as it is nontoxic and forms a gel (Gan et al., 2005). For this approach, as depicted in Figure 3.7, chitosan is dissolved in aqueous acidic solution for example an acetic acid solution. Next, it is then added dropwise to TPP, a polyanion solution (Dash et al., 2011). Chitosan undergoes ionic gelation and precipitates to form spheres due to the presence of oppositely charged species (Tiyaboonchai, 2003). Calvo and colleagues were first to report the use of this technique for the production of hydrophilic chitosan-polyethylene oxide nanoparticles. It was discovered that the particles had an apparent entrapment capacity and allowed for continued release of proteins for an extended amount of time. The size of these chitosan-polyethylene oxide nanoparticles ranged from 200- 1000 nm depending upon the concentration of polyethylene oxide (Calvo et al., 1997).

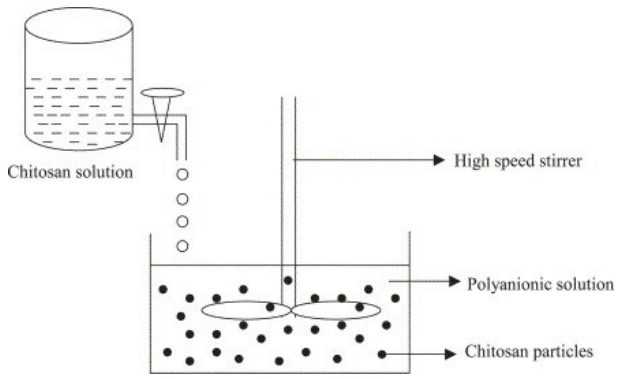

Figure 3.7: Scheme of the preparation of chitosan nanoparticles by ionictropic gelation (Agnihotri et al., 2004)

3.7.2 Emulsion Solvent Diffusion

Emulsion solvent diffusion is based on the limited miscibility of water with an organic solvent and is best used for entrapment of hydrophobic drugs (Tiyaboonchai, 2003; Nagpal et al., 2010).

The first step, shown below in Figure 3.8, is to obtain oil-in-water (o/w) emulsion by injecting an organic (oil) phase into chitosan solution that comprises a stabilizing agent. The emulsion is then diluted with water while under continuous stirring to surpass organic solvent miscibility of water. As the organic solvent diffuses into the water, the polymer precipitates and forms nanoparticles (Tiyaboonchai, 2003; Nagpal et al., 2010). Niwa and coworkers developed emulsion solvent diffusion methods for creating nanoparticles; nanospheres of d,l-lactide/glycolide copolymer (PLGA) were prepared loaded with both water-soluble and insoluble drugs (Niwa et al., 1993). Yang and coworkers (2009) were successful in preparing chitosan-modified paclitaxel-loaded PLGA nanoparticles by the w/o emulsion solvent diffusion method. The chitosan nanoparticles formed after acetone diffused from the droplets into the water phase. The average size and encapsulation efficiency of the produced particles were 105 nm and 91.2%, respectively (Yang et al., 2009). This process has a few drawbacks such as harsh processing conditions, high shear forces and use of organic solvents (Nagpal et al., 2010).

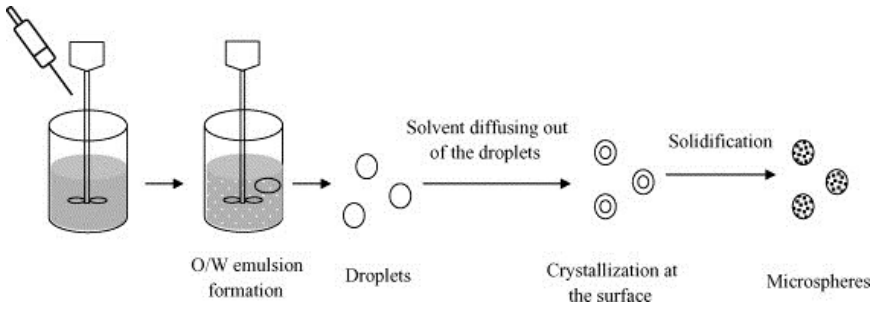

Figure 3.8: Schematic representation of preparation of chitosan particulate systems by emulsion solvent diffusion (Gao et al., 2006)

3.7.3 Coacervation

Coacervation is based on the chitosan physiochemical property of being insoluble in alkaline pH medium, while coacervating when in contact with alkaline solution. The nanoparticles are formed when chitosan solution is blown using a compressed air nozzle into an alkali solution such as sodium hydroxide as shown below in Figure 3.9 (Agnihotri et al., 2004; Dash et al., 2011). Particle size can be controlled by modifications in compressed air pressure or diameter of the nozzle. Bozkir and Saka used complex coacervation with sodium hydroxide to prepare

chitosan nanoparticles for plasmid DNA delivery. They investigated the effect of several parameters for encapsulation efficiency, including molecular weight and DDA of chitosan. It was found that there is a directly proportional relationship between encapsulated efficiency of plasmid DNA and DDA but an inverse proportional relationship between encapsulated efficiency of plasmid DNA and molecular weight of chitosan. Depending upon the DNA:Chitosan ratio as well as the molecular weight of the chitosan, the average particle size and entrapment efficiency was found to be 512-820 nm and 85-98%, respectively (Bozkir and Saka, 2004).

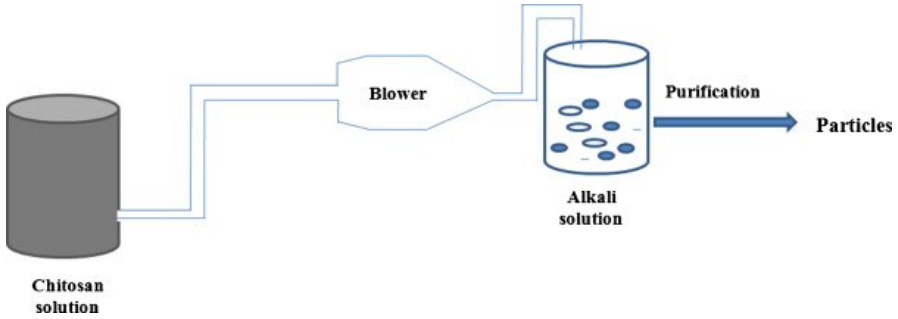

Figure 3.9: Schematic representation of preparation of chitosan particulate systems by coacervation (Dash et al., 2011)

3.7.4 Spray Drying

Spray drying (Figure 3.10) is a well-known process used to produce dry powders, granules, or agglomerates from the mixture of drug and excipient solutions from drying of droplets in a stream of hot air. Oliveira and coworkers prepared spray dried chitosan microspheres that were crossed-linked with D.L-glyceraldehyde. The average size of these particles ranged from 3.4- 6.7 μm depending on the chitosan concentration (Oliveira et al., 2005).

A peristaltic pump feeds the liquid solution to the nozzle where it is forced though by compressed air into small droplets. The droplets are then blown into a chamber in a stream of hot air. During this phase the solvent in the droplets evaporates and discharges though an exhaust tube leading to the formation of free flowing particles. The end product, the dry powder, is gathered in the collection bottle (He et al., 1999). Numerous process parameters can be controlled to get the preferred size of particles; for example the size of the nozzle, spray flow

rate, atomization pressure, inlet air temperature and extent of crosslinking in the solution (Agnihotri, et al. 2004). Spray-drying can be separated into four stages: liquid feed is atomised into a spray of droplets, spray air contact (mixing and droplet/particle flow), drying and particle formation, and particle separation from drying air and dries product discharge.

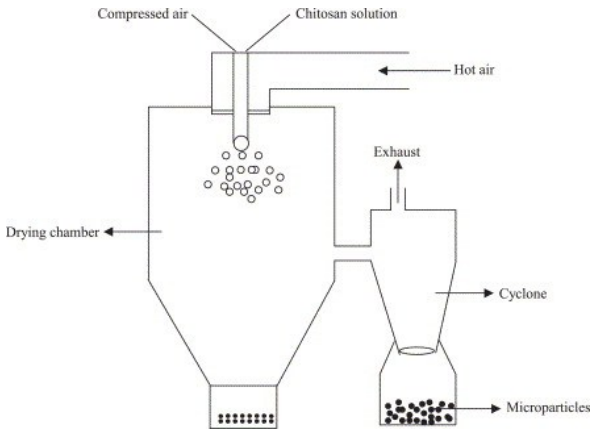

Figure 3.10: Schematic representation of preparation of chitosan particulate systems by spray drying (Agnihotri et al., 2004)

3.7.5 Freeze Drying

Freeze-drying or lyophilization is a commonly used process for drying and refining the stability of various pharmaceutical products such as nanoparticle drug carriers (Franks, 1997). Water must be eliminated in order to increase the chemical and physical stability of these systems. Freeze drying occurs under vacuum and uses sublimation and desorption to eliminate water from a frozen sample. However, this practice is rather slow and costly. Freeze-drying cycles can be separated into three steps: freezing (solidification), primary drying (ice sublimation) and secondary drying (desorption of unfrozen water).

Freezing is the initial stage of freeze-drying. Freezing is an effective dehydration phase where majority of the solvent, commonly water, is separated from the solutes to form ice. Further water confined in the liquid freezes as the freezing process continues resulting in growing concentration of the remaining liquid (Tang and Pikal, 2004). Additional crystallization is induced as the liquid suspension becomes more concentrated and its viscosity increases. The

liquid solidifies, resulting in an amorphous, crystalline, or combined amorphous-crystalline phase (Abdelwahed, et al. 2006). The primary drying phase requires sublimation of ice from the frozen product by dropping the pressure and applying enough heat. Pressure is controlled by partial vacuum; the vacuum speeds sublimation. A porous plug results by the end of the primary drying stage. Its pores correlate to the areas that were occupied by ice crystals (Abdelwahed, et al. 2006). Secondary drying aims to remove absorbed, unfrozen water from the product seeing as the ice was removed during the primary drying stage (Tang and Pikal, 2004). Here, the physico-chemical interfaces that have developed among the water molecules and frozen material are broken by raising the temperature higher than in the primary drying phase (Abdelwahed, et al. 2006). The pressure can also be lowered at this phase to assist desorption.

4.0 METHODS AND MATERIALS

4.1 Chemicals

High purity, low molecular weight chitosan from crab shells in the form of powder (degrees of deacetylation: 90%) was purchased from CarboMer, Inc., San Diego (USA). Chitosan with a degree of deacetylation of 90% was chosen based on the work of Domaratzki (208). Sodium tripolyphosphate (85%), adenosine, dimethylsulphone (certified standard for quantitative $_1$H-qNMR), and D-(+)-trehalose dihydrate were supplied by Sigma-Aldrich (USA). Fisher Scientific, New Jersey (USA) supplied potassium chloride, sodium chloride, sodium phosphate monobasic, and potassium phosphate monobasic, the chemicals required to mix PBS media for release studies. Deionized water was used throughout except for the re-suspension of particles for sizing where purified water was used provided by Sigma-Aldrich (USA) and preparing samples for liquid nuclear magnetic resonance (NMR) where deuterium oxide also provided by Sigma-Aldrich (USA) was used.

4.2 Preparation of Chitosan-TPP Nanoparticles

Chitosan nanoparticles were prepared according to the ionotropic gelation procedure (Figure 4.1) developed by Calvo et al. and modified by Domaratzki (Calvo et al., 1997; Domaratkzi, 2008). The accurate weight of chitosan (1mg/mL) was dissolved in 0.175% acetic acid (v/v). Sodium tripolyphosphate (TPP) was dissolved in deionized water at the concentration of 2mg/mL. Both the chitosan and TPP solutions were dissolved under constant magnetic stirring at room temperature for 30 minutes at 900 rpm. Once both solutions were individually mixed they were passed through a syringe filter. A 0.45 μm syringe filter was used for chitosan and a 0.22 μm filter was used for TPP. The TPP was added to chitosan to form nanoparticles. A chitosan to TPP ratio of 5:1 was chosen based on the work of Zhang and coworkers (2004) and confirmed by Domaratkzi (2008). Chitosan-TPP nanoparticles spontaneously formed by the TPP-initiated ionic gelation mechanism, upon the addition of aqueous TPP solution to the chitosan solution (at chitosan to TPP volume ratio of 5:1). This was done under mild constant magnetic stirring at room temperature for 1 minute at 100 rpm. The solution was centrifuged (Beckman Coulter Ultra-centrifuge, California, USA) for 30 minutes at 52 000 x g, to isolate the nanoparticles.

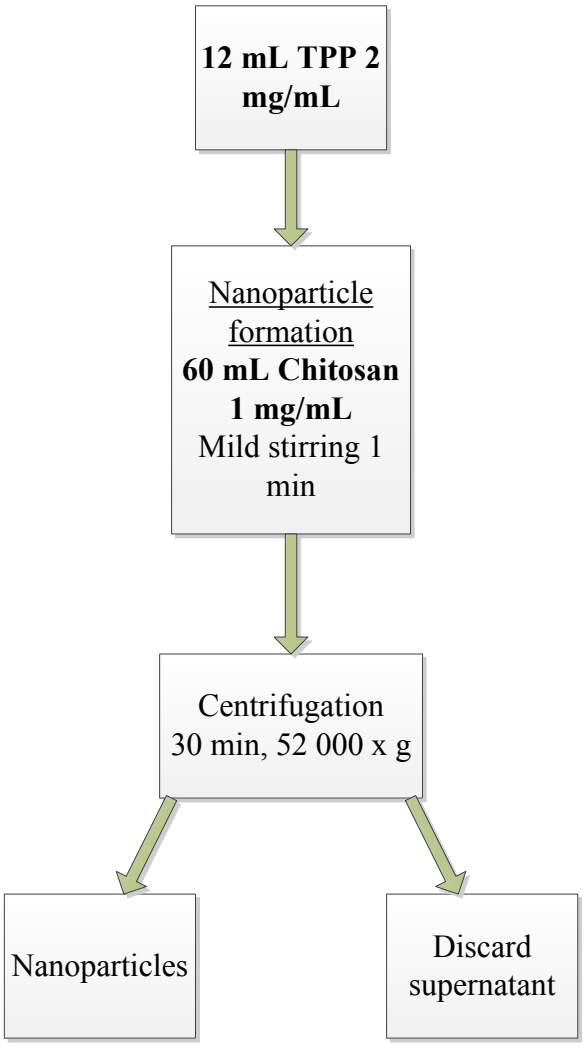

Figure 4.1: Procedure of chitosan nanoparticle formation.

4.3 Drug Loading/Incorporation into Nanoparticles of Chitosan

The drug was incorporated into chitosan nanoparticle systems either by entrapment during the preparation of the particles or by adsorption onto the surface of the particles – these methods are described in the sections below. In the second method the nanoparticles were incubated in a drug solution, which resulted in the drug being entrapped directly on the surface of the nanoparticle. For both methods, adenosine stock solution was prepared by dissolving 7.5 mg/ml of adenosine in 0.9% NaCl (aq).

4.3.1 Internal Entrapment of Adenosine into Chitosan Matrix

For the association of adenosine with chitosan-TPP nanoparticles, adenosine stock solution (pH= 6.27) was added to the TPP solution (pH= 9.00) before adding it to the chitosan solution (pH= 3.35) as shown below in Figure 4.2. Likewise, adenosine-chitosan nanoparticles can be formed according to Figure 4.3, by adding adenosine to the chitosan solution before the addition of the TPP solution. The adenosine-chitosan nanoparticles are formulated following the procedure outlined in section 4.2, with adenosine first added to the TPP or the chitosan. It is theorised that adenosine will be entrapped into the chitosan matrix during the ionotropic gelation process. For both methods the initial loading of adenosine was manipulated (16, 39, 56 % (w/w, with respect to initial chitosan weight)). The effect of the chitosan pH on adenosine entrapment was also investigated by first altering the pH of the chitosan solution to 4.20 with NaOH (40N).

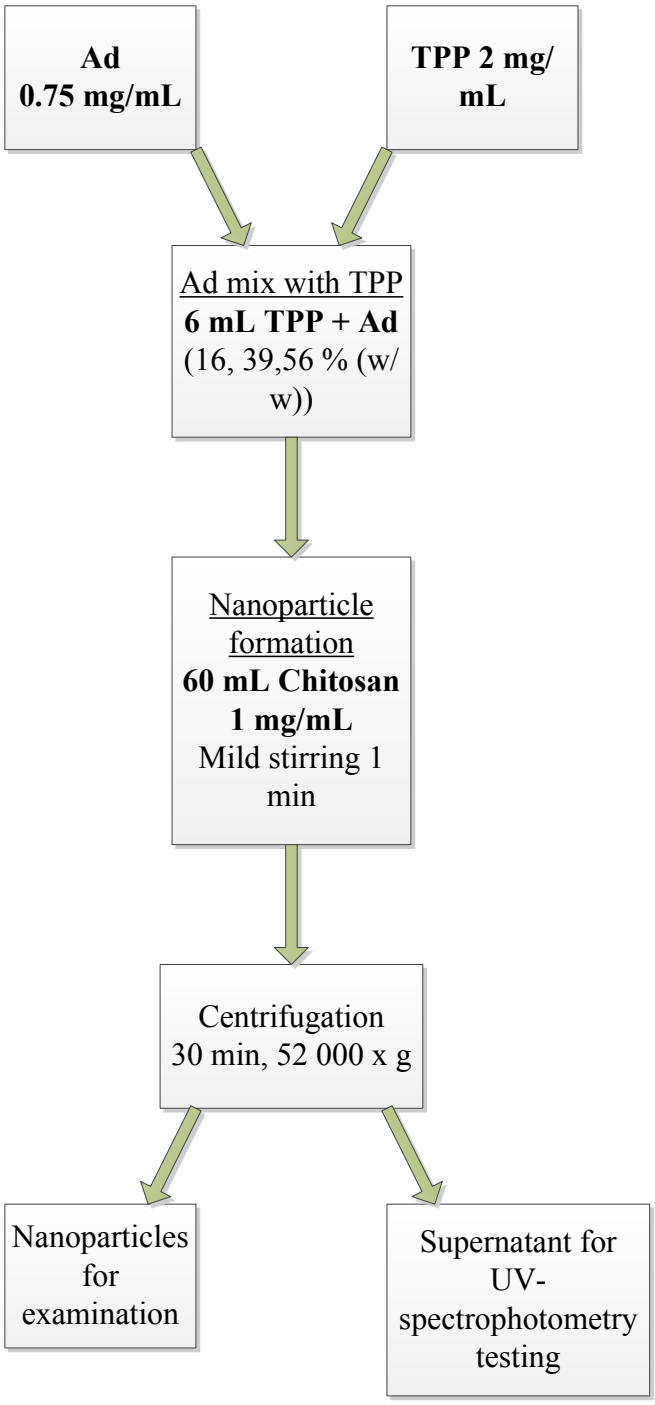

Figure 4.2: Procedure of internal entrapment of adenosine into chitosan nanoparticles, adenosine first mixed with TPP.

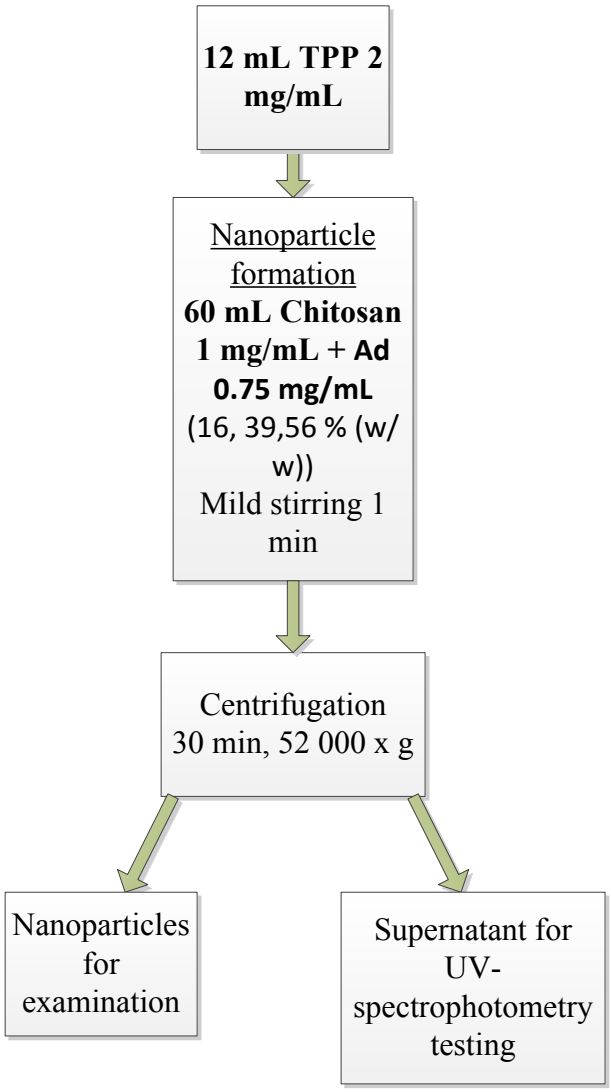

Figure 4.3: Procedure of internal entrapment of adenosine into chitosan nanoparticles, adenosine first mixed with chitosan.

4.3.2 Adsorption of Adenosine onto Chitosan Matrix

Chitosan-TPP nanoparticles are formed according to the ionotropic gelation method described in section 4.2. The chitosan-TPP nanoparticles were then dispersed in deionized water. To adsorb adenosine onto the surface of the nanoparticles, adenosine stock solution (39 (w/w)) was added to 120 ml of chitosan nanoparticle suspension solution. The particles were then incubated at 37°C for 24 hours under constant magnetic stirring at 100 rpm (Figure 4.4). Adenosine-chitosan nanoparticles were recovered by centrifuging at 52 000 x g for 30 minutes and the supernatant was decanted.

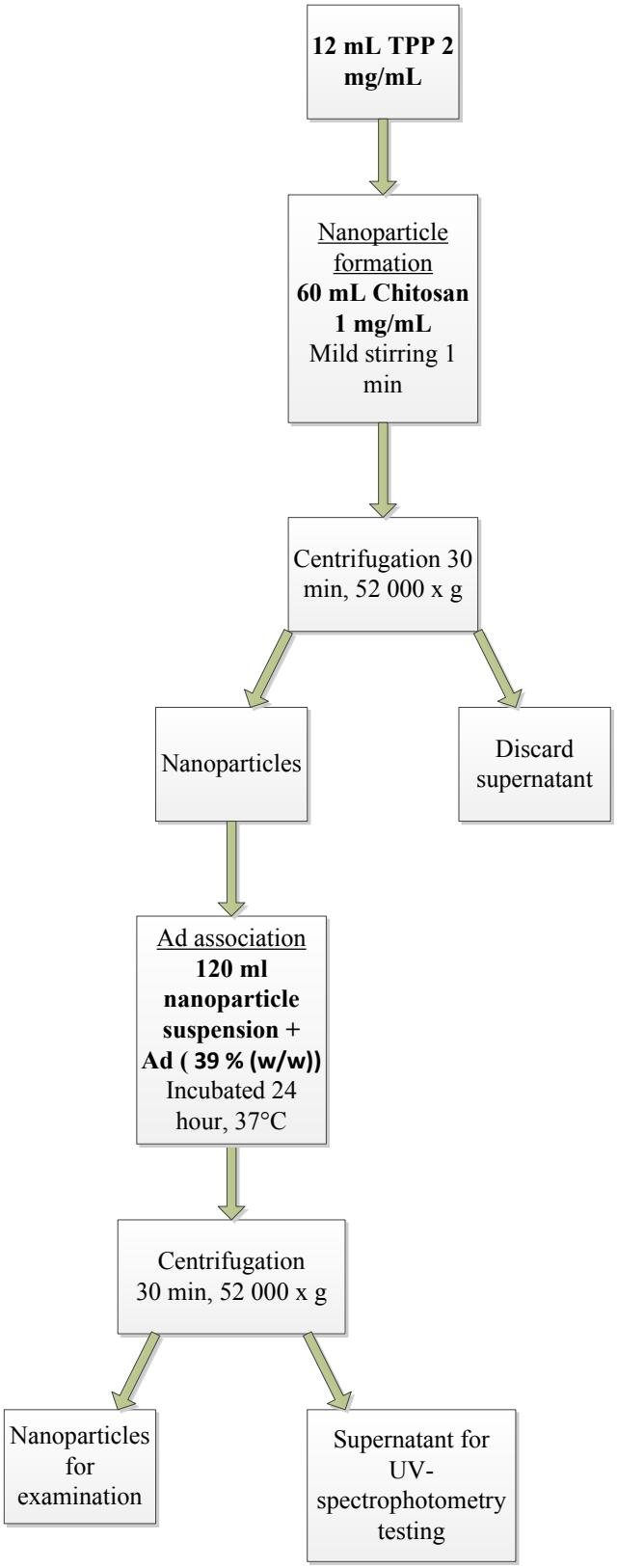
12 mL TPP 2 mg/mL
Nanoparticle formation
60 mL Chitosan 1 mg/mL
Mild stirring 1 min
Centrifugation 30 min, 52 000 x g
Nanoparticles
Discard supernatant
Ad association
120 ml nanoparticle suspension + Ad (39 % (w/w))
Incubated 24 hour, 37°C
Centrifugation 30 min, 52 000 x g
Nanoparticles for examination
Supernatant for UV-spectrophotometry testing

Figure 4.4: Procedure of adsorption of adenosine onto the surface of the chitosan matrix.

4.4Characterization of Nanoparticles of Chitosan

For size and morphology characterization of chitosan nanoparticles, the supernatant was discarded after ultra-centrifugation and the nanoparticles were re-suspended with 2 mL of purified water (W4502 Sigma, USA).

4.4.1 Dynamic Light Scattering

Measurement of the mean particle diameter (z-average), polydispersity (size distribution) and zeta potential of chitosan-TPP nanoparticles in the hydrated state were performed using dynamic light scattering (DLS) on Zetasizer Nano ZS (Malvern Instruments, UK) in the Dalhousie Department of Civil Engineering. The measurements of particle size for 3 mL samples were made at 20°C with an angle of 90° in triplicate to obtain an average after 2 minutes of autocorrelation.

The zeta potential of the chitosan nanoparticles were also calculated with the Malvern Zetasizer. Samples were inserted into the universal dip cell by using a syringe and measurements were made at 20°C in triplicate to obtain an average. First the Electrophoretic Mobility was calculated and then the Henry equation was applied. By assessing the velocity of the particles using Laser Doppler Velocimetry and executing an electrophoresis experiment on the samples the Electrophoretic Mobility can be acquired (Malvern, 2004).

4.4.2 Transmission Electron Microscopy

A Philips Tecnai-12 (Eindhoven, The Netherlands) transmission electron microscope (TEM) in the Dalhousie Department of Biology was used to characterize the size and morphology of dried chitosan nanoparticles. The TEM sample was obtained by using a pastor pipette to place a drop of the chitosan nanoparticle suspension onto carbon-coated copper grids. The samples were dried at room temperature and then examined without any further modification or negative staining.

4.5 Lyophilisation

All samples for the Solid-state NMR (ssNMR) were lyophilized by a freeze dryer, Labconco Freezone® 4.5 Freezedry (Kansas City, MI, USA). After the nanoparticles were formed and centrifuged, the supernatant was decanted and the separated nanoparticles were resuspended in trehalose solution before being placed in a Labconco beaker and freeze-dried for 40 hours at a maximum temperature of -46°C and maximum vacuum of 100 x 10^{-3} mbar to obtain dried chitosan nanoparticles. A Coolpix 995 camera and Eclipse TS100 microscope both by Nikon (Japan) was used to view and record the microstructure of the freeze-dried chitosan nanoparticles.

A cryoprotectant was added to prevent aggregation and stress from freezing and drying of the samples post-lyophilisation. Trehalose was used as the cryoprotectant, as it has minimal chemical reactivity and prevents the leakage of the active ingredient during the freeze-drying process (Abdelwahed et al., 2006). After ultra-centrifugation the supernatant was discarded and the nanoparticles were resuspended in deionized water with 5% trehalose prior to lyophilisation (Lopez-Leon et al., 2005). The concentration of the nanoparticles was 2 mg/ml (Hafner et al., 2011).

4.6 Adenosine Measurement

4.6.1 UV-Spectrophotometry

UV-spectrophotometry was used to quantify the amount of adenosine entrapped as well as the amount of adenosine released from chitosan nanoparticles (Arias et al., 2010; Du et al., 2010; Katas and Alpar, 2006; and Papadimitriou et al., 2008). Absorbance readings of the samples were determined using PharmaSpec UV-1700 ultraviolet-visible spectrophometer (Shimadzu, Kyoto, Japan). All spectrophotometric measurements were conducted at an operating wavelength of $\lambda = 280$ nm in optically homogeneous quartz cuvettes. The operating wavelength was chosen based on the wavelength scans of adenosine, chitosan and TPP (Appendix A). At 280 nm the wavelength peaks of chitosan and TPP do not interfere with the peak of adenosine.

4.6.2 Solid-State NMR

The solid-state ^{13}C and ^{31}P spectra were obtained on a Bruker Avance 400 (Massachusetts, USA) NMR spectrometer located at Dalhousie University's Nuclear Magnetic Resonance Research Resource Center. The spectrometer had a 9.4 T magnet (400.24 MHz proton Larmor frequency, 100.65 MHz ^{13}C Larmor frequency, 162.02 ^{31}P Larmor frequency). Liquid-state NMR was performed on selected samples to verify results from UV spectrometry.

All samples were lyophilized prior to being packed well into 4 mm diameter rotors. The experimental parameters for the ^{13}C NMR trials were established from the H NMR spectral parameters. With single pulse excitation and background suppression the ^{1}H NMR spectra were developed. Inversion-recovery sequences were used to find the ^{1}H spin lattice relaxation times, T_1. The lattice relation times of the ^{1}H spin was found to be on the order of 2.5-4.2 seconds. All samples were measured at 9.5 kHz sample spinning for the ^{13}C NMR spectra except for a few that were spun at 7 or 10.5 kHz in order to differentiate isotropic chemical shift peaks from spinning sidebands. For the developing of the ^{13} C CP/MAS spectra a repetition time of 240 s was used. For the ^{13} C cross- polarization (CP) / magic angle spinning (MAS) experiments a recycle delay of 9-28 seconds was used for chitosan containing samples. The ^{13}C CP/MAS test performed with TPPM proton decoupling were improved on glycine. Glycine's carbonyl resonance also functioned as external, secondary chemical shift standard at 176.06 ppm. For the concluding ^{13}C CP/MAS NMR spectra, 16 scans for the pure Adenosine and up to 400 scans for the other samples were collected operating at 2.6 ms CP contact time.

To detect the isotropic shifts and spinning sidebands for the ssNMR ^{31}P CP/MAS spectra the spinning speeds were 7.0 and 8.0 kHz. Spinning sidebands are intense in systems like these owing to the wide anisotropic chemical shifts. Scans were collected with repetition times of 9 s using CP contact times of 500 microseconds, up to 80 seconds. NHHPO at 0.81 ppm was used as a secondary standard to externally reference the chemical shift scale against.

4.6.3 Liquid-State NMR

Quantitative liquid-state NMR (qNMR) ^{1}H spectra were obtained on a Bruker Avance 500 (Massachusetts, USA) NMR spectrometer also located at Dalhousie University's Nuclear Magnetic Resonance Research Resource Center. The NMR spectrometer had a 11.74 T magnet (500 MHz frequency, tunable to all frequencies between ^{14}N and ^{31}P). Due the intrinsic sensitivity and its high comparative abundance the ^{1}H nucleus was chosen for qNMR experiments. Liquid-state NMR was performed on selected samples to verify results from UV spectrometry.

The supernatant collected from nanoparticles that were formulated following the procedure outlined in section 4.3.1 was used for testing. The only change made to this procedure was that deuterium oxide was used as a solvent instead of deionized water. One-millilitre samples of supernatant were spiked with a known amount of standard solution and packed into NMR tubes for testing. Dimethyl sulphone ($DMSO_2$) was chosen as a reference standard as it has a low volatility, structurally unrelated to the analyte, and has a resonance that does not cover areas in spectrum where the adenosine signal is expected. As well $DMSO_2$ is chemically inert and does not have any additional salts or ions that interact with molecules in the supernatant. The internal standard is used as a reference point to calibrate the chemical shifts in the resultant spectrum. The area under the peak of the standard in a spectrum is directly proportional to the number of nuclei giving rise to that peak and its molar concentration. From this information the concentration of adenosine can be calculated using Equation 4-1.

$$C_{Ad} = \frac{C_S \times A_{Ad}}{A_S} \times n \qquad [4\text{-}1]$$

where

C_{Ad} = concentration of adenosine (mg)

C_S = concentration of standard (mg)

A_{Ad} = integral area of adenosine

A_S = integral area of standard

n = 6 (signal from reference compound is due to 6 equivalent protons)

A calibration curve was created by diluting known amounts of adenosine solution with the supernatant from blank loaded chitosan nanoparticles and spiking it with measured volumes of $DMSO_2$. This was done for both chitosan at its original pH of 3.35 and chitosan with a pH change to 4.2. The concentrations of adenosine that were acquired from the qNMR measurements were calibrated using the appropriate calibration curve equation in order to convert the readings to be comparable to the prepared weighed amounts of adenosine. Entrapment efficiency (Equation 4-2) can then be calculated from the converted from the converted readings.

4.7 Adenosine Quantification Calculations

4.7.1 Drug Loading

Adenosine-loaded chitosan nanoparticles were prepared as described in section 4.3. The amount of adenosine entrapped and absorbed was evaluated indirectly from the difference between the total quantity added to the loading solution (initial loading) and the quantity of non-entrapped adenosine remaining in the supernatant. Based on the absorbance of the samples determined using the UV spectrophometer the adenosine concentration in the supernatant can be found (Calvo et al., 1997; Dudhani and Ksaraju, 2010; Grenha et al., 2005; Katas and Alpar, 2006). The supernatant samples from nanoparticles with 16, 39, 56 (% (w/w)) initial drug loadings were diluted 1:3, 1:5, and 1:6 respectively with deionized water to ensure the absorbance readings were within the parameters of the assay, the linear region of the standard curve. A standard curve (concentration vs. UV absorbance) was prepared using the supernatant of blank nanoparticles and diluting a standard solution of adenosine to various concentrations. By use of External Standard Method (Appendix B) the amount of free adenosine in the supernatant of drug loaded nanoparticles can be calculated. This value was then subtracted from the known initial loading to find the measure of drug entrapped.

After nanoparticle formation, the entrapment or association efficiency and loading capacity can be determined from the supernatant. Entrapment efficiency (EE) indicates the efficiency of the

preparation method to incorporate the drug into the carrier system as it expresses the amount of the drug entrapped within the nanoparticle compared to the initial drug loading (Judefedind and de Villiers, 2009). An entrapment efficiency of 100% means that the total initial drug loaded was integrated into the nanoparticles. The performance of the drug delivery system can be determined by the amount of drug entrapped as it impacts the rate and extent of drug release from that system (Judefeind and de Villiers, 2009). Entrapment efficiency was determined according to the following equation:

$$EE = \frac{m_e}{m_i} \times 100 \qquad [4\text{-}2]$$

where

EE = entrapment efficiency (%)

m_e = mass of drug entrapped in nanoparticles (μg)

m_i = mass of initial drug loading (μg)

The association efficiency (AE) can be determined analysing the un-bound drug in the supernatant as described above. The association efficiency is comparable to the entrapment efficiency as it is a percent measurement of the efficiency of the preparation method of associating the drug onto the carrier system. The drug is absorbed onto the surface instead of entrapped within the nanoparticles; consequently the term association is used in place of entrapment to designate drug incorporation. The association efficiency expresses the amount of drug associated with the nanoparticles compared to the initial drug loading. Association efficiency was determined according to the following equation:

$$AE = \frac{m_i - m_s}{m_i} \times 100 \qquad [4\text{-}3]$$

where

AE = association efficiency (%)

m_s = mass of drug remain in solution (μg)

m_i = mass of initial drug loading (μg)

4.7.2 Drug Release

In vitro adenosine release profiles from chitosan nanoparticles were implemented over time in release media (Figure 4.5). After ultra-centrifugation the supernatant was discarded from the adenosine-loaded chitosan nanoparticles. The adenosine-loaded chitosan nanoparticles were re-dispersed in 2.5 mL of deionized water.

The *in vitro* release studies were conducted using dialysis tubing to contain the adenosine-loaded chitosan nanoparticles in order to minimize the effect that nanoparticles and other large molecules could have on the spectrophotometric absorbance of the samples. The chosen dialysis tubing (Spectra/Pro 1, Spectrumlabs USA) had a molecular weight cut off (MWCO) of 6000 to 8000 Da to ensure that adenosine, molecular weight of 267, would diffuse though the pores in the membrane. The dialysis tubing was first soaked for 20 minutes in deionized water. Then the 2.5 mL sample of re-suspended adenosine-loaded nanoparticles were pipetted into the dialysis tubing (60 mm length with a dry diameter of 24 mm). In order to ensure proper tubing length the following Equation 4-5 from Spectrumlabs was used (Spectralab, 1995-2013). To ensure there were no leaks in the system, each end of the dialysis tubing was sealed with dialysis tubing closures that had a sealing width of 4 mm longer than the flat width of the dialysis tubing (Spectralab, 1995-2013). When sealing the dialysis tubing a portion of the length was left void to allow for headspace (air) to keep the sample buoyant.

$$Total\ length = \frac{sample\ volume}{\left(\frac{volume}{length}\right)} = +(additional\ 10-20\%) + 4\ cm \qquad [4\text{-}4]$$

The samples were incubated in 50 mL buffered reservoirs (pH= 7.4) at 37°C with 120 rpm agitation (Arulmozhi et al., 2013). By use of a pipette, 3 mL samples of release media were removed from the beakers at appropriate time intervals (Wu et al., 2005). The quantity of adenosine in the release media was assessed by absorption using UV-spectrophotometric examination. A standard curve (concentration vs. UV absorbance) was prepared using the release media and diluting a standard solution of adenosine to various concentrations in the appropriate range. From the equation fitted to the standard curve (Appendix C) the amount of

free adenosine in the release media was calculated. To maintain the original volume, each time, the 3 mL samples were returned to the beaker once testing was completed. Each release measurements were repeated in triplicate.

Phosphate-buffered saline (PBS) was selected as the release medium as the pH remains nearly constant and it is isotonic, the osmolarity and ion concentrations generally equivalent those of human fluids (Zhia et al., 2009). Polleux and Ghosh's recipe for PBS was employed; 80 g NaCl, 2 g KCl, 11.5 g $Na_2HPO_4 \bullet 7H_2O$, 2 g KH_2PO_4, and 1 L of deionized water (Polleux and Ghosh, 2002). The pH of the PBS was changed to 7.4 in order to mimic physiological conditions with NaOH (40N) (Hossain et al., 2013). In order to maintain a driving force and the rate of dialysis the total volume of medium was replaced with fresh medium after 2.5 days. This was done to ensure that the rate of diffusion did not slow down as it approached equilibrium.

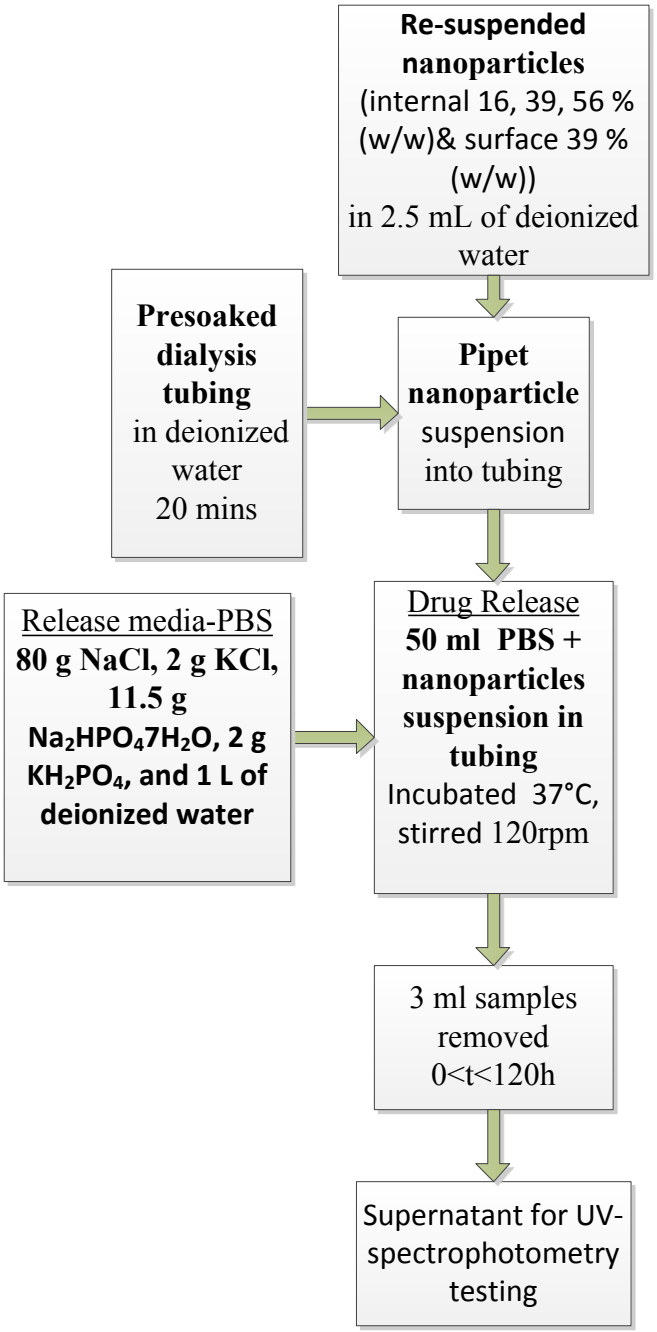

Figure 4.5: Process summary for drug release experiment.

4.8 Summary of Experiments

Below in Figures 4.6 and 4.7 a pictorial representation is displayed of the summary of experiments preformed on entrapped/associated adenosine chitosan-TPP nanoparticles and the outcome for each.

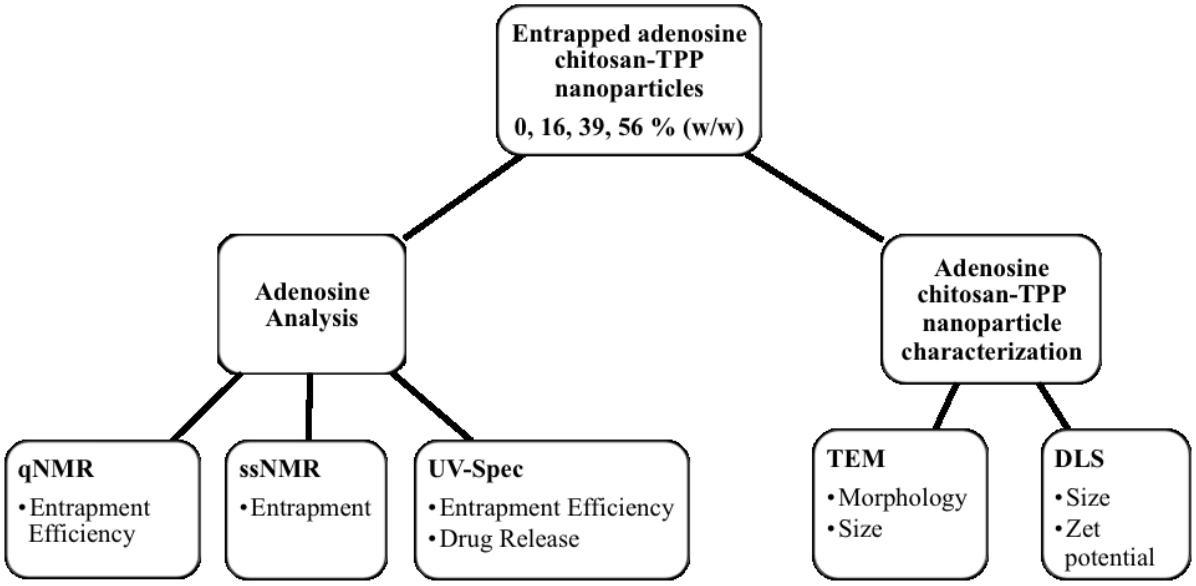

Figure 4.6: Summary of experiments preformed on entrapped adenosine chitosan-TPP nanoparticles with varied with initial Ad loading

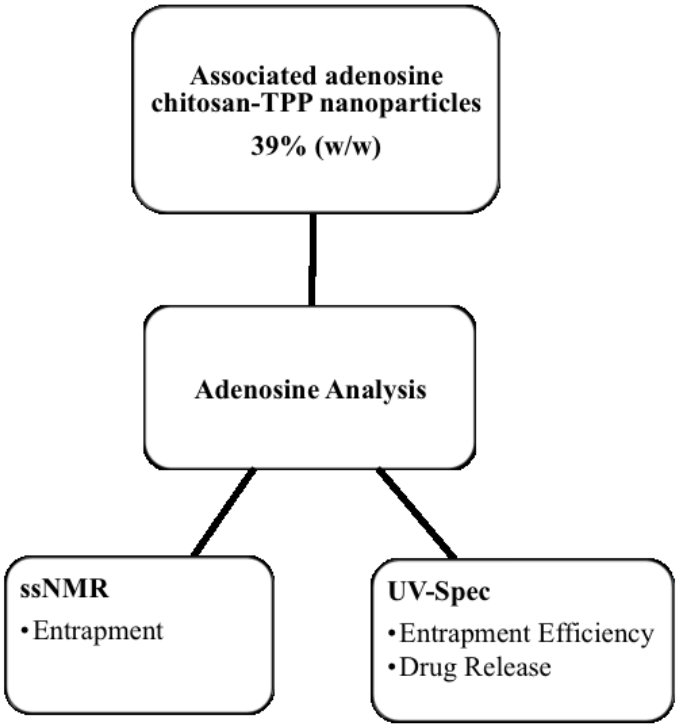

Figure 4.7: Summary of experiments preformed on associated adenosine chitosan-TPP nanoparticles with 39% (w/w) Ad loading

4.9 Statistical Analysis

Each experiment was performed in triplicate and repeated several times. All results are expressed as means ± standard deviation. Data was analyzed using Sigma Plot version12 by t-test to determine the normality of the sample ($P \geq 0.05$ indicating significance). Mann-Whitney Rank Sum Test was then used to determine statistical significance of the data.

5.0 RESULTS AND DISCUSSION

5.1 Nanoparticle Formation Observations

The formation of chitosan nanoparticles by ionic gelation occurs spontaneously upon the incorporation of the anion TPP solution into the chitosan solution. The results are confirmed visually, as the appearance of the solution changed from clear to one that is opalescent and colloidal upon the contact of chitosan and TPP. This change in solution appearance signified a modification of the physical state of the chitosan to form nanoparticles. Conversely, the addition of adenosine to either the chitosan solution or TPP solution before the chitosan interaction with TPP resulted in a final solution that was more translucent than opalescent. The pellet that remained in the bottom of the centrifuge tube after ultra-centrifugation of the internally entrapped adenosine nanoparticles had a greater volume and appeared to be more translucent and gel-like than that of the nanoparticles with adenosine absorbed on the surface and the nanoparticles with no drug loaded. The pellets from the latter two nanoparticles were more opaque, dense and cakey.

There is possibly an interaction between TPP and adenosine, which could affect crosslinking. One possible reason for this is that adenosine could preferentially complex with the TPP. If TPP and adenosine molecules form a complex due to close contact there could be less vacant anionic sites for the TPP to interact with the cationic chitosan sites. Therefore chitosan and TPP may not form a tightly bound matrix causing the nanoparticles to occupy a greater volume. This adenosine and TPP complex that may form from interacting may also be the reason why the solution appears translucent, implying that there are fewer particles being formed and that more chitosan remained in solution.

5.2 Characterization of Nanoparticles of Chitosan

The Malvern zetasizer and TEM were used to observe the size and characteristics of both adenosine-loaded chitosan-TPP nanoparticles and chitosan-TPP nanoparticles. Table 5.1 displays the hydrated diameter, polydispersity index (PDI), count rate and zeta potential of empty and varying adenosine-loaded chitosan nanoparticles.

5.2.1 Dynamic light scattering

DLS as reviewed in section 4.4.1 was employed to measure the hydrodynamic diameter of the chitosan nanoparticles. Drug loading affected the size of the chitosan nanoparticles. The average diameters of unloaded particles were large and outside the range to be considered a nanoparticle, 1450 ± 489 nm. However, the average diameter decreased upon the incorporation of adenosine. This decrease in diameter seen in the adenosine loaded nanoparticles from the unloaded chitosan nanoparticles is significant (Mann-Whitney Rank Sum Test, $P \leq 0.001$). Within the tested range of conditions, the increase in particle size showed a simple linear relationship (Figure 5.1) with increase in adenosine concentrations: 425.6 ± 133.7, 447.4 ± 176.3, and 514.7 ± 190.5 nm for 16, 39 and 56 % (w/w) initial Ad loading, respectively. Increases in adenosine concentration correlated to an increase in particle size. As the quantity of adenosine increased so did the size of the particle. This increase in particle bulk is attributable to increase of adenosine molecules contained within the nanoparticles. However, this increase in particles size due to increases amounts of adenosine loaded is not significant (Mann-Whitney Rank Sum Test, P= 0.479)

Table 5.1: Characteristics of chitosan nanoparticles, n ≥ 20

Ad loading (%(w/w))	Hydrated nanoparticle diameter (nm)	Polydispersity index	Count rate (kcps)	Zeta potential (mV)	Mass of Ad loaded (mg)
0	1450 ± 489	0.825 ± 0.064	227.9 ± 113.1	37.20 ± 5.62	---
16	425. 6 ± 133.7	0.755 ± 0.187	227.9 ± 79.4	56.73 ± 5.08	1.626 ± 0.167
39	447.4 ± 176.3	0.680 ± 0.025	227.9 ± 90.3	63.34 ± 7.19	17.843 ± 0.339
56	514.7 ± 190.5	0.699 ± 0.154	227.9 ± 140.8	65.43 ± 15.52	35.092 ± 0.930

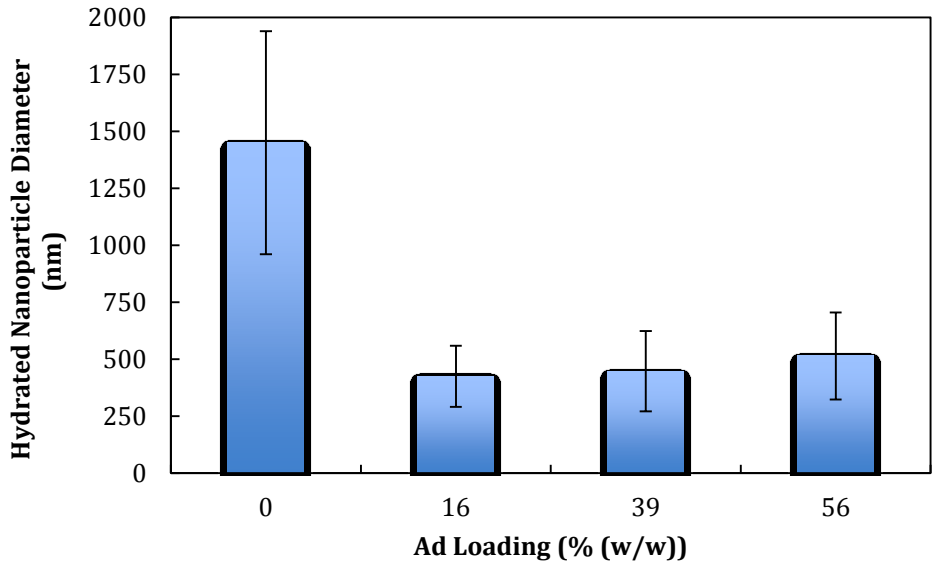

Figure 5.1: Average diameter of hydrated chitosan nanoparticles, as varied with initial Ad loading. Mean ± standard deviation, n ≥ 20.

Polydispersity, a measure of size distribution, is often measured by the PDI. The PDI measured for each drug loading as well as the empty chitosan nanoparticles was more than 0.5 as displayed in Figure 5.2. According to Wu, et al., 2011 this indicates a broad particle size distribution. A PDI value of 0.1 to 0.25 would have been related to a narrow size distribution. Aggregation of the nanoparticles is likely the cause of such large PDI values. The reason for the aggregation is that chitosan is a self-adhesive hydrogel polymer that tends to produce larger particles as a result of strong inter-particle interactions (Banejee et al., 2002). Consequently, through Brownian motion chitosan nanoparticles interact between themselves when in an aqueous solution to form clusters (Jin-Oh et al., 2006). As a result, for interacting particles, the average diameter is always larger than that of the actual. The PDI values for the unloaded and adenosine loaded chitosan nanoparticles (16, 39, and 56 % (w/w)) is not significantly different (Mann-Whitney Rank Sum Test, P=0.478).

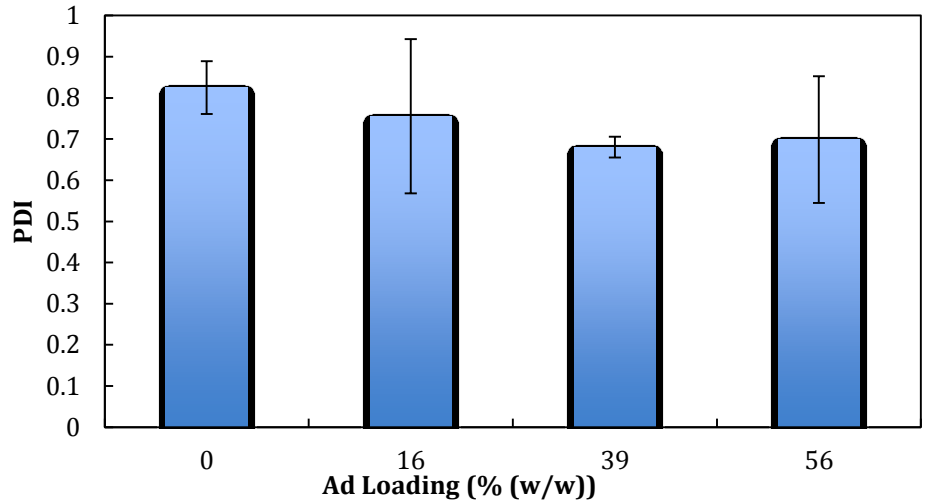

Figure 5.2: Average polydispersity Index of hydrated nanoparticles, as varied with initial Ad loading. Mean ± standard deviation, n ≥ 20.

Zeta Potential, also known as surface charge, can impact the stability of particles in suspension by the electrostatic repulsion amongst particles. The average zeta potential of adenosine loaded chitosan nanoparticles at 63.01 ± 11.04 mV increases significantly from that of unloaded chitosan nanoparticles at 37.20 ± 5.62 mV (Mann-Whitney Rank Sum Test, $P \leq 0.001$). The incorporation of increasing amounts of adenosine led to an increase on their surface charge that ranged from 56.73 ± 5.08 to 65.43 ± 15.52 as seen in Table5.1 and Figure 5.4. The difference between the zeta potentials for the adenosine loaded chitosan nanoparticles (16, 39, and 56 % (w/w)) is not significantly different (Mann-Whitney Rank Sum Test, P=0.479).

The positive zeta potential greater than 30 mV indicates that the colloidal system is stable. The degree of the zeta potential can advise the stability of the colloidal system. If the particles in suspension have a large positive or negative zeta potential (more positive than +30 mV and more negative than -30 mV) then they will be stable and tend to repel each other. However, if the zeta potential falls between +30 and – 30 mV the system will be unstable as there are no forces to prevent the particles from coming together or flocculating (Malvern, 2013). The pH is the most important factor to affect the zeta potential. Problems can arise with dispersion stability with pH

values between 4 and 7.5 as shown in Figure 5.3. This stability of this chitosan nanoparticle system can be attributed to two factors, the residual amino groups on the chitosan as well as the pH being below 4 at 3.35.

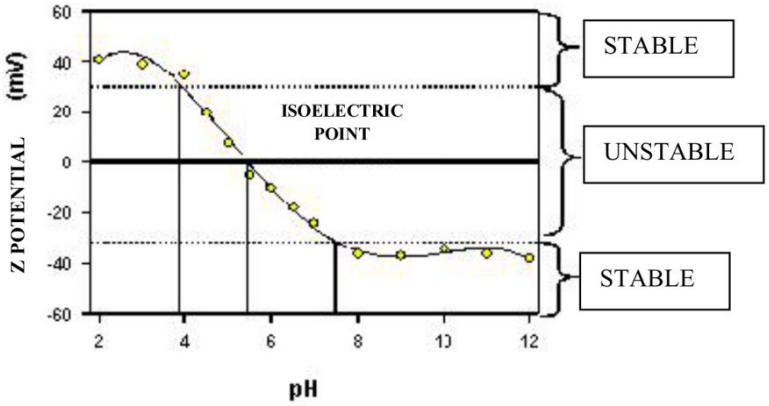

Figure 5.3: Zeta potential verus pH plot exhibiting the isoelectric point and the pH values where the dispersion would be predicted to be stable (Talero et al., 2013)

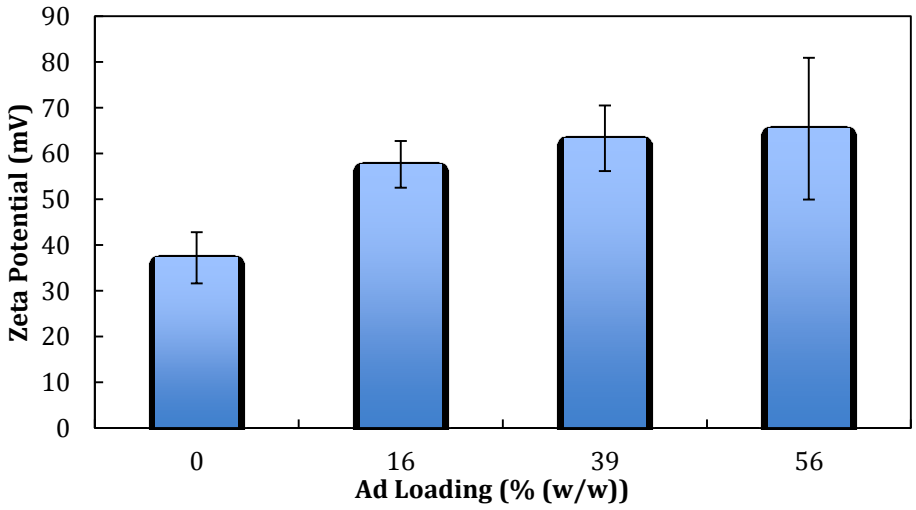

Figure 5.4: Average zeta potential of hydrated nanoparticles, as varied with initial Ad loading. Mean ± standard deviation, n ≥ 10.

Count rate, expressed in kilo counts per second (kcps), is the sample scattering intensity measured by the number of photons detected per second by the photodetector (Wu et al., 2007; Malvern, 2004). The count rate is useful determining two things: 1) the quality of the data and 2) the comparative concentration of the sample. A reduction in data precision will result if the particle suspension is too dense. As the count rate increases so does the concentration of the sample, this would designate a higher number of particles are present (Isa et al., 2007). The concentration should produce a minimum count rate of 10kcps (Malvern, 2004). The average count for all nanoparticles regardless of the quantity of drug loaded was 227.9 kcps as shown in Figure 5.5 and Table 5.1, there was no significant difference (Mann-Whitney Rank Sum Test, P=0.179). This proposes that the concentration of nanoparticles in each sample were nearly equivalent. In this case the count rates fell within the ideal average count rate in the 50-300 kcps range (Williams et al., 1999). This constant count rate value for all nanoparticles could indicate that after fabricating and transferring there were no loss of particles.

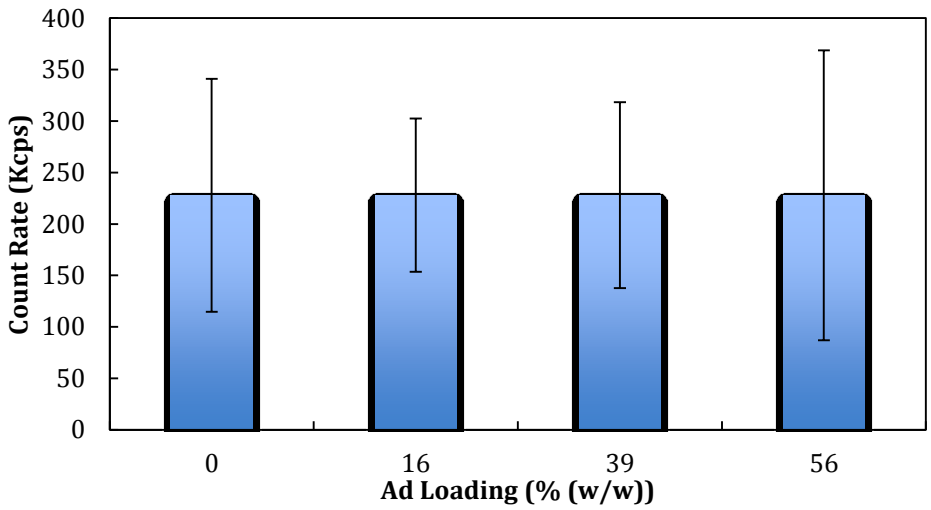

Figure 5.5: Particle analyzer average count rate, as varied with initial Ad loading. Mean ± standard deviation, n ≥ 20.

5.2.2 Transmission Electron Microscopy

The visualization of loaded and unloaded chitosan nanoparticles size and morphology was performed in a dried state by TEM. The averaged measured diameter of the unloaded nanoparticles was 194 ± 72 nm. The average dried diameter of the adenosine loaded nanoparticles was 135 ± 48 nm, 180 ± 66 nm, 183 ± 64 nm for 16, 39 and 56 %(w/w) initial Ad loading, respectively (Figure 5.6). There was no significant difference between the average dried diameter of the chitosan nanoparticles regardless of the amount of adenosine initially loaded (0, 16, 39 and 56 %(w/w)) (Mann-Whitney Rank Sum Test, P=0.29) .The TEM revealed that the size and morphology of particles were not affected by adenosine loadings up to 56%. The morphology study of the nanoparticles revealed that the nanoparticles possessed a regularly spherical shape and smooth surface; this can be seen in Figures 5.9 and 5.10. From Figure 5.7 and Figure 5.8 it can been that there is some aggregation of the particles, this could be why the standard deviation is high. This aggregation seen in the TEM images can also prove that the hydrated diameter of unloaded chitosan nanoparticles was high due to particle aggregation. Figure 5.8 shows an aggregation of three individual particles with distinctive joining boundaries formed at the side of the polyhedron shaped nanoparticles.

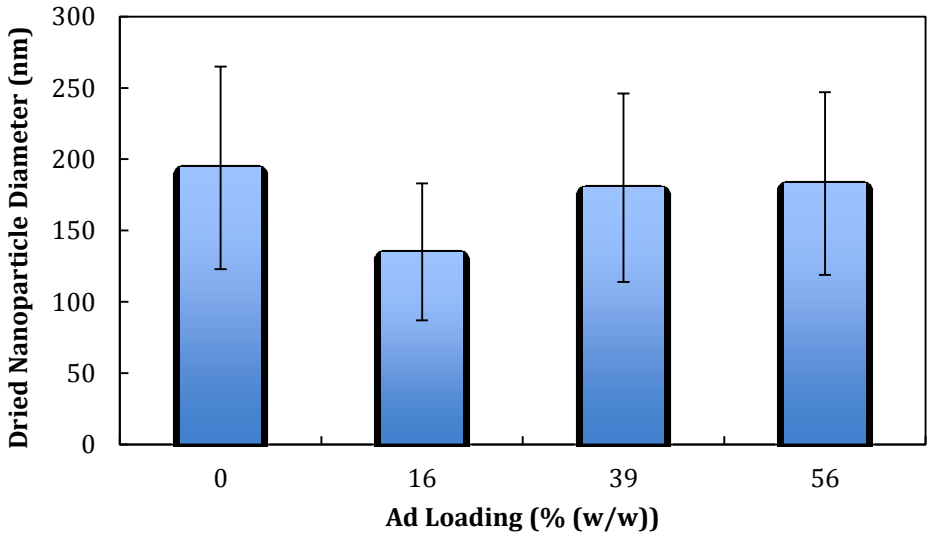

Figure 5.6: Average diameter of air dried nanoparticles, as varied with initial Ad loading. Mean ± standard deviation, n ≥ 15.

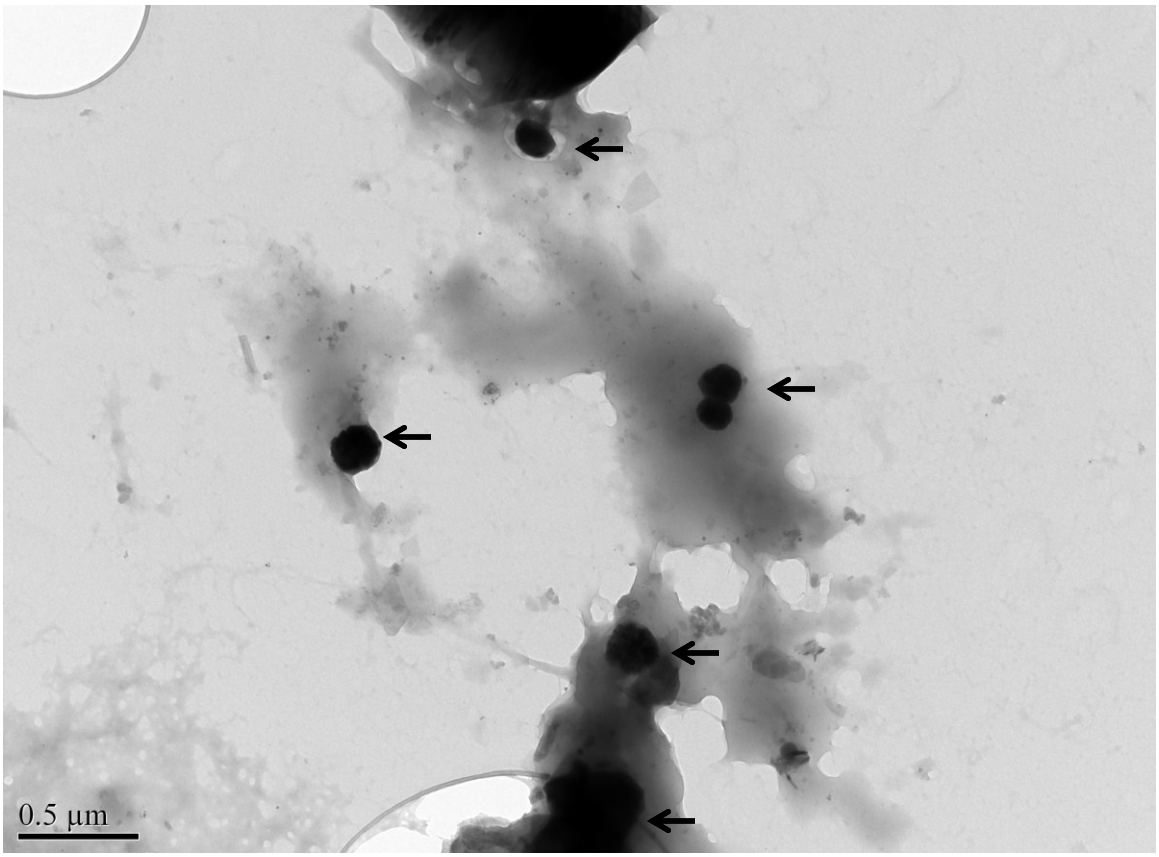

Figure 5.7: TEM image of an air-dried single and large aggregate of unloaded chitosan nanoparticles at 30 000 x magnification. Arrows point out the particles present.

Figure 5.8: TEM image of an air-dried aggregate of three single 16% initial Ad loading chitosan nanoparticles with distinctive polyhedron shapes at 150 000 x magnification. Arrows point out the particles present.

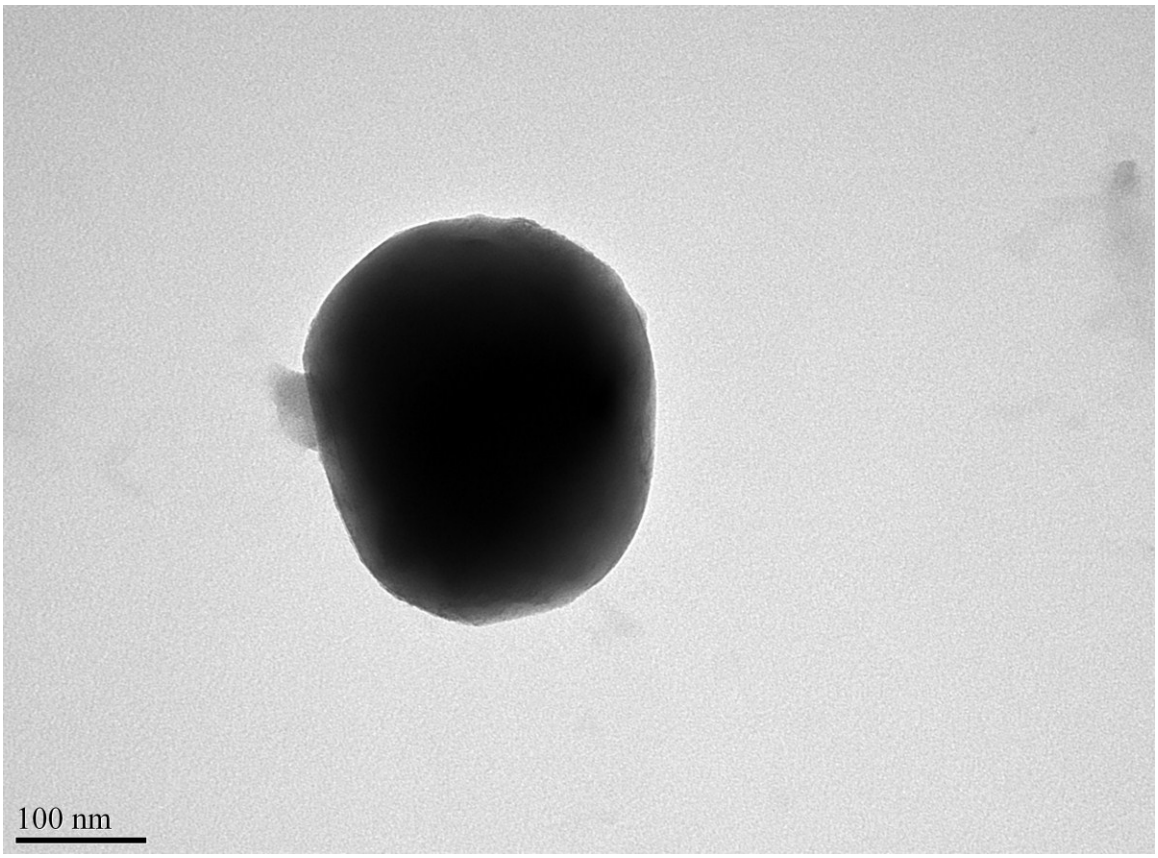

Figure 5.9: TEM image of an air-dried single spherical 39% initial Ad loading chitosan nanoparticle at 150 000 x magnification.

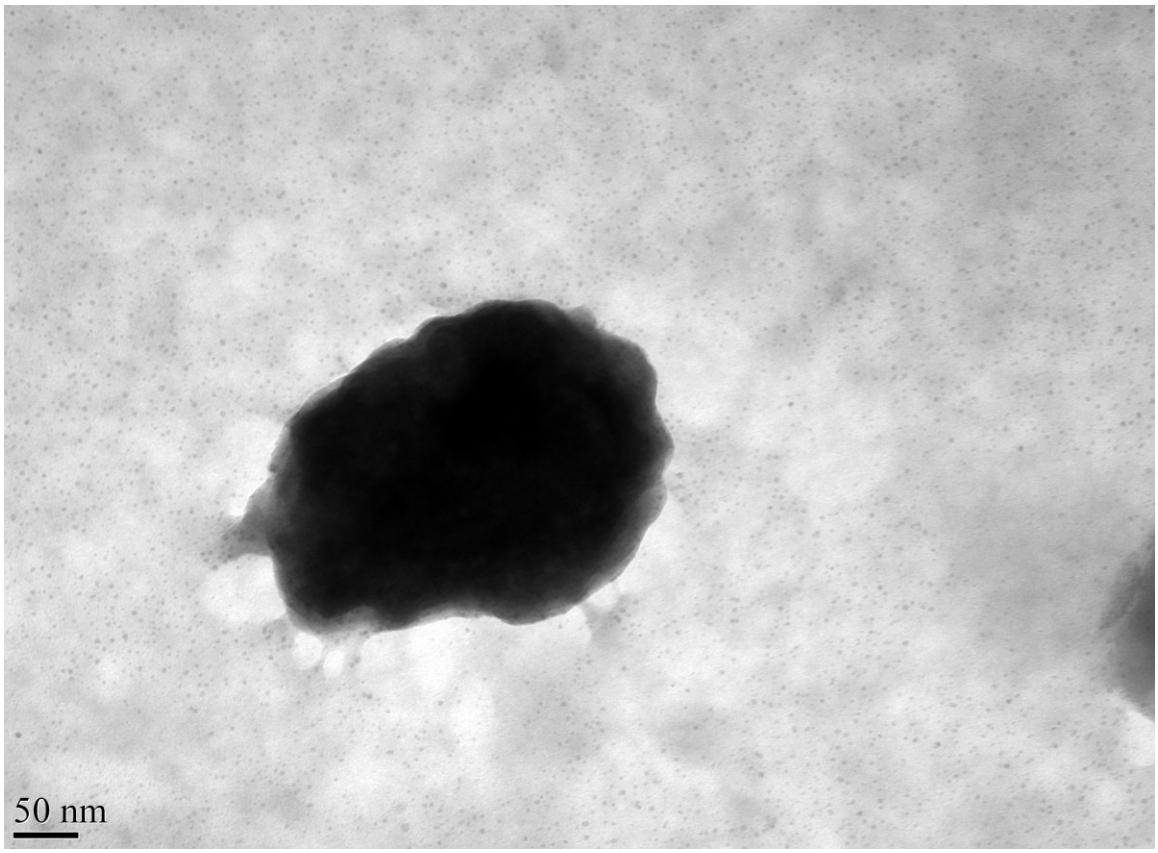

Figure 5.10: TEM image of an air-dried single spherical 56% initial Ad loading chitosan nanoparticle at 150 000 x magnification.

The dried adenosine-loaded chitosan nanoparticles showed a similar narrow diameter size range as the hydrated nanoparticles. A significant diameter reduction of 68, 60, and 64% from the fresh hydrated state for 16, 39 and 56% initial Ad loading, respectively was observed (Mann-Whitney Rank Sum Test, $P \leq 0.001$). For unloaded chitosan nanoparticles a significant diameter decrease of 86% was verified (Mann-Whitney Rank Sum Test, $P \leq 0.001$). A comparison of the diameter size range for the hydrated and dried chitosan nanoparticles can be seen below in Figure 5.11. The dried chitosan nanoparticles were smaller with a narrower size range than the swollen hydrated particles obtained by DLS due to the different conditions required for each, in a dried form for TEM and in an aqueous suspension for DLS.

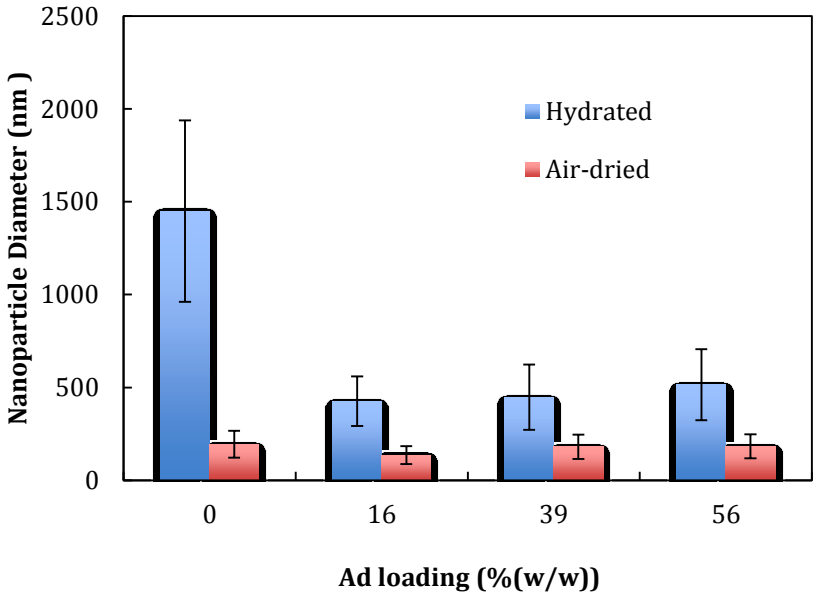

Figure 5.11: Comparison of diameters of hydrated and air-dried chitosan nanoparticles, as varied with initial Ad loading. Mean ± standard deviation, n ≥ 15.

5.3 Lyophilisation

Unloaded chitosan nanoparticles and 39 % (w/w) adenosine loaded chitosan nanoparticles were freeze-dried prior to ssNMR analysis following the procedure in section 4.5. After lyophilisation the nanoparticles formed a white solid intact cake that occupied the same shape and volume as the original frozen suspension. A small amount of force applied to the solid cake caused it to break into a particulate form. Both the chitosan and adenosine-loaded chitosan nanoparticles had a fully crystalline structure after freeze-drying as shown below in Figure 5.12 and 5.13.

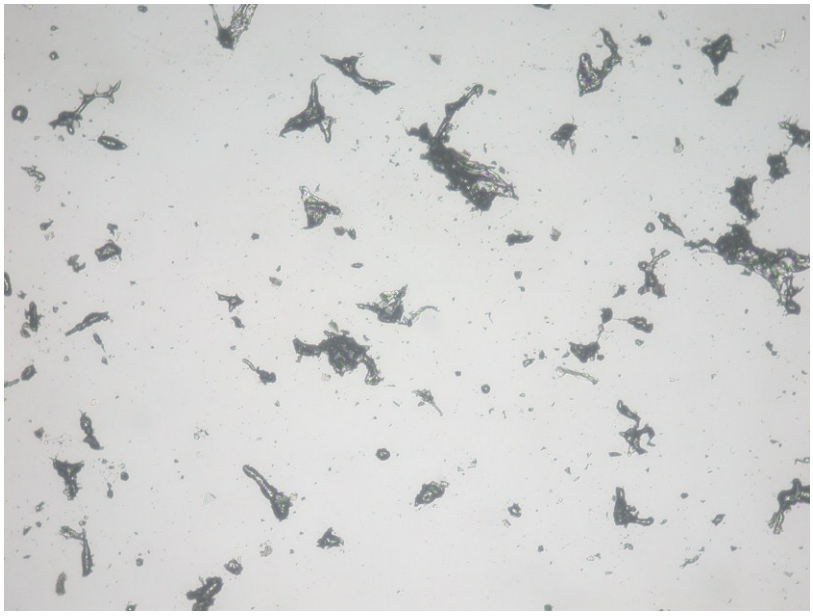

Figure 5.12: Broken up particulate of lyophilised chitosan nanoparticles, 4 x magnification

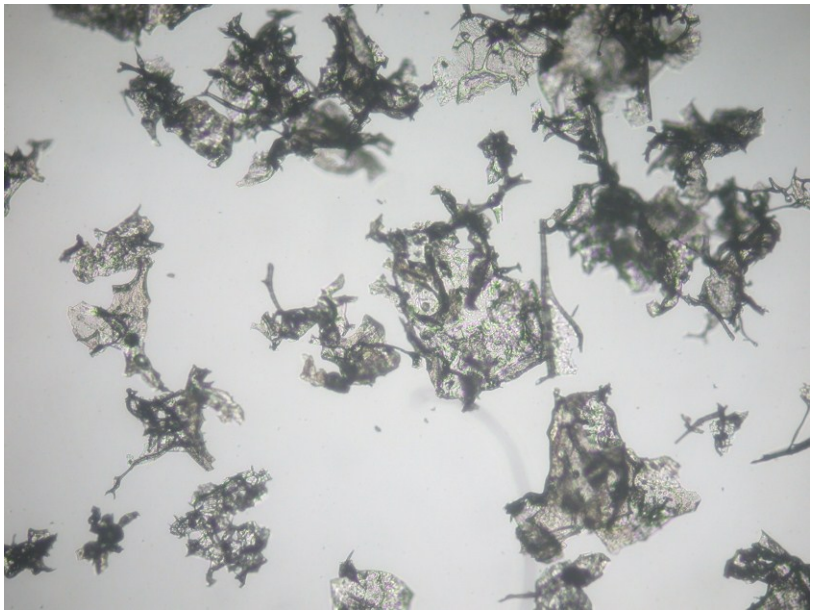

Figure 5.13: Broken up particulate of lyophilised chitosan nanoparticles, 20 x magnification

5.4 Adenosine Entrapment Results using UV Spectrometry

5.4.1 Internal Entrapment

Figure 5.14 summarizes the entrapment efficiency results from the incorporation of adenosine into chitosan –TPP nanoparticles by (i) loading adenosine into TPP solution prior to incorporation with chitosan solution and (ii) loading adenosine into chitosan solution prior to incorporation with TPP solution. It can be seen that the drug incorporation method has a weak influence on entrapment efficiency of adenosine into chitosan nanoparticles. The entrapment efficiency was 72.25 ± 7.42, 79.07 ± 1.58, and 77.98 ± 2.07 % when 16, 39, and 56 % (w/w) initial adenosine loading was first added to the TPP solution, respectively. Similarly, there was no significant change in the entrapment efficiency, 72.53 ± 3.77, 78.88 ± 1.541, and 77.24 ± 1.756 %, when 16, 39, and 56 %(w/w) initial adenosine loading was first added to the chitosan solution before being added to the TPP solution. The difference between the entrapment efficiency for both methods was not significant (t-test, two-tailed paired P=0.429). The first method of adding adenosine to the TPP was chosen for all following tests.

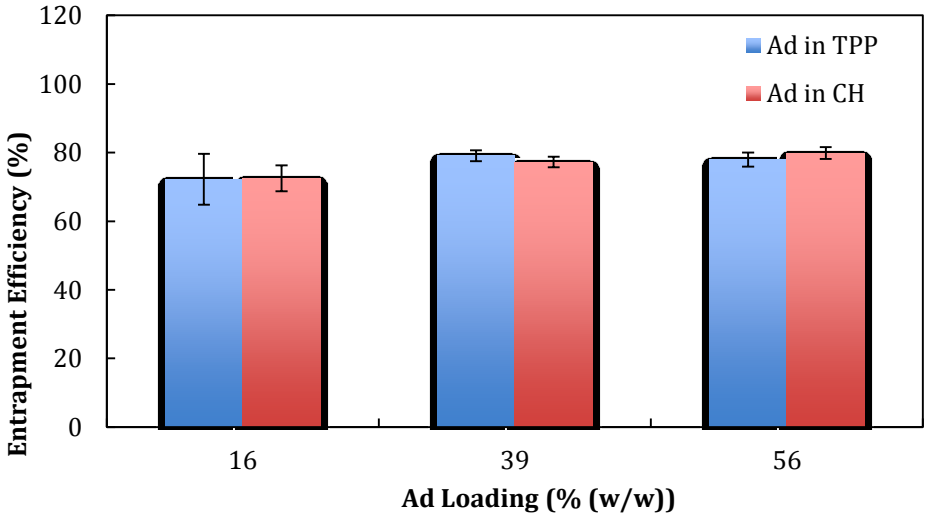

Figure 5.14: Ad entrapment efficiency, as varied with initial Ad loading. Mean ± standard deviation, n ≥ 20.

Adenosine concentration shows no remarkable influence on the entrapment efficiency of the particles. One reason for the entrapment efficiency not being affected by the initial adenosine loadings is that the nanoparticles have not reached their full potential for loading, they could carry more drug.

It was hypothesized that for the internal entrapment experiments, adenosine could become protonated when added to the chitosan, as the pH of the solution (around 3.35) was below the pKa of adenosine (which is 3.5). Being protonated, adenosine could be preferentially complex with the TPP, which would potentially decrease the entrapment efficiency. To test this, the pH of the chitosan solution was changed from 3.35 to 4.2 with sodium hydroxide prior to ionic gelation to see if this would increase drug incorporation into the chitosan matrix. By changing the pH of the chitosan solution to be above the pKa of adenosine, the adenosine would not be protonated when added to chitosan and not be complexed with TPP. The average entrapment efficiency determined by UV-spectrophotometer for 39 % (w/w) initial adenosine loading was 75.78 ± 1.99%. At 39 % (w/w) initial adenosine loading, the entrapment efficiency of chitosan nanoparticles with a pH change is not significantly different (Man-Whitney Rank Sum Test, P=0.065) to the entrapment efficiencies at the original pH (Figure 5.15). Thus the change in chitosan pH shows no remarkable influence on entrapment efficiency of the particles.

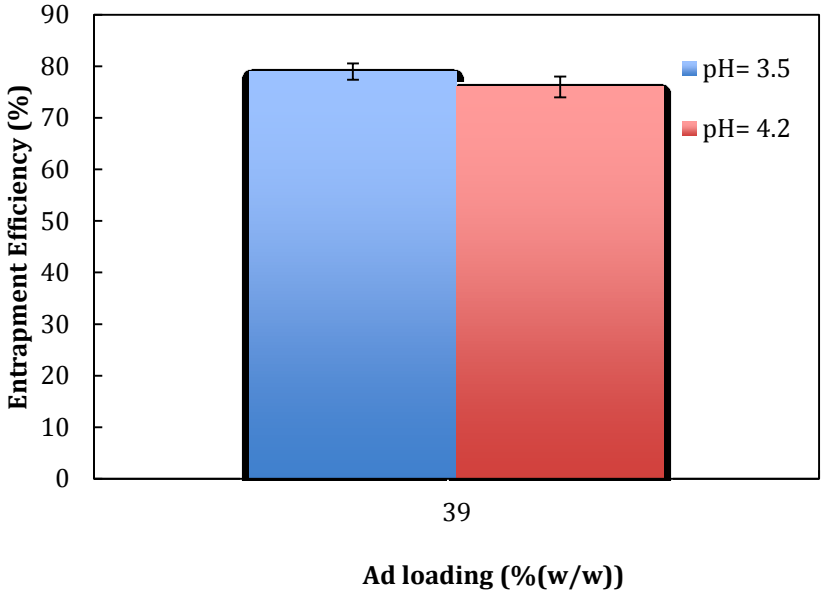

Figure 5.15: Comparison of Ad entrapment efficiency for 39 % (w/w) initial Ad loading at the original pH of 3.35 and new pH of 4.2. Mean ± standard deviation, n ≥ 5.

5.4.2 Surface Association

The average association efficiency for surface absorbed adenosine is 83.97 ± 3.28%. At 39 % (w/w) initial adenosine loading, the association efficiency is significantly greater (Mann-Whitney Rank Sum Test, P≤0.001) than the entrapment efficiency (Figure 5.16).

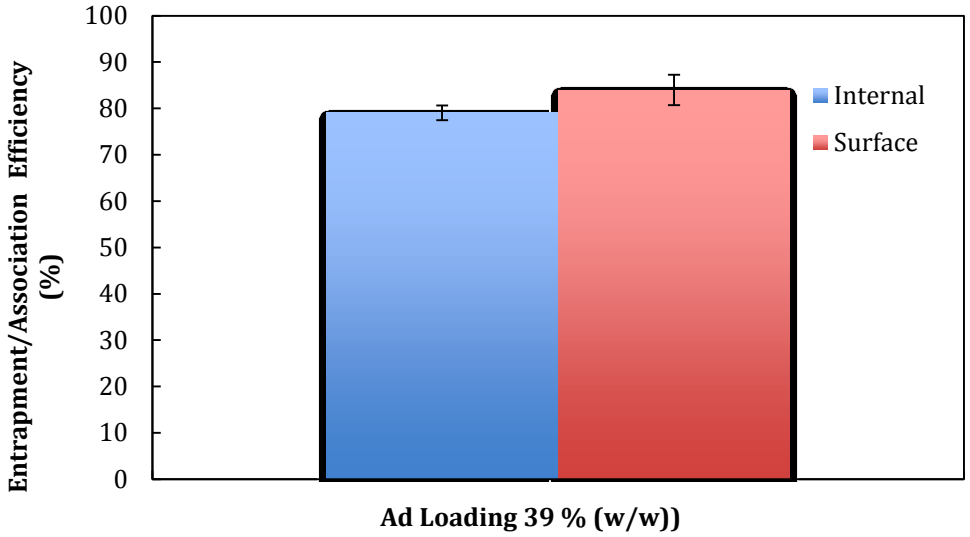

Figure 5.16: Ad entrapment efficiency compared to association efficiency for 39 %(w/w) initial Ad loading. Mean ± standard deviation, n ≥ 15.

5.5 Adenosine Entrapment Results using Solid State NMR

Solid-state nuclear magnetic resonance was employed to confirm the entrapment/association efficiencies calculated using data from the UV-spectrophotometer and to validate the UV-spectrophotometer results which indicate that adenosine is entrapped within the chitson-TPP nanoparticles. SsNMR spectrometry differs from UV spectrometry as it is founded on the absorption of electromagnetic radiation by nuclei (generally protons) rather than the absorption of the wavelength of light. NMR spectra plots (radio frequency applied vs. absorption) display the characteristic chemical shifts (i.e. absorption frequencies) of hydrogen atoms from different functional groups. These chemical shifts allow the functional groups present in a molecule to be known as well as its structure. The nuclear spin of the hydrogen atoms produces a magnetic field effects the chemical shift of adjacent hydrogen atoms.

The acquisition and interpretation of the NMR data was performed by Dr. Ulrike Werner-Zwanziger from the Nuclear Magnetic Resonance Resource Center at Dalhousie University. An experimental spectrum of pure adenosine (Figure 5.20) was measured to determine the positions of the peaks. The peaks of this spectrum will be compared to the drug loaded chitosan

nanoparticle spectrums to identify if adenosine is present. The frequency prediction spectrum in Figure 5.18 matches reasonably well with the experimental peak positions of the adenosine spectrum. This permits the assignment of the resonances to the carbon nuclei. Though, it is important to note the predicted resonances for 156 and 153 ppm are not set under the experimental peak at 154 ppm. There are actually two lines under the resonance peak as shown by a shoulder to the high ppm side.

Figure 5.22 will be used for the experimental spectrum of chitosan and will be compared to the drug loaded chitosan nanoparticle spectrums to determine which peaks belong to chitosan. The chitosan spectrum peaks at 60 and 62 ppm correspond to carbons 3 and 13, the peak at 72 ppm correspond to the alcoholic carbons 4,5 and 6, while the peak at 92 ppm corresponds to the acetal carbon. A figure of the chitosan structure with the carbon positions numbered can be found below in Figure 5.17. Figure 5.19 allows a comparison between adenosine and the chitosan containing nanoparticles. The unsaturated ring carbons of the adenosine are in the aromatic range of 199-154 ppm resonate outside the frequency of the chitosan peaks. As well the substituted aliphatic region from 92-60 ppm of chitosan do not overlap the adenosine resonance at 84.5 ppm. This information allows the identification of the presence of adenosine in the chitosan matrix.

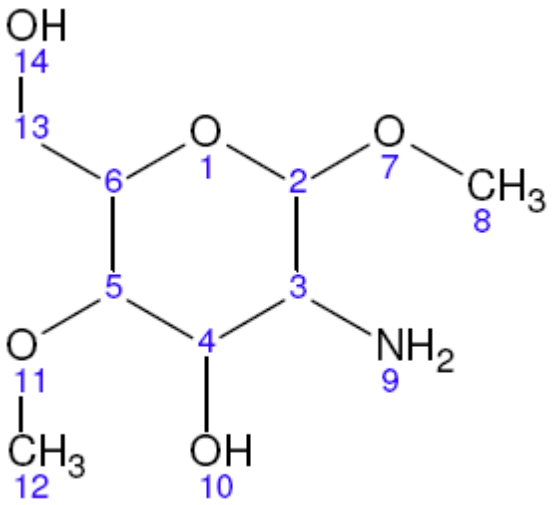

Figure 5.17: : Structure of chitosan with the position of carbon atoms numbered

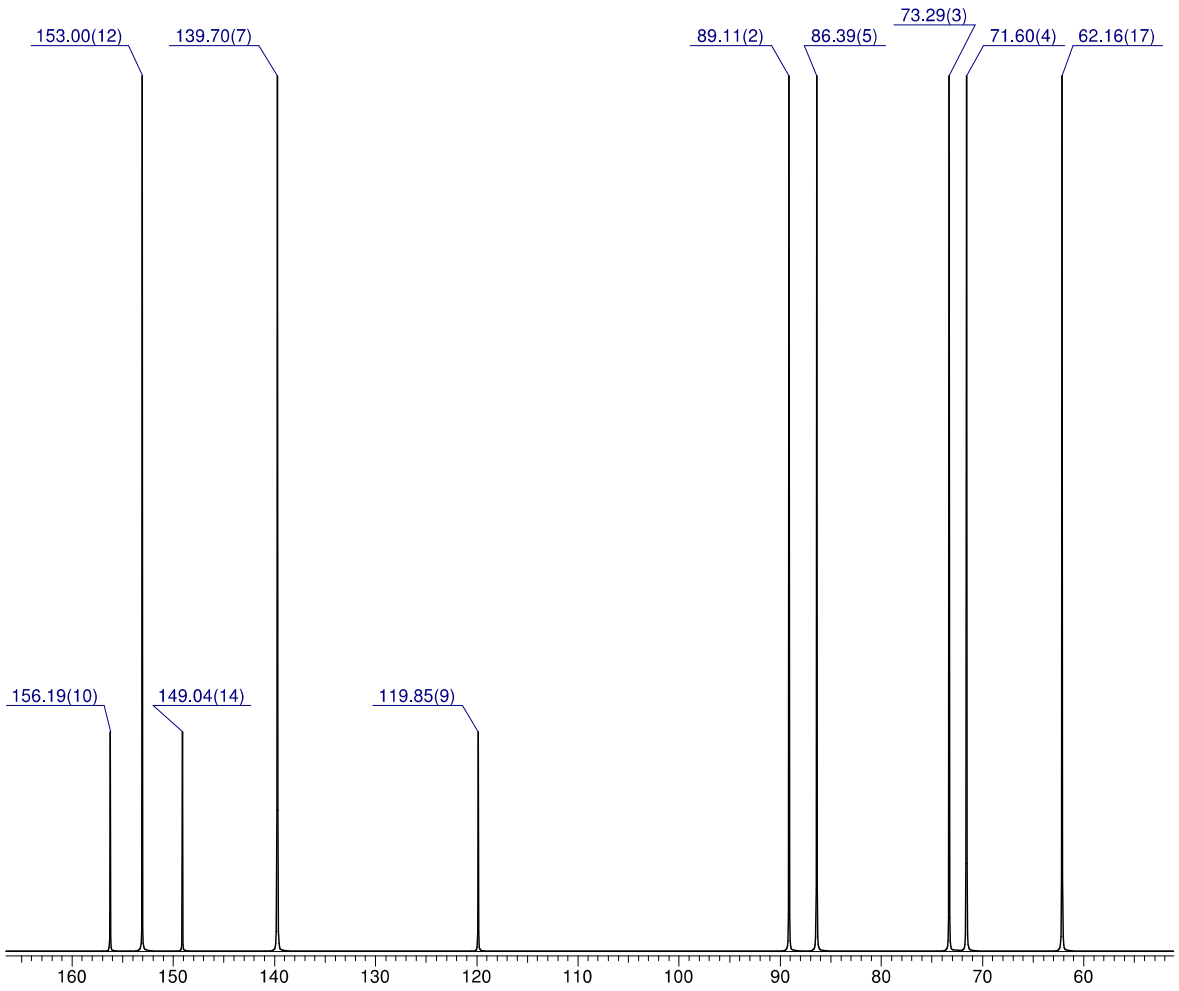

Figure 5.18: Computer (ACD) simulated spectrum of adenosine

5.5.1 Internal Entrapment

The results of the NMR ^{13}C experiments for internally entrapped adenosine chitosan-TPP nanoparticles are given in Figures 5.19- 5.24. A comparison amongst the various ^{13}C NMR spectra is displayed below in Figure 5.19 whereas Figure 5.20-5.24 gives the single ^{13}C NMR spectra with experimental parameters and peak positions. The ^{13}C spectra of the chitosan compounds (Figures 5.21-5.23) are identical and show no appreciable amounts of adenosine.

This is surprising, as the ssNMR result from entrapment of adenosine in chitosan-TPP nanoparticles (Figures 5.23) differ from the UV spectrophotometric results that show incorporation of adenosine in the nanoparticles, as discussed in section 5.4. Even the chitosan samples prepared with adenosine do not show as much as a weak adenosine resonance. Therefore, the ssNMR indicates that adenosine is not incorporated into the material to a significant amount (i.e., less than 2% molar). The only features shown are that of chitosan, specifically the resonances at 92.3 ppm, 72.1 ppm and the group around 60.6 ppm. While the supernatant from the internally entrapped adenosine nanoparticles include both chitosan and adenosine, it cannot be concluded from the spectra (Figure 5.24) whether this is a heterogeneous mixture freeze-dried together or actual bonding.

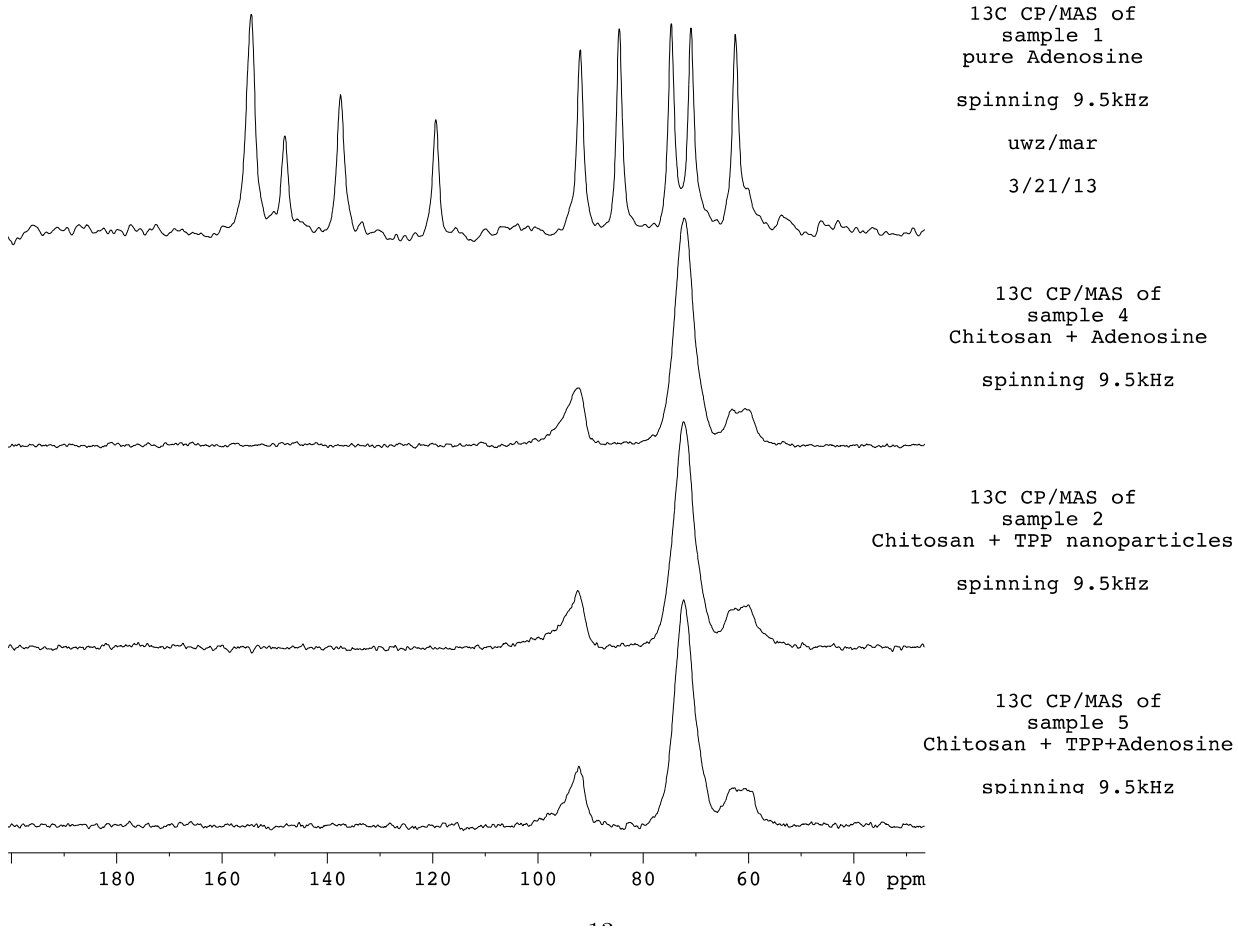

Figure 5.19: Comparison of the ^{13}C CP/MAS NMR spectra of adenosine (top) followed by chitosan and adenosine, blank chitosan-TPP nanoparticles and adenosine loaded chitosan-TPP nanoparticles (bottom).

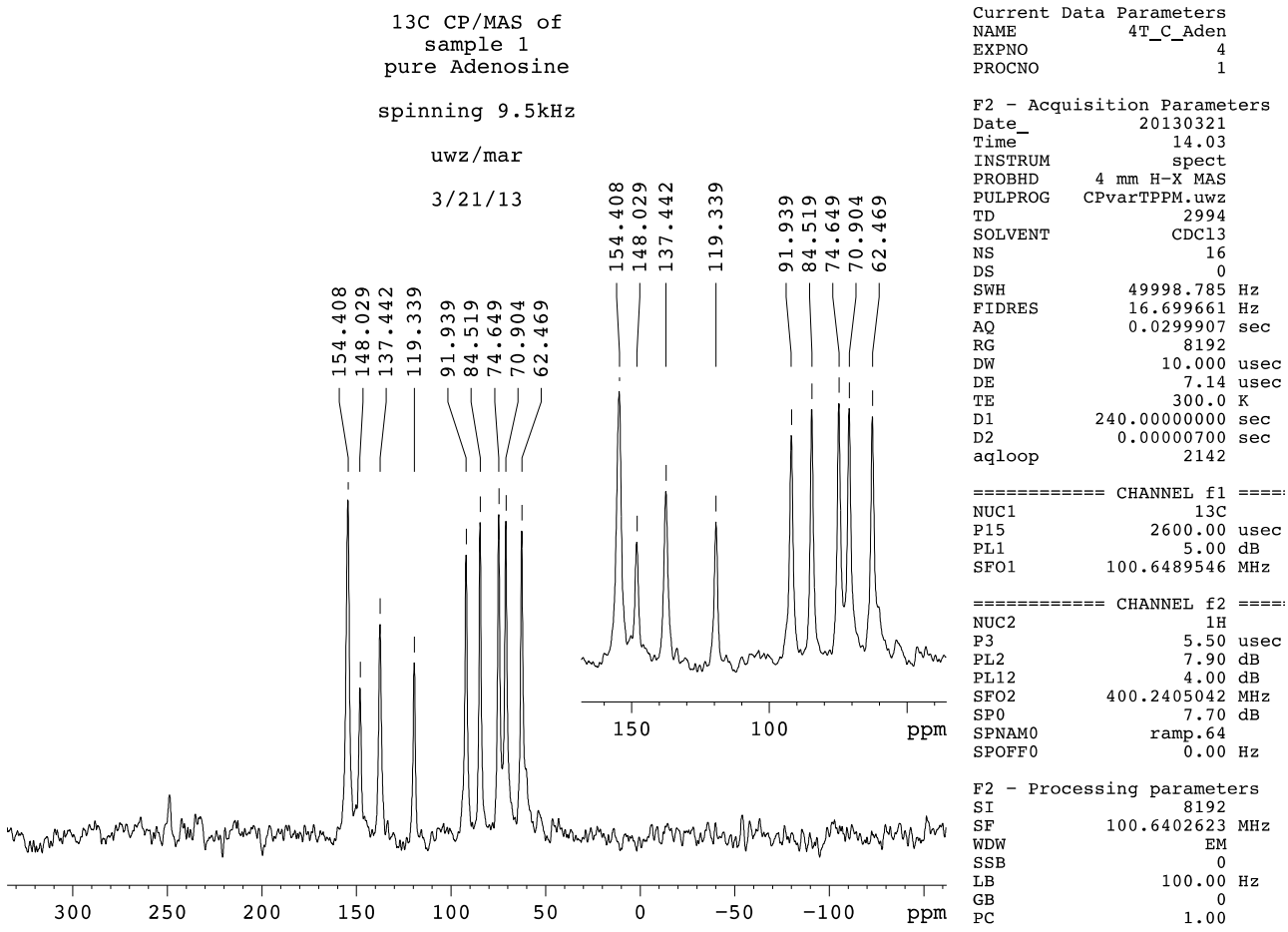

Figure 5.20: ^{13}C CP/MAS NMR spectra of pure adenosine powder

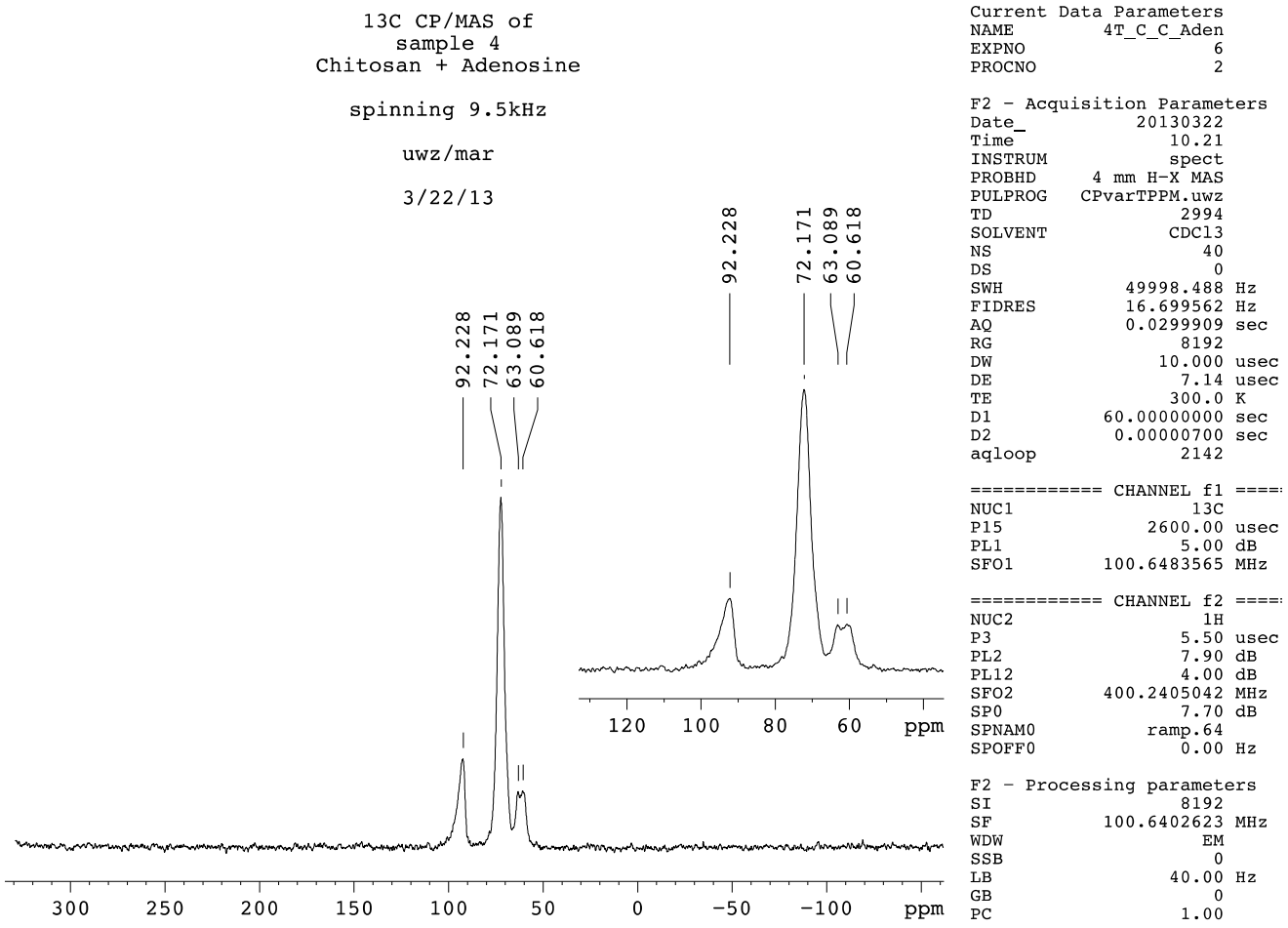

Figure 5.21: ^{13}C CP/MAS NMR spectra of chitosan mixed with adenosine solution then centrifuged

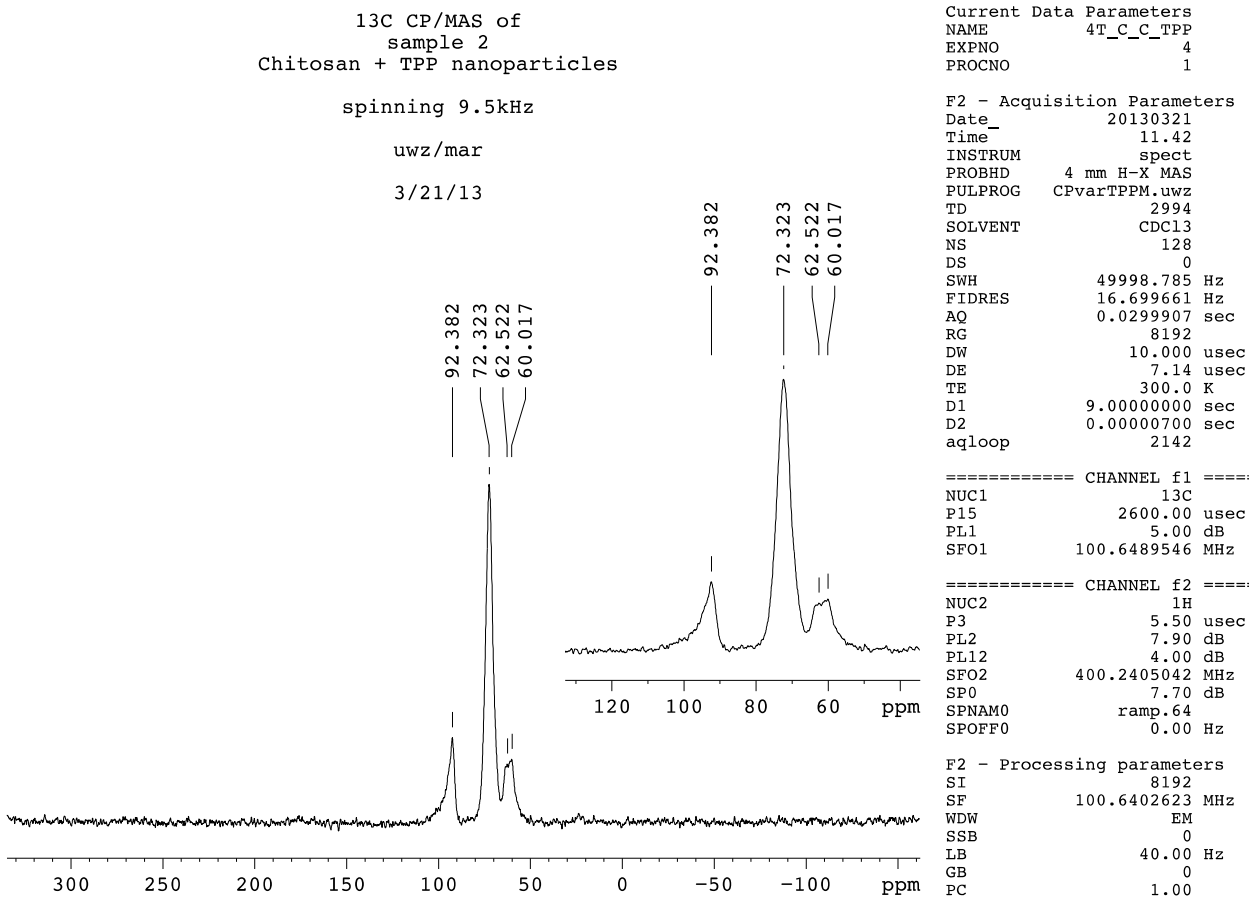

Figure 5.22: ^{13}C CP/MAS NMR spectra of chitosan-TPP nanoparticles with no adenosine

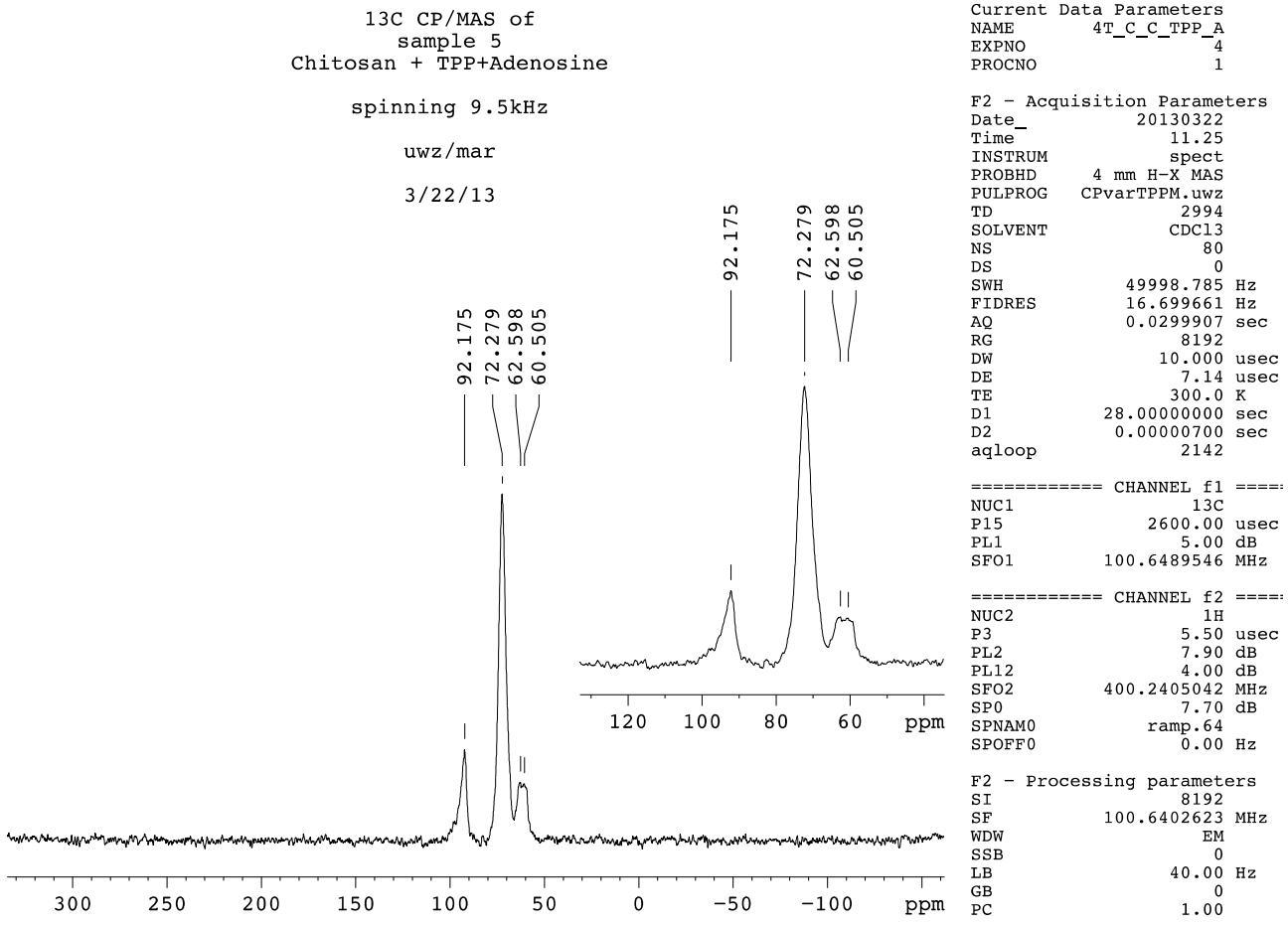

Figure 5.23: ^{13}C CP/MAS NMR spectra of adenosine entrapped chitosan-TPP nanoparticles

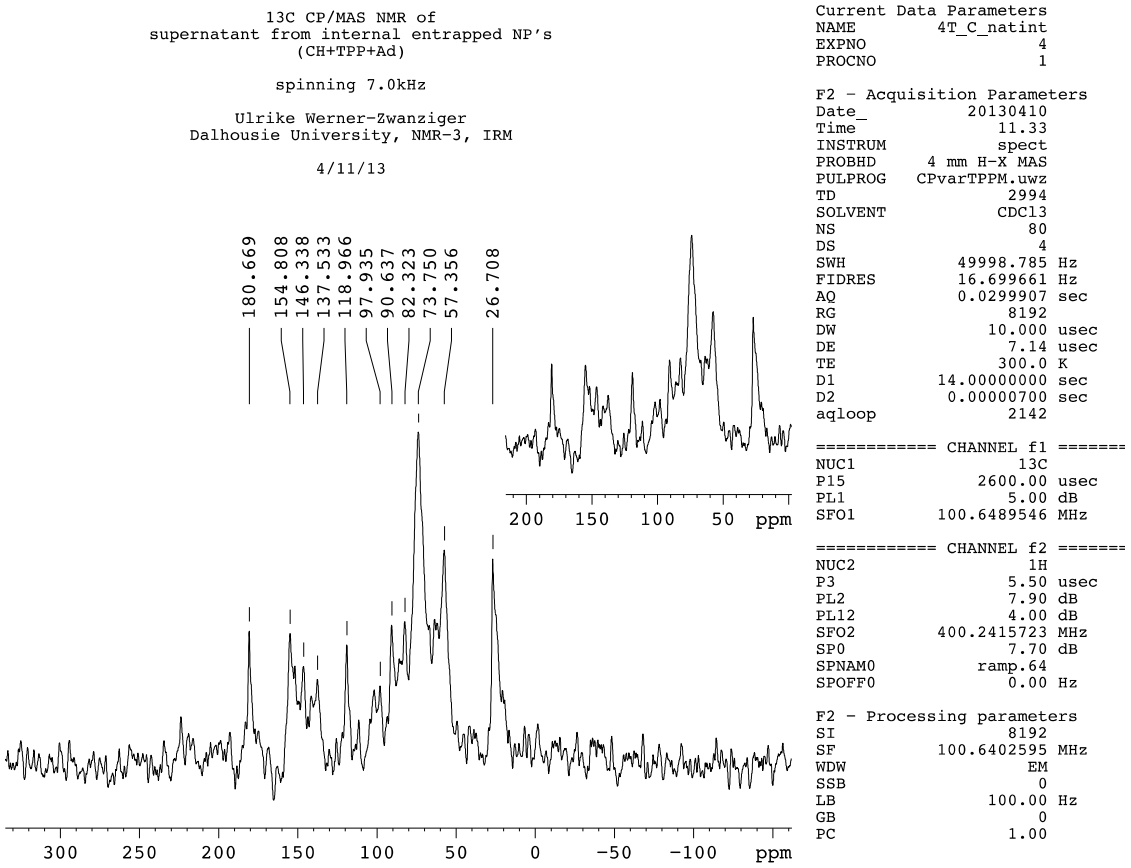

Figure 5.24: ^{13}C CP/MAS NMR spectra of supernatant from adenosine entrapped chitosan-TPP nanoparticles

To determine, whether the samples prepared with TPP did indeed contain TPP, a ^{31}P NMR spectra was acquired to check for the presence of phosphorous. The results from the NMR ^{31}P experiments are given in Figures 5.25- 5.28. Figure 5.25 displays a comparison amongst the different ^{31}P NMR spectra. Figure 5.26 allow for the distinction between isotopic peaks and spinning side bands to be made by comparing spinning speeds. While Figures 5.27 and 5.28 give the experimental parameters and peak positions for individual ^{31}P NMR spectra. The spectra of the two TPP containing nanoparticle samples do show some signal of the presence of phosphorous but the total quantity appears to be low (Figure 5.25). The amount of TPP appears to be especially low in the adenosine loaded chitosan nanoparticles (Figure 5.28). This amount cannot be quantified, as this test is only qualitative.

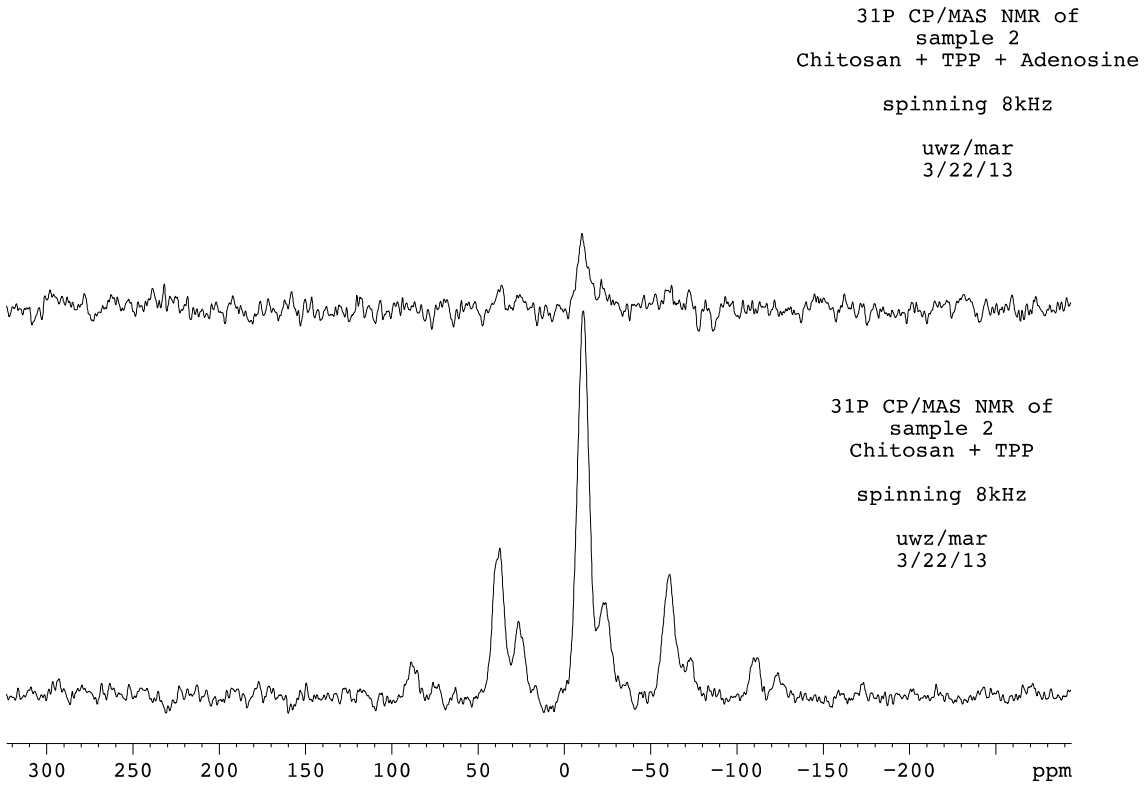

Figure 5.25: Comparison of the ^{31}P CP/MAS NMR spectra of the two compounds containing TPP: adenosine loaded chitosan-TPP nanoparticles (top) and the blank chitosan-TPP nanoparticles

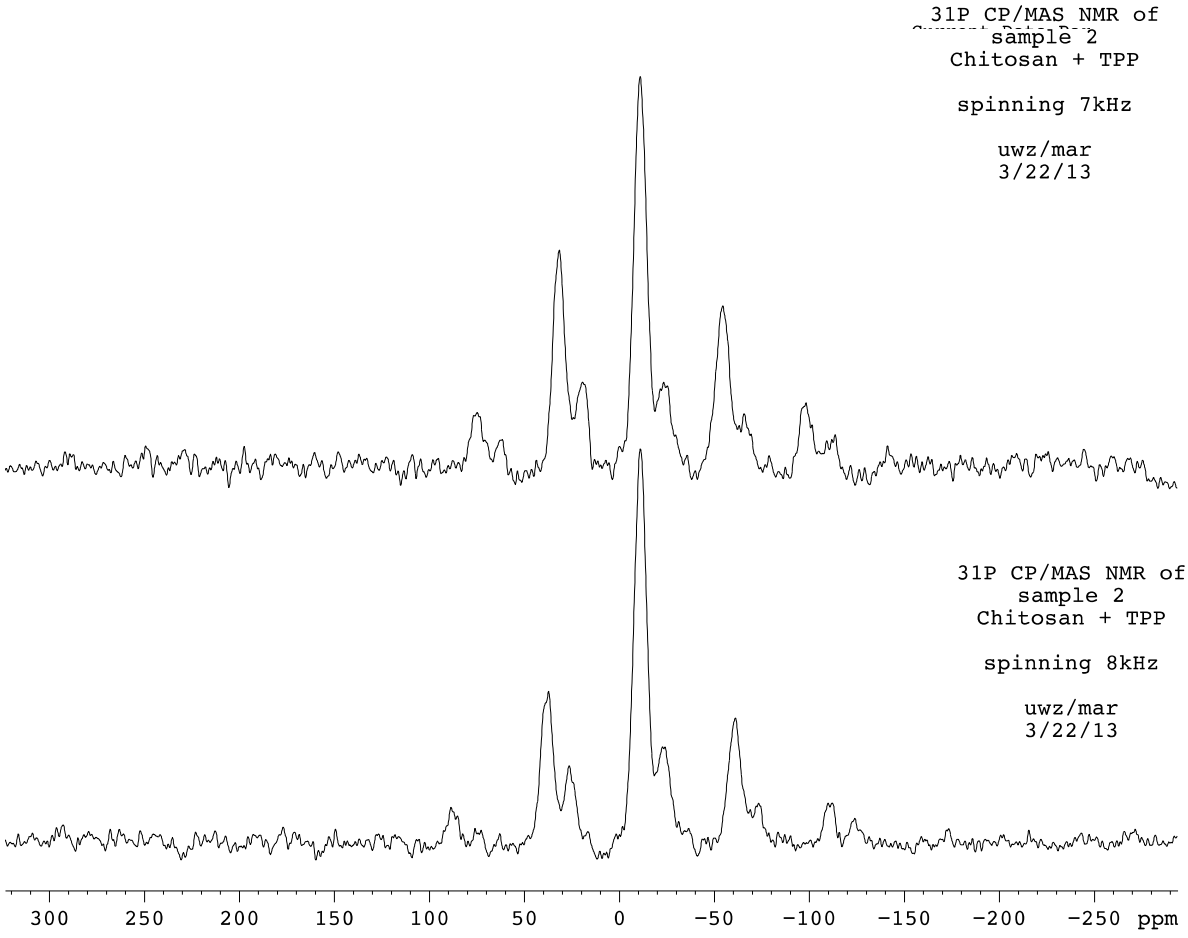

Figure 5.26: Spinning speed comparison on the blank chitosan nanoparticles to determine the distinction between isotopic peaks and spinning side bands

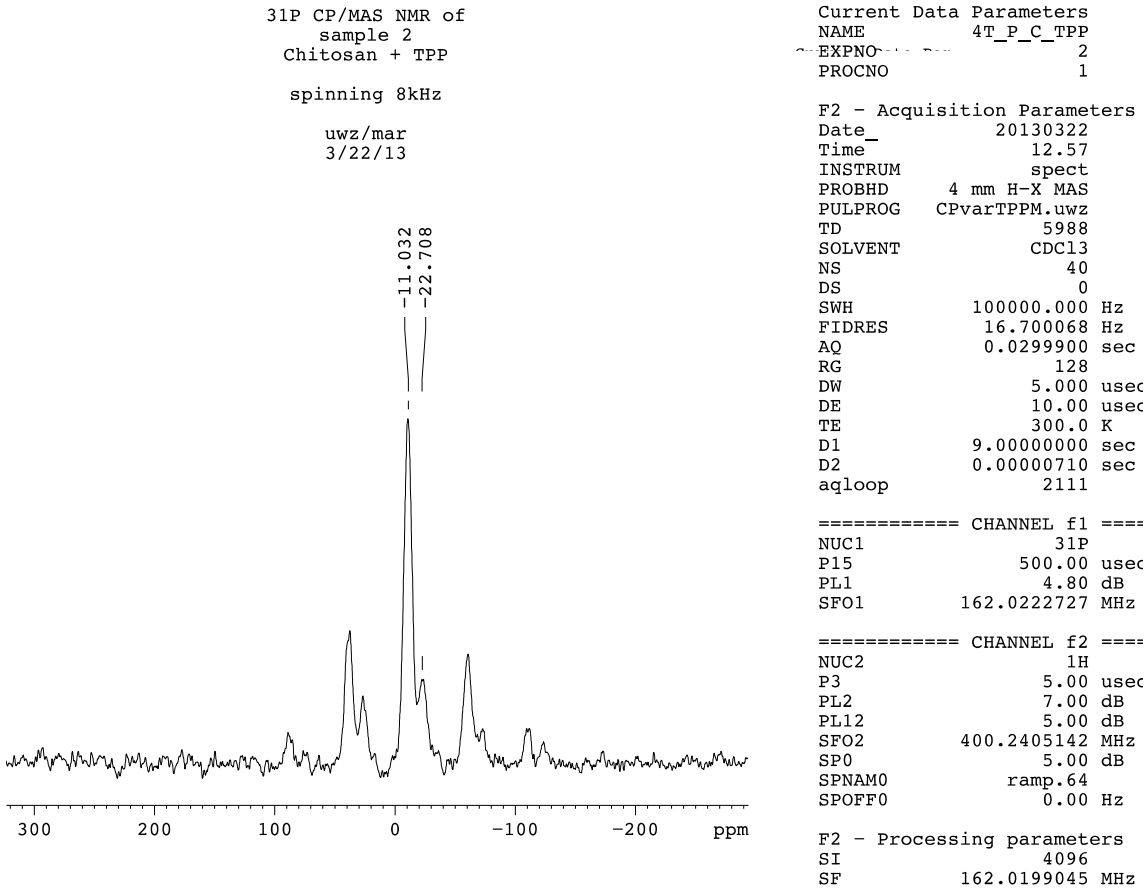

Figure 5.27: ^{31}P CP/MAS NMR spectra of blank loaded chitosan-TPP nanoparticles

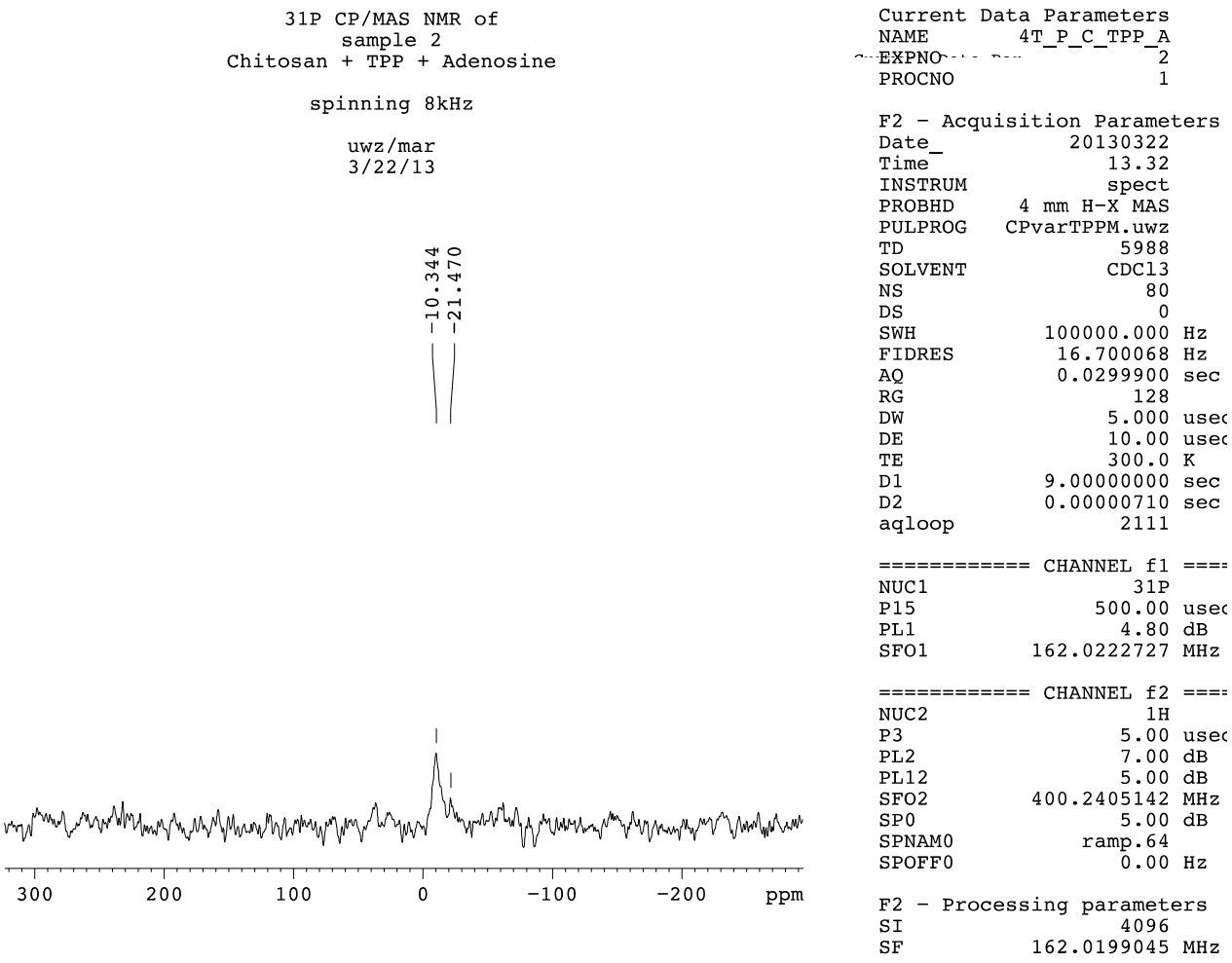

Figure 5.28: ^{31}P CP/MAS NMR spectra of adenosine loaded chitosan-TPP nanoparticles

5.5.2 Surface Association

The ^{13}C spectra for adenosine associated chitosan-TPP nanoparticles (Figures 5.29) show no appreciable amounts of adenosine, comparable to the results obtained from the ^{13}C spectra of the chitosan compounds containing adenosine. The ssNMR result from the association of adenosine to chitosan-TPP nanoparticles differ from the UV spectrophotometric results that show association of adenosine to the nanoparticles, as discussed in section 5.4. Consequently, the ssNMR implies that adenosine is not associated into the material to a significant amount (i.e., less than 2% molar).

. Adenosine is retained in the supernatant from the surface entrapped nanoparticles, as all the peaks found in this sample are also present in the adenosine spectrum (Figure 5.26).

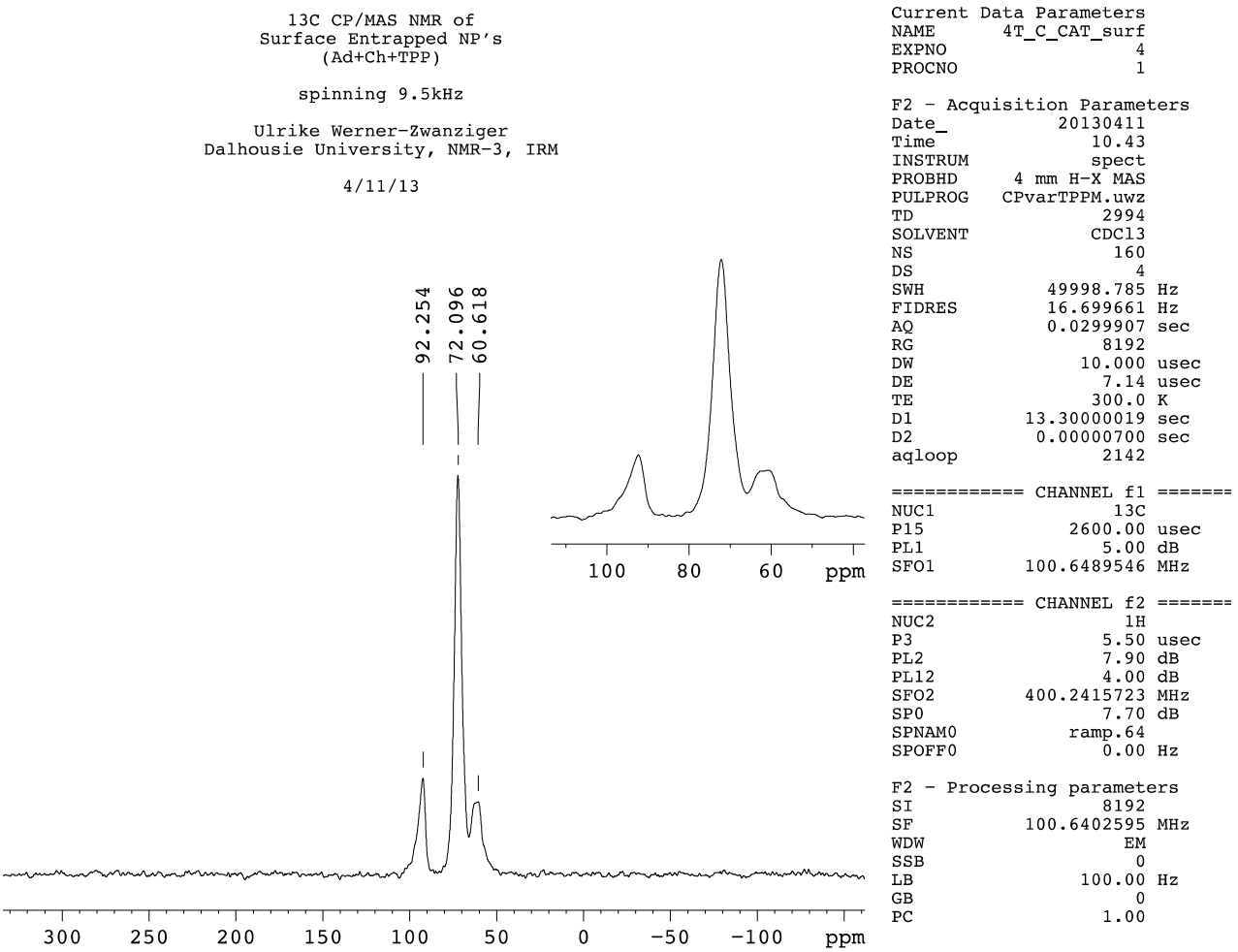

Figure 5.29: ^{13}C CP/MAS NMR spectra of adenosine absorbed onto surface of chitosan-TTP nanoparticles

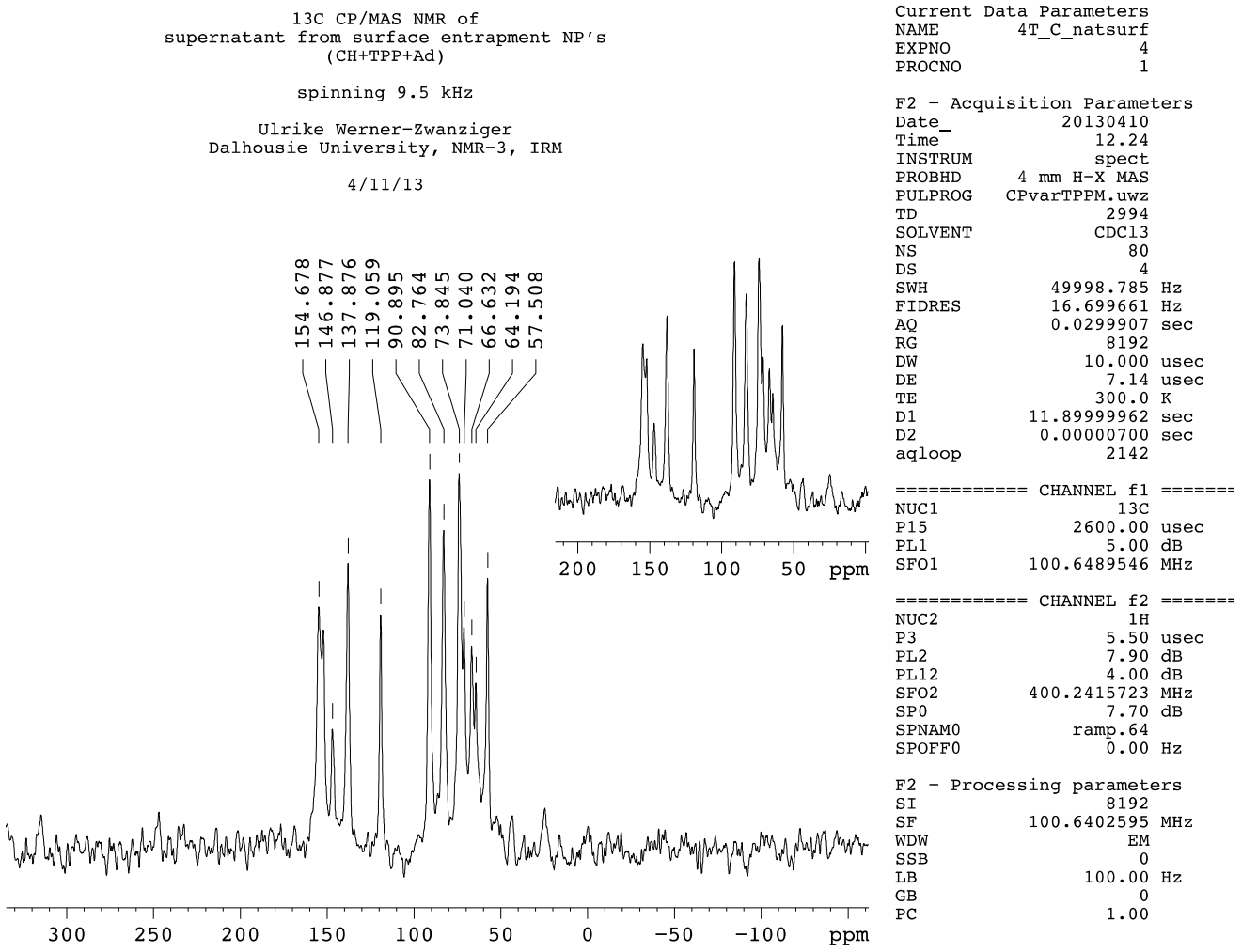

Figure 5.30: ^{13}C CP/MAS NMR spectra of supernatant from adenosine absorbed onto the surface of chitosan-TPP nanoparticles

5.6 Adenosine Entrapment Results using Liquid State NMR

Liquid state NMR (qNMR) was performed to confirm either the UV-spectrophotometer or ssNMR findings for adenosine entrapment in the nanoparticles. Liquid and solid state NMR spectra differ in the appearance and information of the content. In liquid state NMR a sharp line is observed for each nucleus as molecular tumbling averages out orientation-dependent

interactions. The resultant line widths for ssNMR are at least ten times wider than that of liquid state. This is a result of observing the distribution frequencies for every nucleus and not averaging out each samples orientation-dependent interaction. Solid state NMR distribution echoes the bond orientations distribution comparative to the magnetic field for that type of nucleus (Yang et al., 2001). Solid state NMR is reliant on ^{13}C isotopic labeling and provides data on the structure or motion in the area of the labeled nuclei.

Chemical shifts were used to determine the amount adenosine in the supernatant. The chemical shifts were represented in parts per million (ppm) and can be calibrated via the internal standard $DMSO_2$. The resultant spectrums of the qNMR experiments can be found in Appendix D. The concentrations of adenosine that were acquired from the qNMR measurements were calibrated using the appropriate calibration curve equation in order to convert the readings to be comparable to the prepared weighed amounts of adenosine (Appendix D). The average entrapment efficiency determined by qNMR for 39 % (w/w) initial adenosine loading was 76.73 ± 9.44 % at a pH of 3.35 and 67.72 ± 5.54 at a pH of 4.2. At 39 % (w/w) initial adenosine loading, the entrapment efficiency of chitosan nanoparticles with a pH change from 3.35 to 4.2 is statistically significant (Mann-Whitney Rank Sum Test, P=0.002). These results differ from the results discussed in section 5.4.1 (Figure 5.31) where the entrapment efficiency of chitosan nanoparticles with a pH change from 3.35 to 4.2 was not significantly different. Here, a change in chitosan pH shows little influence on entrapment efficiency of the particles.

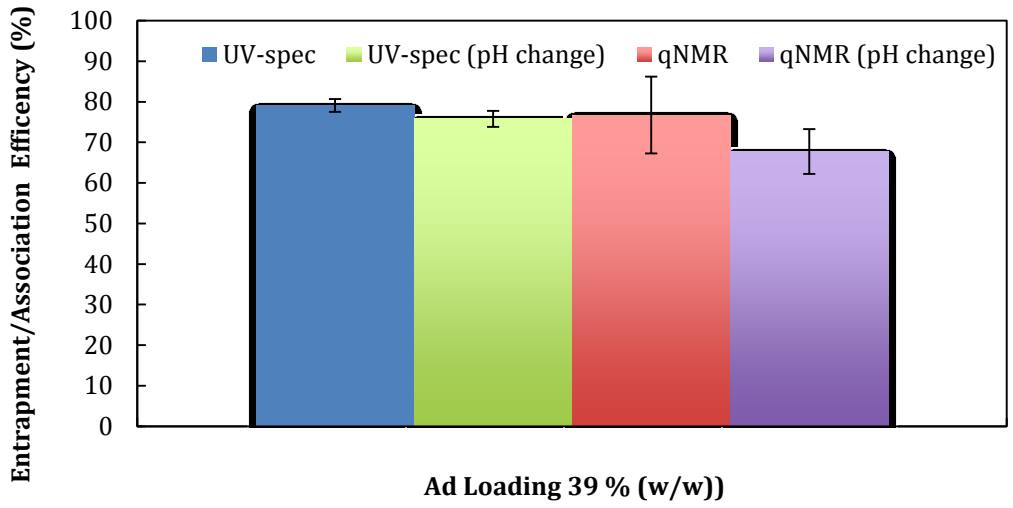

Figure 5.31: Comparison of Ad entrapment efficiency calculated from UV-spectrophotometry and qNMR for 39 %(w/w) initial Ad loading. Mean ± standard deviation, n ≥ 3.

When compared to the UV-spectrophotometer results the qNMR findings are comparable. Both methods for measuring entrapment efficiency confirm a decrease in entrapment efficiency when the pH of the chitosan solution is raised from 3.35 to 4.2. Both entrapment efficiencies calculated at the original pH of 3.35 using UV-spectrophotometry and qNMR are nearly equivalent with the UV-spectrophotometer results being slightly greater. Whereas, the entrapment efficiency calculated using qNMR with a pH change to 4.2 is lower than that calculated from UV-spectrophotometry, nonetheless they are in the same range (Figure 5.31).

The results from ssNMR differ a great deal from those obtained from qNMR and UV-spectrophotometry. The results from qNMR and UV-spectrophotometry agree with each other, both claim that over 70% of adenosine was incorporated into the chitosan matrix. In contrast, according to ssNMR spectra there is no drug present in the chitosan matrix. There are constraints that need to be overcome for ssNMR; the most vital is low sensitivity. According to Yang and coworkers (2001) samples must contain 0.5 mmol of material at a concentration of 1 mM. The samples in this research prepared for ssNMR contained 0.067 mmol of adenosine and 0.032 mmol of TPP. Due to the sensitivity of Bruker Avance 400, the low amount of adenosine and TPP present in the samples were not detected. This explains why the spectrums acquired via

ssNMR conclude that no adenosine was entrapped into the chitosan nanoparticles when there is over 70% of the drug incorporated into the chitosan matrix.

5.7 Drug Release

Prior to release studies, the stability of diluted adenosine solutions in deionized water and Phosphate Buffer Solution (PBS) at room temperature was studied. Samples were prepared in triplicate by diluting a stock solution of adenosine to various concentrations with either PBS or deionized water. The samples were assayed using UV-spectrophotometrics directly after preparation (time zero) and each 24 hour time interval for up to 7 days. All measurements were done in triplicate. An equation formulated from a calibration curve of standards was used to calculate the concentrations. Visual inspection was also executed to monitor clarity, color, and the presence of crystalline particulate matter. Stability was defined as retaining at least 90% of the initial adenosine concentration. All samples retained greater than 97% of the starting adenosine concentration after 7 days, with no indication of detectible precipitation signifying negligible loss of adenosine owed to degradation (Appendix F).

In vitro release studies of the adenosine from loaded chitosan-TPP nanoparticles were then performed, with the aim of investigating the ability of these delivery systems to release the entrapped and associated adenosine over time. The *in vitro* release of adenosine from the nanoparticles was measured over a 5 day period in PBS at a pH of 7.4 to characterize features of the nanoparticle release mechanism as described in section 4.7.2. This study of adenosine being released from nanoparticles is significant as it gives an indication of the degree of the drug release and the time at which it takes to occur. The concentration of adenosine in the release medium is measured to detect the drug released over a time period. It was postulated that the drug release of the adenosine loaded chitosan-TPP nanoparticles *in vitro* would happen over two phases. The first phase would show a rapid initial burst due to the diffusion of adenosine molecules close to the surface of the matrix into solution, and then followed by a slow drug release during the plateau phase. In the second phase the release of adenosine would increase when the chitosan matrix begins to degrade.

Table 5.2: Release data of Ad from chitosan nanoparticles, as varied with initial Ad loading. Mean ± standard deviation, n ≥ 5.

Adenosine loading (%(w/w))	Average mass of adenosine entrapped/ associated (mg)	Average accumulative mass of adenosine released (mg)
16	1.63 ± 0.17	0.342 ± 0.006
39	17.84 ± 0.34	0.121 ± 0.001
56	35.09 ± 0.93	0.321 ± 0.050
39 (Surface)	17.73 ± 0.33	0.214 ± 0.010
39 (Free drug)	22.5	1.229 ± 0.063

The release profiles from chitosan nanoparticles varied with initial Ad loading are shown in Figures 5.32-5.37 and the accumulative mass of adenosine released for each drug loading is presented in Table 5.2. It was apparent by looking at the trend in the release profiles that adenosine released from the internal entrapped nanoparticles agreed with the postulated initial burst followed by the plateau phase. However, no second phase of drug release transpired. The initial burst was a result of drug being released that was on surface of the particle and not entrapped into the chitosan matrix. Looking thoroughly at the quantities in the release profile it can be established that little adenosine was released over the 120 hours. The cumulative average release of adenosine was 21.06 ± 0.0062%, 0.6909 ± 0.0005%, and 0.9139 ± 0.0499% for 16, 39 and 56 %(w/w) initial Ad loading, respectively.

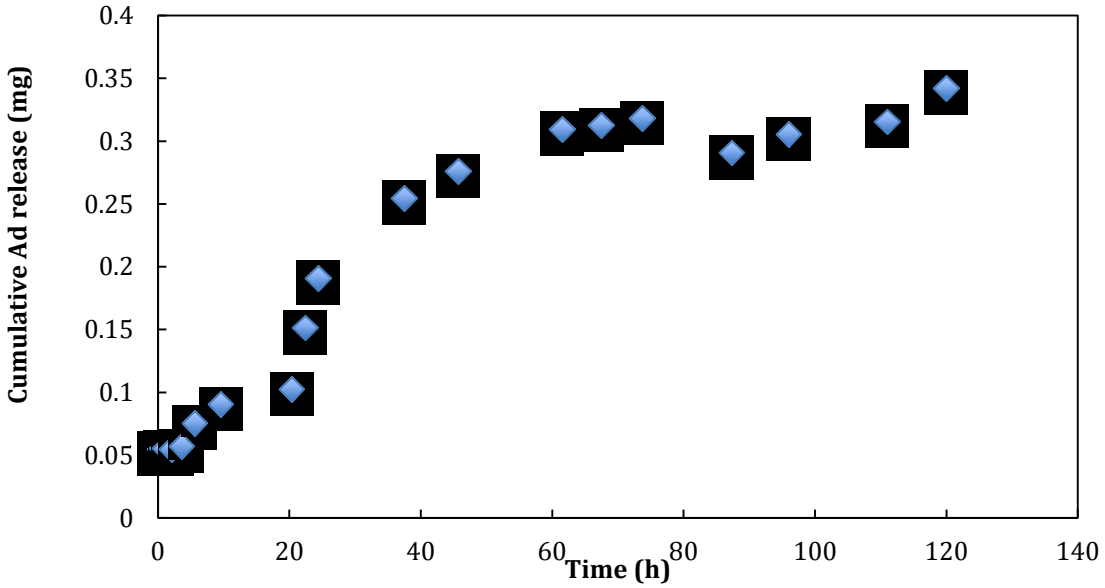

Figure 5.32: Release of Ad from 16% initial Ad loading entrapped nanoparticles into PBS, pH 7.4. Mean ± standard deviation, n ≥ 5.

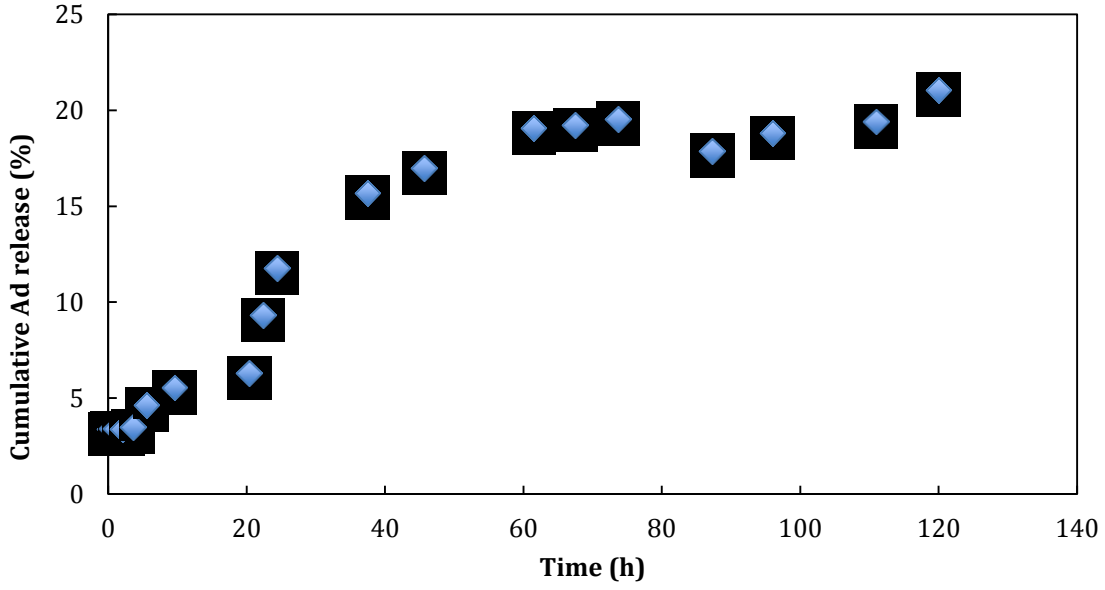

Figure 5.33: Release of Ad from 16% initial Ad loading entrapped nanoparticles into PBS, pH 7.4. Mean ± standard deviation, n ≥ 5.

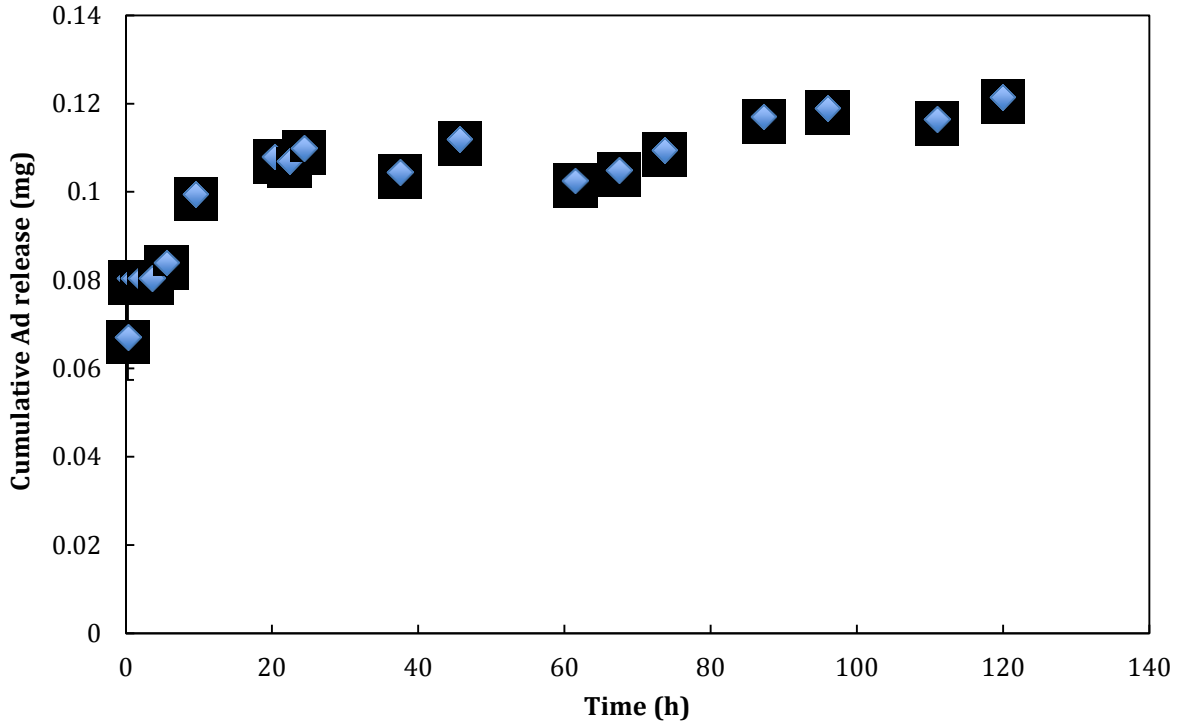

Figure 5.34: Release of Ad from 39% initial Ad loading entrapped nanoparticles into PBS, pH 7.4. Mean ± standard deviation, n ≥ 5.

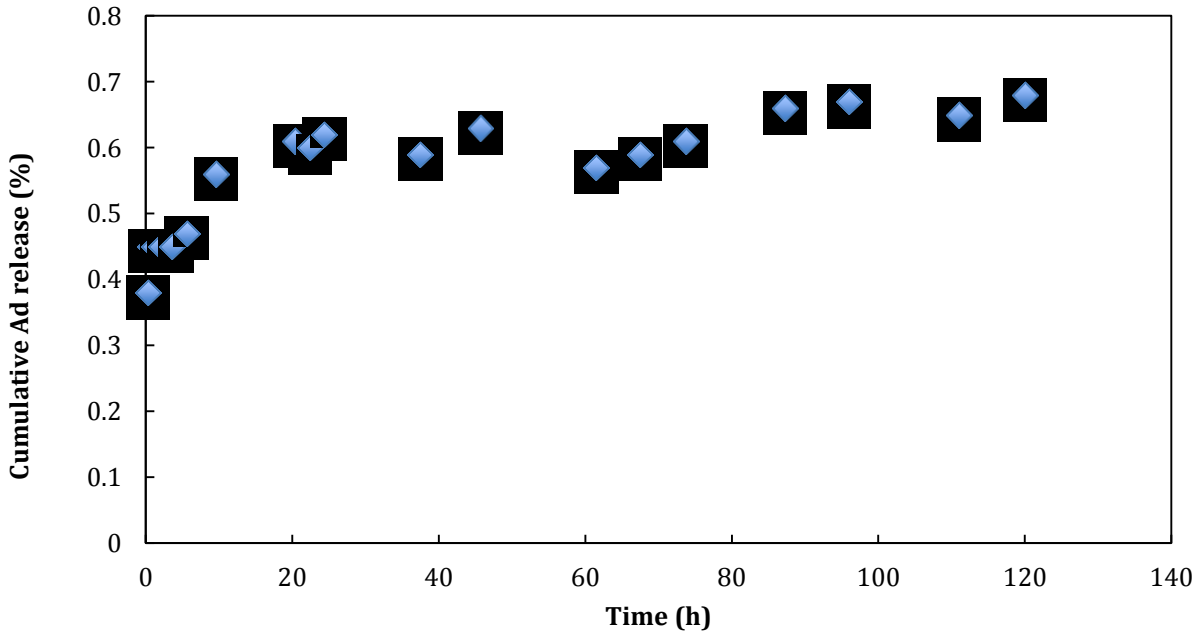

Figure 5.35: Release of Ad from 39% initial Ad loading entrapped nanoparticles into PBS, pH 7.4. Mean ± standard deviation, n ≥ 5.

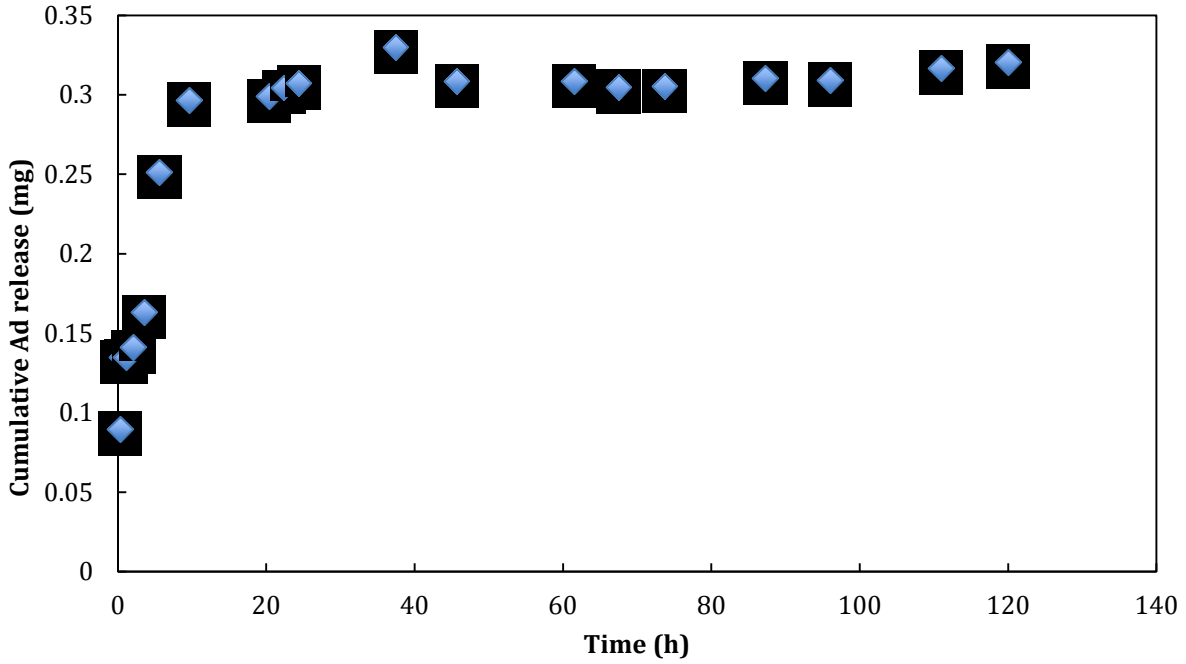

Figure 5.36: Release of Ad from 56% initial Ad loading entrapped nanoparticles into PBS, pH 7.4. Mean ± standard deviation, n ≥ 5.

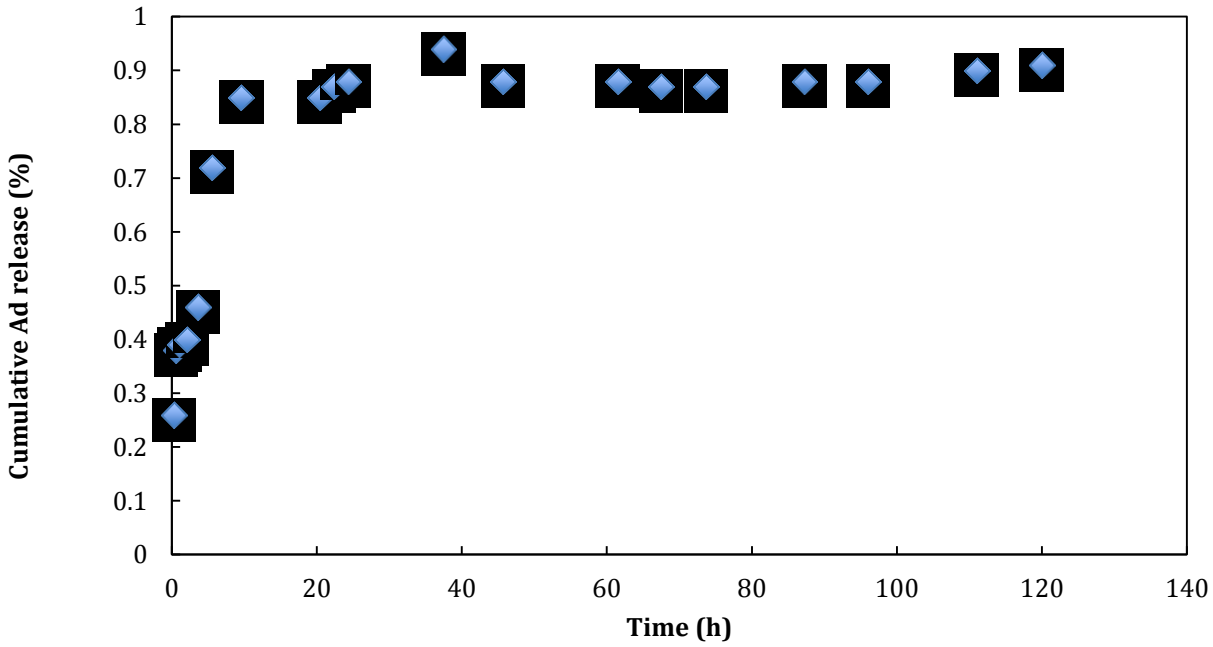

Figure 5.37: Release of Ad from 56% initial Ad loading entrapped nanoparticles into PBS, pH 7.4. Mean ± standard deviation, n ≥ 5.

The release profiles of adenosine surface associated nanoparticles (Figures 5.38 and 5.39) in PBS were similar to those for the internal entrapped nanoparticles. For the 39 %(w/w) associated adenosine nanoparticles about 1 ± 0.0163 % of drug was released during the first hour, and the release amount reached the maximum at 72 hours. The cumulative release of adenosine from surface associated adenosine nanoparticles was about 1.14 ± 0.0098 %.

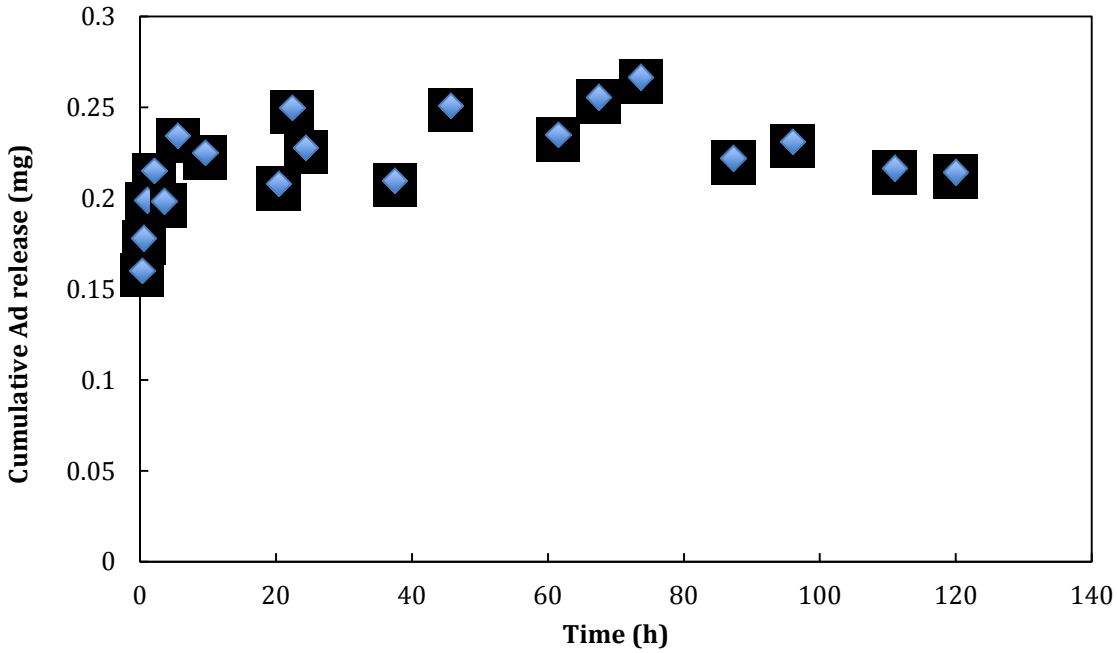

Figure 5.38: Release of Ad from 39% initial Ad loading associated nanoparticles into PBS, pH 7.4. Mean ± standard deviation, n ≥ 5.

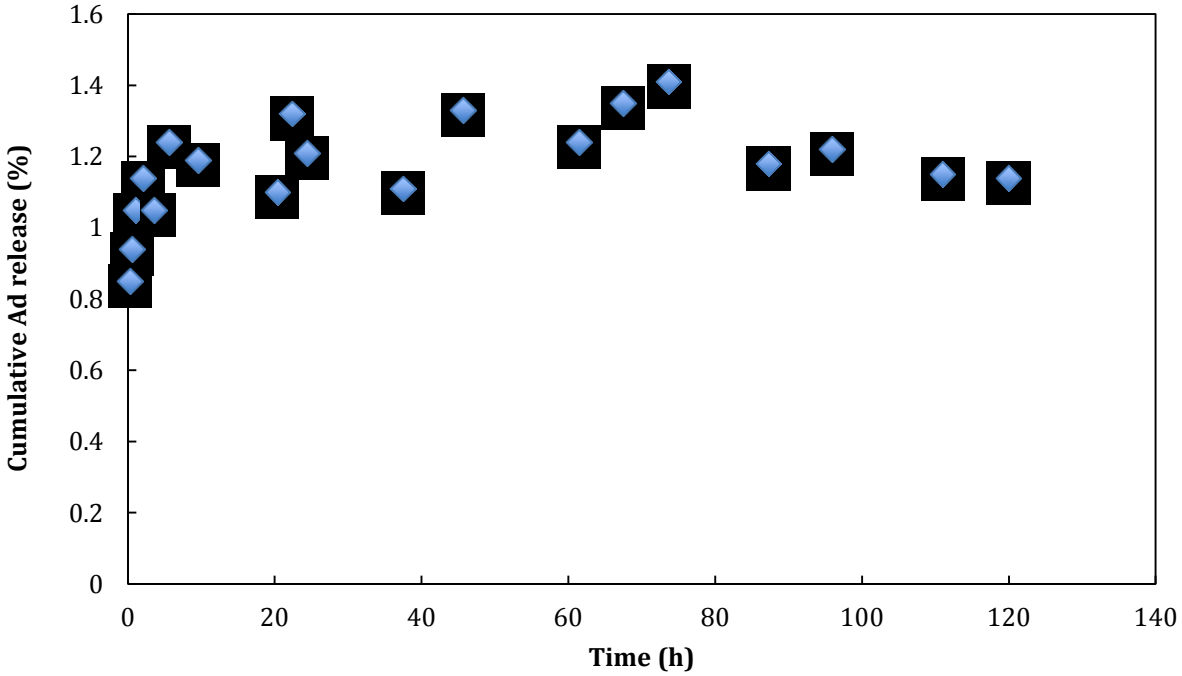

Figure 5.39: Release of Ad from 39% initial Ad loading associated nanoparticles into PBS, pH 7.4. Mean ± standard deviation, n ≥ 5.

The release results from this study suggest that there is an insignificant quantity of drug being released from the adenosine-loaded chitosan-TPP nanoparticles. The low detected release was not expected as the entrapment and association efficiency was so high, thus it was originally thought that there may have been an issue with the UV-spectrophotometer, however the qNMR analysis validated the UV-spectrometer results. It was also thought that use of the PBS solution as a release media may have been an issue, however it has been used by other researchers to study the release of drugs from chitosan nanoparticles (Arias et al, 2010; Du et al., 2010; Papadimitriou et al., 2008). The postulated two-phase release profiles were not observed. It is likely that adenosine did not release from the chitosan nanoparticles as the TPP may have formed a strong complex with the adenosine. Moreover, it is apparent from the release profile (Figure 5.36) of the free drug (no chitosan-TPP nanoparticles present just adenosine stock solution) that the assay used to measure drug release is ineffective as a mere 5.46 ± 0.0631% adenosine release was measured over the time period.

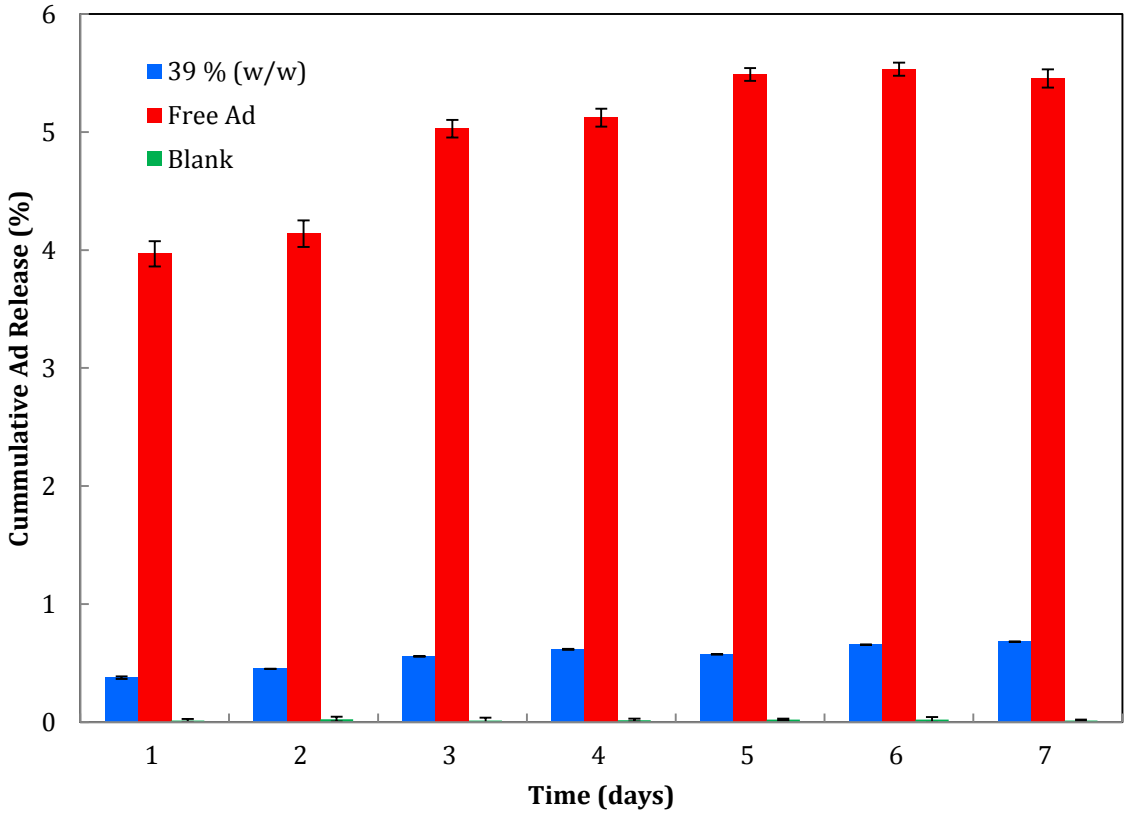

Figure 5.40: Release of Ad from 39% initial Ad loading entrapped nanoparticles into PBS compared to release of blank and free Ad into PBS, pH 7.4, as varied with initial Ad loading. Mean ± standard deviation, n ≥ 5.

Although the use of UV spectrophotometry and PBS release media has not been a successful tool for measuring drug release from chitosan-TPP nanoparticles that were prepared from ionotropic gelation in this research it has been for many other researchers as reported from previous works. Du et al. (2010) quantified the *in vitro* release of ATP encapsulated chitosan oligosaccharide nanoparticles in PBS by using UV spectrophotometry. Through the use of the UV spectrophotometer the ATP loading efficiencies were found to be in the range of 40.6-69.5%. They were successful with their findings as they reported that over 80% of the ATP encapsulated was released from chitosan oligosaccharide nanoparticles over 24 hours. Arias and coworkers (2010) concluded drug entrapment efficiencies varying from 18.1-36.9%. *In vitro* release studies of tegafur from chitosan nanoparticles were performed in PBS following a similar dialysis bag method as previously mentioned in section 4.7.2. By means of spectrophotometric determinations it was concluded that the release of tegafur displayed a biphasic release profile.

Within the first hour 30% of tegafur was released due to the burst effect followed by a sustained release of the remaining drug over the next 143 hours. Likewise, Papadimitriou and coworkers (2008) were able to entrap 17.8 to 29.1% of the initial drug loaded. This research also used the dialysis bag method in PBS to measure drug release of Dorzo from chitosan nanoparticles. The findings from this experiment were similar to those found by Arias and coworkers. A biphasic release profile for Dorzo was recorded with 50-60% of the drug being released during the initial burst effect in the first 45 minutes trialed by a period of slower release for the remainder drug.

6.0 CONCLUSION AND FUTURE WORK

Chitosan-TPP nanoparticles are an effective and efficient drug delivery system for the drug adenosine. The work in this thesis was conducted to further develop controlled drug delivery systems which could increase the uptake, half-life and bioavailability of adenosine by protecting it from degrading enzymes. The literature review in section 3 clearly specified the need for experimental studies on particle fabrication technique, particle characterization, drug entrapment efficiency, and drug release characteristics when using chitosan nanoparticles. The main objective of this thesis and experimental work was to validate a proof-of-concept of a novel drug delivery system for adenosine. This chapter will summarize the conclusions that can be drawn from the research and experimentation that went into developing a novel chitosan-adenosine nanoparticle formulation, in addition, it will recommend future work that should be done.

6.1 Conclusion

Along with it properties, chitosan can provide a valuable solution for the progression of drug delivery systems. Spherical chitosan nanoparticles were successfully fabricated by ionotropic gelation. The polydispersity index for chitosan and adenosine-chitosan nanoparticles was greater than 0.5 indicating a broad size distribution. The average hydrated diameter of unloaded chitosan nanoparticles was 1450 ± 489 nm. Adenosine loaded chitosan-TPP nanoparticles saw an increase in average hydrated diameter from 425.6 ± 133.7 to 514.7 ± 190.5 nm as the amount of initial loaded drug increased. Similar results were observed in previous studies on chitosan nanoparticles (Calvo et al., 1997; Liu et al., 2007). The size of the hydrated adenosine-chitosan nanoparticles are slightly too large to diffuse through the endothelia cells of leaky tumors where the cutoff size of the pores are 400 nm. However, the size of the air dried chitosan nanoparticles decreased for both unloaded, 194 ± 72 nm, and adenosine loaded, 135 ± 48 nm to 183 ± 64 nm. However, these particles would rehydrate once introduced to body fluids, but likely not to the initial amount.

Entrapment efficiencies were calculated using UV-spectrophotometry and confirmed by qNMR. From UV- spectrophotometry it was proven that the drug incorporation method had no influence on entrapment efficiency of adenosine into chitosan nanoparticles. The entrapment efficiency

was 72.25 ± 7.42, 79.07 ± 1.58, and 77.98 ± 2.07 % when 16, 39, and 56 % (w/w) initial adenosine loading was first added to the TPP solution, respectively. Similarly, the entrapment efficiency was 72.530 ± 3.77, 78.886 ± 1.541, and 77.249 ± 1.756 %, when initial adenosine loadings of 16, 39, and 56 %(w/w) were first added to the chitosan solution. From these results above it can also be stated that initial adenosine loadings had little effect on the entrapment efficiency. The average entrapment efficiency confirmed by qNMR for the 39 % (w/w) initial adenosine loading was 76.73 ± 9.44 % which is on par with the results from the UV-spectrophotometer. The effect of chitosan pH change from 3.35 to 4.2 had on entrapment efficiency was also verified. The entrapment efficiency based on UV-spectrophotometer was 75.78 ± 1.99% for 39 % (w/w) initial adenosine loading, this is similar to results found at the original pH. Liquid state NMR analysis resulted in a lower entrapment efficiency of 67.72 ± 5.54%. Entrapment efficiency data was presented for the carrier system, and these results show promising potential for future work on chitosan nanoparticles for the delivery of adenosine. In particular, the entrapment efficiency results demonstrate drug entrapment efficiencies of chitosan nanoparticles is greater than that observed by liposomes and chitosan oligosaccharide nanoparticles in previous studies (Chien, 2009; Du et al., 2010; Hartner et al., 2009).

The average association efficiency for surface absorbed adenosine is 83.97 ± 3.28%. At 39 % (w/w) initial adenosine loading, the association efficiency is slightly greater but comparable to that of the entrapment efficiency.

Due to the sensitivity of Bruker Avance 400 the low amount of adenosine and TPP present in the samples, 0.067 mmol and 0.032 mmol respectively, were not detected. This is why the spectra acquired by means of ssNMR indicated that no adenosine was entrapped into the chitosan nanoparticles even though over 70% of the drug was incorporated into the chitosan matrix. It is for this reason that these ssNMR results cannot be used to form any conclusions on the entrapment of adenosine into chitosan nanoparticles.

The results showed that the two-phase *in vitro* release profiles that were expected from the chitosan nanoparticles did not occur. There is a negligible amount of drug released from the chitosan nanoparticles, regardless the initial adenosine loading. The cumulative average release of

adenosine over 120 hours was 21.06 ± 0.0062%, 0.6909 ± 0.0005%, and 0.9139 ± 0.0499% for 16, 39 and 56 %(w/w) initial Ad loading, respectively and 1.14 ± 0.0098 % for surface associated adenosine nanoparticles. The low quantity of drug released was not expected as the entrapment and association efficiency was so high. One possible reason for the low amount of drug release could be a result of TPP and adenosine might be forming a tightly bounded complex within the chitosan nanoparticles. Additionally, there may be a problem with the drug release assay in PBS solution even though the standard curve indicated that adenosine could be detected using the UV-spectrophotometer as there was only 5.46 ± 0.0631% of free adenosine (no chitosan-TPP nanoparticles present just adenosine stock solution) released from the dialysis tubing. Further development work is required to demonstrate the drug release profile of adenosine from chitosan nanoparticle. Apart from the drug release data, this work can be considered as the first step for further studies on the application of adenosine loaded chitosan nanoparticles.

6.2 Future Work

It is recommended that future work be focused on improving the drug release experiment. Methods of improving adenosine release from chitosan nanoparticles should be investigated. One suggestion is to see if enzymatic degradation would increase the rate and extent of release of adenosine from the chitosan nanoparticles by suspending the loaded chitosan nanoparticles in a lysozyme solution instead of deionized water before pipetting into the presoaked dialysis tubing. Lysozyme is the main enzyme found in the human body to degrade chitosan (Wei et al., 2011). Lysozyme facilitates the hydrolysis of chitosan by acting on the β(1,4) linkages between N-acetylglucosamine and glucosamine (Don et al., 2002; Han et al., 2010). Therefore, the degradation rate of chitosan will increase and so should the release rate of adenosine. Another suggestion for measuring the adenosine release from chitosan nanoparticles would be to use a more direct method. One such method would be to centrifuge the chitosan nanoparticles after a period of time and then dissolve the loaded chitosan nanoparticles in an acid medium. The UV-spectrophotometer or high performance liquid chromatography (HPLC) can be used to measure the concentration of drug remaining in the nanoparticles. In order to help facilitate drug release from the chitosan nanoparticles chitosan with a lower degree of deacetylation could be used. This will create faster degradation rates of chitosan seeing as a lower degree of deacetylation aids in quicker

biodegradation rates as higher degree of deacetylation possesses a slower degradation rate. The chitosan used for this research had a degree of deacetylation of 90%.

Because the novel chitosan nanoparticle drug delivery system for adenosine was designed with intravenous infusion administration in mind it would be ideal to maintain a diameter smaller than 100 nm to help facilitate the transport of adenosine-chitosan nanoparticles through the cell membrane and increase delivery efficiency. One proposal would be to try using chitosan with a lower molecular weight. Research has proven that as the molecular weight of chitosan increases so does the size of the chitosan nanoparticles (Luangtana-anan et al., 2005; Vandana and Sahoo, 2009).

REFERENCES

Abdelwahed, W., Degbert, G., Stainmesse, S., & Fessi, H. (2006). Freeze-drying of nanoparticles: formulation, process and storage considerations. *Advance Drug Deliver Reviews*, *58*(15), 1688-1713.

Agnihotri, A., Mallikarjuna, N., & Aminabhavi, M. (2004). Recent advances on chitosan-based micro- and nanoparticles in drug delivery. *Journal of controlled release*, *100*(1), 5-28.

Aiba, S. (1989). Studies on chitosan: 2. Solution stability and reactivity of partially N-acetylated chitosan derivatives in aqueous media. *International journal of macromolecules*, *11*(4), 249-252.

Arakawa, A., Ishiguro, S., & Tamai, M. (1998). Preparation of liposome-encapsulating adenosine triphosphate. *Tohoku Journal of Experimental Medicine*, *184*(1), 39-47.

Aranaz, I., Harris, R., & Heras, A. (2010). Chitosan amphiphilic derivatives: chemistry and applications. *Current Organic Chemistry*, *14*(3), 308-330.

Arias, J., Lopez-Viota, M., Gallardo, V., & Ruiz, M. (2010). Chitosan nanoparticles as a new delivery system for the chemotherapy agent tegafur. *Drug Development and Industrial Pharmacy*, *36*(6), 744-750.

Arulmozhi, V., Pandian, K., & Mirunalini, S. (2013). Ellagic acid encapsulated chitosan nanoparticles for drug delivery system in human oral cancer cell line (KB). *Colloids and Surfaces B: Biointerfaces*, *110* (Oct 13), 313-320.

Banerjee, T., Mitra, S., Singh, A. K., Sharma, R. K., & Maitra, A. (2002). Preparation, characterization and biodistribution of ultrafine chitosan nanmparticles. *International Journal of Pharmaceutics*, *243*(1-2), 93-105.

Barthelmes, J., Dunnhaupt, S., Hombach, J., & Bernkop-Schnurch, A. (2011). Thiomer nanoparticles: stabilization via covalent cross-linking. *Drug Delivery*, *18*(8), 613-619.

Beachley, V., & Wen, X. (2009). Stem cells and nanostructured materials. In D. Shi (Ed.), Nanoscience in biomedicine (pp 1-19). Berlin: Springer.

Benet, L., & Zia-Amirhosseini, P. (1995). Basic principles of pharmacokinetics. *Toxicologic Pathology, 23*(2), 115-123.

Bhowmik, D., Gopinath, H., Kumar, B., Duraivel, S., & Kumar, K. (2012). Control release drug delivery systems. *The Pharma Innovation*, *1*(10), 24-32.

Biagini, G., Bertani, A., Muzzarelli, R., Damadei, A., DiBenedetto, G., Riccotti, B., Zucchini,C., & Rizzoli, C. (1991). Wound management with N-carboxybutyl chitosan. *Biomaterials*, *12*(30), 281-286.

Bodnar, M., Hartmann, J., & Borbely, J. (2005). Preparatin and characterization of chitosan-based nanoparticles. *Biomolecules*, *6*(5), 2521-2527.

Bowman, K., & Leong, K. (2006). Chitosan nanoparticles for oral drug and gene delivery. *International Journal of Nanomedicine*, *1*(2), 117-128.

Bozkir, A., & Saja, O. M. (2004). Chitosan nanoparticles for plasmid DNA delivery: effect of chitosan molecular structure on formulation and release characteristics. *Drug Delivery*, *11*(2), 107-112.

Brannon-Peppas, L. (1997, November 1). Polymers in controlled drug delivery. *Medical Plastics and Biomaterials*. Retrieved from http://www.mddionline.com/article/polymers-controlled-drug-delivery

Bryant, B., & Knights, K. (2011). Pharmacokinetics and dosing regimens. In B. Bryant, & K. Knights (Eds.), *Pharmacology for health professionals* (pp. 156-166). Chatswood: Elsevier.

Buranachai, T., Praphairaksit, N., & Muangsin, N. (2010). Chitosan/polyethylene glycol beads crosslinked with tripolyphosphate and glutaraldehyde for gastrointestinal drug delivery. *AAPS PharmSciTech*, *11*(3), 1128-1137.

Calcagno, A. M., & Siahaan, t. J. (). Physiological, biochemical, and chemical barrierts to oral drug delivery. In B. Wang, T. J. Siahaan, & R. Soltero, (Eds.), *Drug delivery: principles and applications* (pp 15-27). New Jersey: Wiley.

Calvo, P., Remunan-Lopez, C., Vila-Jato, J. L., & Alonso, M. J. (1997). Novel hydrophilic chitosan-polyethylene oxide nanoparticles as protein carries. *Journal of Applied Polymer Science*, *63*(1), 125-132

Castro, E., & Kumar, A. (2013). Nanoparticles in drug delivery systems. In A. Kumar, H. M. Mansour, A. Friedman, & E. R. Blough (Eds.), *Nanomedicine in drug delivery* (pp 1-22). Boca Raton: CRC Press.

Chan, P., Kurisawa, M., Chung, J., & Yang, Y. (2007). Synthesis and characterization of chitosan-g-poly(ethylene glycol) folate as a non-viral carrier for tumor-targeted gene delivery. *Biomaterials*, *28*(3), 540-549.

Chellat, F., Tabrizian, M., Dumitriu, S., Chornet, E., Rivard, C., & Yahia, L. (2000). Study of biodegradation behaviour of chitosan-xanthan microspheres in simulated physiological media. *Journal of Biomedical Materials Research*, *53*(5), 592-599.

Chien, S. (2010). Intracellular ATP delivery using highly fusogenic liposomes. In V. Weissig (Ed.), *Liposomes: Methods in molecular biology* (pp 377-391). New York: Humana press.

Cho, K., Wang, X., Nie, S., Chen, Z., & Shin, D. M. (2008). Therapeutic nanoparticles for drug delivery in cancer. *Clinical Cancer Research*, *14*(5), 1310-1316.

Christian, P., von der Kammer, F., Baalousha, M., & Hofmann, T. (2008). Nanoparticles: structure, properties, preparation and behaviour in environmental media. *Ecotoxicology*, *17*(5), 326-343.

Cohen, M. V., & Downey, J. M. (2009). Adenosine at reperfusion. *Journal of the American College of Cardiology, 53*(8), 718-719.

Danhier, F., Ansorena, E., Silva, J., Coco, R., Breton, A., & Preat, V. (2010). PLGA-based nanoparticles: an overview of biomedical applications. *Journal of Controlled Release*, *161*(2), 505-522.

Dash, M., Chellini, F., Ottenbrite, R. M., & Chiellin, E. (2011). Chitosan- a versatile semi-synthetic polymer in biomedical applications. *Progress in Polymer Science*, *36*(8), 981-1014.

de Campos, A., Sanchez, A., & Alonso, M. (2001). Chitosan nanoparticles: a new vehicle for the improvement of the delivery of drugs to the ocular surface. Application to cyclosporine A. *International Journal of Pharmaceutics*, *224*(1-2), 159-168.

Desai, M. P., Labhasetwar, V., Walter, E., Levy, R. J., & Amidon, G. L. (1997). The mechanism of uptake of biodegradable microparticles in Caco-2 cells is size dependent. *Pharmaceutical Research*, *14*(11), 1568-1573.

Dhawan S, Singla A, and Sinha V. (2004). Evaluation of Mucoadhesive properties of chitosan microspheres prepared by different methods. *AAPS PharmSciTech*, *5*(4), 122-128.

Dodane, V., Khan, M., & Merwin, J. (1999). Effect of chitosan on epithelial permeability and structure. *International Journal of Pharmaceutics, 182*(1), 21-32.

Don, T., Chuang, C., & Chiu, W. (2002). Studies on the degradation behavior of chitosan-g-poly (acrylic acid) copolymers. *Tamkang Journal of Science and Engineering*, *5*(4), 235-240.

Du, Y., Ying, X., Wang, L., Zhai, Y., Yuan, H., Yu, R., & Hu, F. (2010). Sustained release of ATP encapsulated in chitosan oligosaccharide nanoparticles. International *Journal of Pharmaceutics*, *392*(1-2), 164-169.

Dudhani, A., & Kosaraju, S. (2010). Bioadhesive chitosan nanoparticles: preparation and characterization. *Carbohydrate Polymers*, *81*(2), 243-251.

Deng, M., Laurencin, C. T., Allcock, H. R., & Kumbar, S. G. (2013). Polyphosphazenes as biomaterials. In S. Dumitriu, & V. Popa (Eds.), *Polymeric biomaterials: structure and function* (pp 83-134). Boca Raton: CRC Press.

Dutta, P., Dutta, J., & Tripathi, V. (2004). Chitin and chitosan: chemistry, properties and applications. *Journal of Scientific and Industrial Research*, *63*(1), 20-31.

Dutta, P., & Gupta, S. (2006). Physics of nanotechnology. In P. Dutta, & S. Gupta (Eds.), *Understanding of nano science and technology* (pp 35-74). New Delhi: Global Vision Publishing House.

Eikvar, L., & Kirkeboen, K. (1998). Receptor mediated effects of adenosine and caffeine. *Journal of Norwegian Medical Association*, *118*(9), 1390-1395.

Einbu, A. (2007). *Characterisation of chitin and a study of its acid-catalysed hydrolysis* (Doctorial dissertation). Retrieved from NTNU database. (urn:nbn:no:ntnu:diva-1566)

Ely, S. W., & Berne, R. M. (1992). The protective effects of adenosine in myocardial ischemia. *American Heart Association*, *85*(3), 893-904.

Errington, N., Harding, S. E., Varum, K. M., & Illum, L. (1993). Hydrodynamic characterization of chitosan varying in molecular weight and degree of acetylation. *International Journal of Biological Macromolecules*, *15*(2), 113-117.

Felix, F. (1998). Freeze-drying of bioproducts: putting principles into practice. *European Journal of Pharmaceutics and Biopharmaceutics*, *45*(3), 221-229.

Fishman, P., Bar-Yehuda, S., & Cohn, I. (2002). A3 adenosine receptor as a target for cancer therapy. *Anticancer Drugs*, *13*(5), 437-443

Fishman, P., Bar-Yehuda, S., Synowitz, M., Powell, J. D., Klotz, K. N., Gessi, S., & Borea, P. A. (2009). Adenosine receptors and cancer. In C. N. Wilson, & S. J. Mustafa, *Handbook of Experimental Pharmacology* (pp 399-441). Berlin: Springer Berlin Heidelberg.

Fleige, E., Quadir, M., & Haag, R. (2012). Stimuli-responsive polymeric nanocarriers for the controlled transport of active compounds: concepts and applications. *Advanced Drug Delivery Reviews*, *64*(9), 866-884.

Folkman, J., & Long, D. (1964). The use of silicone rubber as a carrier for prolonged drug therapy. *Journal of Surgical Research*, *4*(3), 139-142.

Freitas, R. A. (2003). *Nanomedicine – Volume IIA: Biocompatibility*. Georgetown: Landes Bioscience.

Gan, Q., & Wang, T. (2007). Chitosan nanoparticle as protein delivery carrier- systematic examination of fabrication conditions for efficient loading and release. *Colloids and Surfaces B: Biointerfaces*, *59*(1), 24-34.

Gan, Q., Wang, T., Cochrane, C., & McCarron, P. (2005). Modulation of surface charge, particle size and morphological properties of chitosan-TPP nanoparticles intended for gene delivery. *Colloids and Surfaces: Biointerfaces*, *44*(2-3), 65-73.

Gao, Y., Cui, F., Guan, Y., Wang, Y., & Zhang, L. (2006). Preparation of roxithromycin-polymeric microspheres by the emulsion solvent diffusion method for taste masking. *International Journal of Pharmaceutics*, *318*(1-2), 62-69.

Gelperina, S., Kisich, K., Iseman, M. D., & Heifets, L. (2005). The potential advantages of nanoparticles drug delivery systems in chemotherapy of tuberculosis. *American Journal of Respiratory and Critical Care Medicine*, *172*(12), 1487-1490.

Gessi, S., Merighi, S., Sacchetto, V., Simioni, C., & Boea, P. (2010). Adenosine receptos and cancer. *Biochimica et Biophysica Acta – Biomembranes*, 1808(5), 140-1412.

Goyal, R., & Dhawan, A. (2006). Further investigations into the oxidation chemistry of adenosine- effect of applied potential on the products formation. International *Journal of Electrochemical Science*, 1, 304-316.

Grenha, A., Seijo, B., & Remunan-Lopez, C. (2005). Microencapsulated chitosan nanoparticles for lung protein delivery. European *Journal of Pharmaceutical Sciences*, *25*(4-5), 427-437.

Haas, N., Pufahl, C., Gessler, P., & Teufel, M. (1994). Adenosine triphosphate for supraventricular tachycardia in newborns and suckling infants. *Deutsche Medizinische Wochenschrift*, *119*(40), 1351-1356.

Hafner, A., Durrigl, M., & Filipovic-Grcic. (2011). Short- and long-term stability of lyophilized melatonin-loaded lecithin/chitosan nanopartilces. *Chemical and Pharmaceutical Bulletin*, *59*(9), 1117-1123.

Han, T., New, N., Furuike, T., Tokura, S., & Tamura, H. (2010). Methods of N-acetylated chitosan scaffolds and its in vitro biodegration by lysozyme. *Journal of Biomedical Science and Engineering, 5*(1), 15-23.

Hartner, C., Verma, D., Levchenko, T., Bernstein, E., & Torchilin, V. (2009). ATP-loaded liposomes for treatment of myocardial ischemia. *Willey Interdisciplinary Reviews: Nanomedicine and Nanobiothecnology*, *1*(5), 530-539.

He, P., Davis, S., & Illum, L. (1998). *In vitro* evaluation of the mucoadhesive properties of chitosan microspheres. *International Journal of Pharmaceutics*, *166*(1), 75-88.

He, P., Davis, S., Illum, L. (1999). Chitosan microspheres prepared by spray drying. *International Journal of Pharmaceutics*, *187*(1), 53-65.

Hoffman, A. (2008). The origins and evolution of "controlled" drug delivery systems. *Journal of Controlled Release*, *132*(3), 153-163.

Hoffman, A. (2013). Stimuli-responsive polymers: biomedical applications and challenges for clinical translation. *Advanced Drug Delivery Reviews*, *65*(1), 10-16.

Hossain, S., Yamamoto, H., Chowdhury, E., Wu, X., Hirose, H., Amranul, H., Doki, Y., Mori, M., & Akaike, T. (2013). Fabrication and intracellular delivery of doxorubicin/carbonate apatite nanocomposites: effect on growth retardation or establish colon tumor. PLoS One 8(4), e60428.

Huang, M., Khor, E., & Lim, L. Y. (2004). Uptake and cytotoxicity of chitosan molecules and nanoparticles: Effects of molecular weight and degree of deacetylation. *Pharmaceutical Research*, *21*(2), 344-353

Illum, L. (1998). Chitosan and its use as a pharmaceutical excipient. *Pharmaceutical Research, 15*(9),1326-1331.

Isa, M., Coragia, D., Frazier, R., & Jauregi, P. (2007). Recovery and purification of surfactin from fermentation broth by a two-step ultrafiltration process. *Journal of Membrane Science*, *296*(1-2), 51-57.

Isha, C., Nimrata, S., Rana, A. C., & Surbhi, G. (2012). Oral sustained release drug delivery system: an overview. *International Research Journal of Pharmacy*, *3*(5), 57-62.

Islam, M., Firdous, J., Choi, Y., Yun, C., & Cho, C. (2012). Design and application of chitosan microspheres as oral and nasal vaccine carriers: an updated review. *International Journal of Nanomedicine*, *7*(December), 6077-6093.

Jin, S., & Ye, K. (2008). Nanoparticle-mediated drug delivery and gene therapy. *Biotechnology, 23*(1), 32-41.

Jin-Oh, Y., Yu-Chuan, L., & Ching-An, P. (2006). Efficient gene transfection using chitosan-alginate core-shell nanoparticles. *International Journal of Nanomedicine*, *1*(2), 173-180.

Jong, W., & Borm, P. (2008). Drug delivery and nanoparticles: applications and hazards. *International Journal of Nanomedicine, 3*(2), 133-149.

Kadam, R., Bourne, D., & Kompella, U. (2012). Nano-advantage in enhanced drug delivery with biodegradable nanoparticles: contribution of reduced clearance. *Drug Metabolism and Disposition*, *40*(7), 1380-1388.

Kalantzi, L., Karavas, E., Koutris, E., & Bikiaris, D. (2009). Recent advances in oral pulsatile drug delivery. *Recent Patents on Drug Delivery and Formulation*, *3*(1), 49-63.

Kalut, S. (2008). Enhancement of degree of deacetylation of chitin in chitosan production (Undergraduate project thesis). Retrieved from UMP open access repository

Kas, H. S. (1996). Chitosan: properties, preparations and application to microparticulate systems. *Journal of Microencapsulation*, *14*(60), 689-711.

Katas, H., & Alpar, H. (2006). Development and characterisation of chitosan nanoparticles for siRNA delivery. *Journal of Controlled Release*, *115*(2), 216-225.

Kean, T., & Thanou, M. (2009). Biodegradation, biodistribution and toxicity of chitosan. *Advanced Drug Delivery Reviews*, *62*(1), 3-11.

Khatri, K., Goyal, A., Gupta, P., Mishra, N., & Vyas, S. (2008). Plasmid DNA loaded chitosan nanoparticles for nasal mucosal immunization against hepatitis B. *International Journal of Pharmaceutics*, *354*(1-2), 235-241.

Kong, M., Chen, X., Xing, K., & Park, H. (2010). Antimicrobial properties of chitosan and mode of action: a state of the art review. *International Journal of Food Microbiology*, *144*(1), 51-63.

Korb, V., Tep, K., Richard, C., Scherman, D., Cynober, L., Chaumeil, J., & Dumortier, G. (2008). Current data on ATP-containing liposomes and potential prospects to enhance cellular energy status for hepatic applications. *Critical Reviews in Therapeutic Drug Carrier Systems*, *24*(4), 305-345.

Krishna Sailaja, A., Amareshwar, P., & Chakravarty, P. (2010). Chitosan nanoparticles as a drug delivery system. *Research Journal of Pharmaceutical, Biological and Chemical Sciences*, *1*(3), 474-484.

Kumar, M. N. V. R. (2000). A review of chitin and chitosan applications. *Reactive and Functional Polymers*, *46*(1), 1-27.

Kumar, G., Smith, P. J., & Payne, G. (1999). Enzymatic grafting of a natural product onto chitosan to confer water solubility under basic conditions. *Biotechnology Bioengineering*, *63*(2), 154-165.

Leader, B., & Golan, D. E. (2011). Protein-based therapies. In D. E. Golan, A. H. Tashjian, E. J. Armstrong, & A. W. Armstrong (Eds.), *Principles of pharmacology: the pathophysiologic basis of drug therapy* (pp 917-934). Philadelphia: Lippincott Williams & Wilkins.

Lerman, B. B., & Belardinelli, L. (1991). Cardiac electrophysiology of adenosine: basic and clinical concepts. *Circulation*, *83*(5), 1499-1509.

Li, S. D., & Huang, L. (2008). Pharmacokinetics and biodistribution of nanoparticles. *Molecular Pharmaceutics*, *5*(4), 496-504.

Liechty, W., Kryscio, D., Slaughter, B., & Peppas, N. (2010). Polymers for drug delivery systems. *Annual Reviews Chemical and Biomolecular Engineering*, *1*, 149-173.

Liu, Z., Jiao, Y., & Zhang, Z. (2007). Heparin/chitosan nanoparticle carriers prepared by polyelectrolyte complexation. *Journal of Biomedical Materials Research*, *83*(3), 806-812.

Lopez-Leon, T., Carvalho, E., Ortega-Vinuesa, J., & Bastos-Gonzalez, D. (2005). Physicochemical characterization of chitosan nanoparticles: electrokinetic and stability beharvior. *Journal of Colloid and Interface Science*, *283*(2), 344 351.

Luangtana-anan, M., Opanasopit, P., Nqawhirunpat, T., Nunthanid, J., Sriamornsak, P., Limmatvapirat, S., & Lim, L. (2005). Effect of chitosan salts and molecular weight on a nanoparticulate carrier for the therapeutic protein. *Pharmaceutical Development and Technology*, *10*(2), 189-196.

Madi, L., Ochaion, A., Rath-Wolfsom, L., Bar-Yehuda, A., Erlanger, A., Ohana, G., Harish, A., Merimski, O., Barer, F., & Fishman, P. (2004). The A3 adenosine receptor is highly expressed in tumor versus normal cells: potential target for tumor growth inhibitor. *Clinical Cancer Research*, *10*(13), 4472-4479.

Malam, Y., Loizidou, M., & Seifalian, A. (2009). Liposomes and nanoparticles: nanosized vehicles for drug delivery in cancer. *Trends in Pharmacological Sciences*, *30*(11), 592-599.

Malvern Instruments Ltd. (2004, July). Zetasizer nano series - User manual. Retrieved from http://www.nbtc.cornell.edu/facilities/downloads/Zetasizer%20Manual.pdf

Malvern Instruments Ltd. 2013. Zeta potential an introduction in 30 minutes. Retrieved from http://www.nbtc.cornell.edu/facilities/downloads/Zeta%20potential%20-%20An%20introduction%20in%2030%20minutes.pdf

Manjunath, S., & Sakhare, P. M. (2009). Adenosine and adenosine receptors: newer therapeutic perspective. *Indian Journal of Pharmacology*, *41*(3), 97-105.

Mark, H., Bikales, N., Overberger, C., & Menges, G. (1985). Encylopedia of polymer science and engineering, vol 1. Wiley, New York: 20.

Mathias, U. (2012). Stimuli-responsive polymer materials. International Conference on Chemical and Material Engineering, Retrieved from http://eprints.undip.ac.id/36940/.

Meena, K. P., Dangi, J. S., Samal, P. K., & Kumar, M. (2011). Nanoparticles technology and recent advances in novel drug delivery systems. *International Journal of Research in Drug Delivery*, *1*(1), 1-5.

Mi, F., Shyu, S., Wu, Y., Lee, S., Shyong, J., & Huang, R. (2001). Fabrication and characterization of sponge-like asymmetric chitosan membrane as a wound dressing. *Biomaterials*, *22*(2), 165-173.

Mitra, A., & Dey, B. (2011). Chitosan microspheres in novel drug delivery systems. *Indian Journal of Pharmaceutical Sciences*, *73*(4), 355-366.

Mitra, S., Gaur, U., & Maitra, A. (2001). Tumour targeting delivery of encapsulated dextran-doxorubicin conjugate using chitosan nanoparticles as carrier. *Journal of Controlled Release*, *74*(1-3), 317-323.

Mourya, V. K., & Inamdar, N. N. (2008). Chitosan-modifications and applications: opportunities galore. *Reactive and Functional Polymers*, *68*(6), 1013–1051.

Nair, K., & Madhavan, P. (1984). Chitosan for removal of mercury from water. *Fishery Technology*, *21*, 109-112.

Nagpal, K., Singh, S. H., & Mishra, D. N. (2010). Chitosan nanoparticles: a promising system in novel drug delivery. *Chemical and Pharmaceutical Bulletin*, *58*(11), 1423-1430.

Narayan R (Ed.). 2009. Biomaterials (pp 419). New York: Springer

Newby, A. C. (1984). Adenosine and the concept of 'retaliatory metabolites'. *Trends in Biomedical Sciences*, *9*(2), 42-44.

Niwa, T., Takeuchi, H., Hino, T., Kunou, N., & Kawashima, Y. (1993). Preparations of biodegradable nanospheres of water-soluble and insoluble drugs with D,L-lactide/glycolide copolymer by a novel spontaneous emulsification solvent diffusion method, and the drug release behavior. *Journal of Controlled Release*, *25*(1), 89-98.

Norouzi, Z., Abdouss, M., Shoushtari, A., & Haji, A. (2012). Electrospinning of β-cyclodextrin grafted chitosan nanofibrous membrane for dye removal. *5th Texteh International Conference*, 275-284. Retrieved from http://www.researchgate.net/publication/236230321_ELECTROSPINNING_OF_-CYCLODEXTRIN_GRAFTED_CHITOSAN_NANOFIBEROUS_MEMBRANE_FOR_DYE_REMOVAL

Oliveira, B., Santana, M., & Re, M. (2005). Crossed-linked with D, L-glyceraldehyde as a potential drug delivery system: preparation and characterization. *Brazilian Journal of Chemical Engineering*, *22*(3), 353-360.

Omidian, H.; & Park, K. (2008). Swelling agents and devices in oral drug delivery. *Journal of Drug Delivery Science and Technology*, *18*(2), 83-89.

Papadimitriou, S., Bikiaris, D., Avgoustakis, K., Karavas, E., & Georgarakis, M. (2008). Chitosan nanoparticles loaded with dorzolamide and pramipexole. *Carbohydrate Polymers*, 73(1), 44-45.

Patel, H., Patel, J., Patel, K., & Patel, R. (2010). Ophtalmic drug delivery systems - A review. *Der Pharmacia Lettre*, *2*(4), 100-115.

Polleux, F., & Ghosh, A. (2002). The slice overlay assay: A versatile tool to study the influence of extracellular signals on neuronal development. *Science: The Signal Transduction Knowledge Environment*, *2002*(136), pl9.

Paul, T., & Pfammatter, J. (1997). Adenosine: an effective antiarrhythmic drug in pediatrics. *Pediatric Cardiology*, *18*(2), 118-126.

Puisieux, F., Fattal, E., Lahiani, M., Auger, J., Jouannet, P., Couvreur, P., & Delattre, J. (1994). Liposomes, an interesting tool to deliver a bioenergetic substrate (ATP). *in vitro* and *in vivo* studies. *Journal of Drug Targeting*, *2*(5), 443-448.

Quiqnard, S., Masse, S., & Coradin, T. (2011). In A. Prokop, *Intracellular delivery: Fundamentals and applications* (pp 333-362). New York: Springer.

Raafat, D., von Bargen, K., & Sahl, H. (2008). Insight into the mode of action of chitosan as an antibacterial compound. *Applied Environmental Microbiology*, *74*(12), 3764-3773.

Rani, M., Agarwal, A., & Negi, Y. (2010). Chitosan based hydrogel polymeric beads as drug delivery system. *Bioresources*, *5*(4), 2765-2807.

Reynolds, T. D., Gehrke, S. H., Hussain, A. S., & Shenouda, L. S. (1998). Polymer erosion and drug release characterization of hydroxypropyl methylcellulose matrices. *Journal of Pharmaceutical Science*, *87*(9), 1115-1123.

Rinaudo, M. (2006). Chitin and chitosan: properties and applications. *Progress in Polymer Science*, *31*(7), 603-632.

Riva, R., Ragelle, H., des Rieux, A., Duhem, N., Jerome, C., & Preat, V. (2011). Chitosan and chitosan derivatives in drug delivery and tissue engineering. In R. Jayakumar, M. Prabaharan, & R. A. A. Muzzarelli (Eds.), Chitosan for Biomaterials II (pp 19-44). Berlin: Springer.

Robins, K., & Lyons, G. (2004). Supraventricular tachycardia in pregnancy. *British Journal of Anaesthesia*, *92*(1), 140-143.

Robitzki, A. A., & Kurz, R. (2010). Biosensing and drug delivery at the microscale. In M. Schäfer-Korting (Ed.), *Handbook of experimental pharmacology 197: Drug delivery* (pp 88-89). Berlin: Springer.

Saxena, V., Sadoqi, M., & Shao, J. (2006). Polymeric nanoparticulate delivery system for indocyanine green: biodistribution in health mice. *International Journal of Pharmaceutics*, *308*(1-2), 200-204.

Shivanand, P., & Devmurari, V. (2010). Osmotic pump drug delivery devices: from implant to sandwich oral therapeutic system. *International Journal of PharmTech Research*, *2*(1), 693-699.

Shryock, J., & Beladinelli, L. (1997). Adenosine and adenosine receptors in cardiovascular system: biochemistry, physiology, and pharmacology. *American Journal of Cardiology*, *79*(12), 2-10.

Siepmann, J., Siegel, R., & Rathbone, M. (2012). Fundamentals and applications of controlled release drug delivery. DOI: 10.1007/978-1-4614-0881-9.

Signh, M., Hemant, K., Ram, M., & Shivakumar, H. (2010). Microencapsulation: a promising technique for controlled drug delivery. *Research in Pharmaceutical Sciences*, *5*(2), 65-77.

Swaraga, M., Charitha, L., & Adinarayana, M. (2005). Mechanism of protection of adenosine from sulphate radical anion and repair of adenosine radicals by caffeic acid in aqueous solution. *Journal of Chemical Sciences*, *117*(4), 345-350.

Takeuchi, H., Matsui, Y., Sugihara, H., Yamamoto, H., & Kawashima, Y. (2005). Effectiveness of submicron-sized, chitosan-coated liposomes in oral administration of peptide drugs. *International Journal of Pharmaceutics*, *303*(1-2), 160–170.

Talero, R., Pedrajas, C., & Rahhal, V. (2013). Performance of fresh Portland cement pastes - Determination of some specific rheological parameters. In R. Durairaj (Ed.), *Rheology - New concepts, applications and methods* (pp. 57-79). New York: InTech.

Tamada, J., & Langer, R. (1993). Erosion kinetics of hydrolytically degradable polymers. *Proceedings of the National Academy of Science of the United States of America*, *90*(2), 552-556.

Tang, X., & Pikal, M. (2004). Design of freeze-drying processes for pharmaceuticals: particles advice. *Pharmaceutical Research*, *21*(2), 91-200.

Terentyuk, G., Akchurin, G., Maksimova, I., Shatrokha, A., Tuchin, V., Maslyakova, G., … Khlebtsov, B. (2009, July 15). Tracking gold nanoparticles in the body. *SPIE*. Retrieved from http://spie.org/x36120.xml

Thanou, M., Verhoef, J., & Junginger, H. (2001). Chitosan and its derivatives as intestinal absorption enhancers. *Advance Drug Delivery Reviews*, *50*(1), S91-S101.

Tiyabooncha, W. (2003). Chistosan: A promising system for drug delivery. *Naresuan University Journal*, *11*(3), 51-66.

Troy, D., & Hauber, M. (2006). Extended-release and targeted drug delivery systems. In D. B. Troy (Ed.), *Remington: The science and practice of pharmacy* (pp 940-941). Philadelphia: Lippincott Williams & Wilkins.

Uchegbu, I. F., & Schatzlein, A. G. (Ed.). 2006. Polymers in drug delivery (pp 161, 243). Florida: Taylor & francis group.

van der Lubben, I., Verhoef, J., Borchard, G., & Junginger, H. (2001). *European Journal of Pharmaceutical Sciences*, *14*(3), 201-207.

Vandana, M., & Sahoo, S. (2009). Optimization of physiochemical parameters influencing the fabrication of protein-loaded chitosan nanoparticles. *Nanomedicine*, *4*(7), 773-785.

Vijayalakshmi, G., Adinarayana, M., & Rao, P. (2009). Kinetics of oxidation of adenosine by tert-butoxyl radicals: protection and repair by chlorogenic acid. *Indian Journal of Biochemistry & Biophysics*, *46*(5), 389-394.

Wang, A. Z., Langer, R., & Farokhzad, O. C. (2011). Nanoparticle delivery of cancer drugs. *Annual Review of Medicine*, *63*,185-198.

Wang, L., Gu, Y., Su, Z., & Ma, G. (2005). Preparation and improvement of release behaviour of chitosan microspheres containing insulin. *International Journal of Pharmaceutics*, *311*(1-2), 187-195.

Wei, L., Cai, C., Lin, J., Wang, L., & Zhang, X. (2011). Degradation controllable biomaterials constructed from lysozyme-loaded ca-alginate microparticles/chitosan composites. *Polymer*, *52*(22), 5139-5148.

Williams, S., Lee, H., & Turner, M. (1999). Size characterization of magnetic cell sorting microbeads using flow field-flow fractionation and photon correlation spectroscopy. *Journal of Magnetism and Magnetic Materials*, *194*(1-3), 248-253.

Wintstanley P, Constable S, and Walley T. 2007. Master medicine: medical pharmacology (12-13). :Churchill Livingstone.

Wittwer, L. K., & Muhr, M. (1997). Adenosine for the treatment of PSVT in the prehospital arena: efficacy of an initial 6 mg dosing regimen. *Prehospital and Sisaster Medicine*, *12*(3), 237-239.

Wright, J., & Hoffman, A. (2012). Overview of long acting injections and implants. In J. Wright, & D. Iurgess (Eds.), *Long acting injections and implants* (pp 11-22). New York: Springer.

Wu, K., Huang, Z., Yang, Y., Chang, C., & Chou, T. (2007). Enhancement of catansome formation by means of cosolvent effect: semi-spontaneous preparation method. *Colloids and Surfaces A: Physicochemical and Engineering Aspects*, *302*(1-3), 599-607.

Wu, Y., Yang, W., Wang, C., Hu, J., & Fu, S. (2005). Chitosan nanoparticles as a novel delivery system for ammonium glycyrrhizinate. *International Journal of Pharmaceutics*, *295*(1-2), 235-245.

Wu, L., Zhang, J., & Watanabe, W. (2011). Physical and chemical stability of drug nanoparticles. *Advance Drug Delivery Reviews*, *63*(6), 456-469.

Yamamoto, H., & Amaike, M. (1997). Biodegradation of cross-linked chitosan gels by a microorganism. *Macromolecules*, *30*(13), 3936-3937.

Yang, R., Han, X., Shi, K., Cheng, G., Shim, C., & Cui, F. (2009). Cationic formulation of paclitaxel-loaded poly D,L-lactic-co-glycolic acid (PLGA) nanoparticles using an emulsion-solvent diffusion method. *Asian Journal of Pharmaceutical Sciences*, *4*(2), 89-95.

Yang, J., Parkanzky, P., Khunte, B., Canlas, C., Yang, R., Gabrys, C., & Weliky, D. (2001). Solid state NMR measurements of conformation and conformational distributions in the membrane-bound HIV-1 fusion peptide. *Journal of Molecular Graphics and Modeling*, *19*(1), 129-135.

Yeh, H., & Lin, J. (2008). Surface characterization and *in vitro* platelet compatibility study of surface sulfonated chitosan membrane with amino group protection-deprotection strategy. *Journal of Biomaterials Science*, *19*(3), 291-310.

Yih, T., & Al-Fandi, M. (2006). Engineered nanoparticles as precise drug delivery systems. *Journal of Cellular Biochemistry*, *97*(6), 1184-1190.

Yuan, F., Dellian, M., Fukumura, D., Leunig, M., Berk, D., Torchilin, V., & Jain, R. (1995). Vascular permeability in a human tumor xenograft: molecular size dependence and cutoff size. *Cancer Research*, *55*(17), 3752-3756.

Zhai, H., Chan, H., Farahmand, S., & Maibach, H. (2009). Measuring human skin buffering capacity: an *in vitro* model. *Skin Research and Technology*, *15*(4), 470-475.

Spectrumlabs. 1995-2013. Laboratory dialysis frequently asked questions. Retrieved from http://www.spectrumlabs.com/dialysis/FAQ.html.

Zhang, G. (2009). Nanotechnology-based biosensors in drug delivery. In M. de Villiers, P. Aramwit, & G. Kwon (Eds.), *Nanotechnology in drug delivery* (pp. 163-189). New York: Springer.

Zhang, H., & Neau, S. (2001). *In vitro* degradation of chitosan by a commercial enzyme preparation: effect of molecular weight and degree of deacetylation. *Biomaterials*, *22*(12), 1653-1658.

Zhang, H., Oh, M., Allen, C., & Kumacheva, E. (2004). Monodisperse chitosan nanoparticles for mucosal drug delivery. *Biomarcomolecules*, *5*(6), 2461-2468.

APPENDIX A: UV- SPECTROPHOTOMETER WAVELENGTH COMPARISON

Literature suggests that absorbance measurements of adenosine to be made at the λ_{max} (260 nm) (Goyal and Dhawan, 2006; Swaraga et al., 2005; and Vijayalakshmi et al., 2009). However, for this research a wavelength of 280 nm was chosen based on the wavelength scans of chitosan, TPP, and adenosine (Figures A.1 – A.3) on a PharmaSpec UV-1700 ultraviolet-visible spectrophometer (Shimadzu, Kyoto, Japan). At 280 nm neither chitosan nor TPP obstruct with the absorbance readings of adenosine.

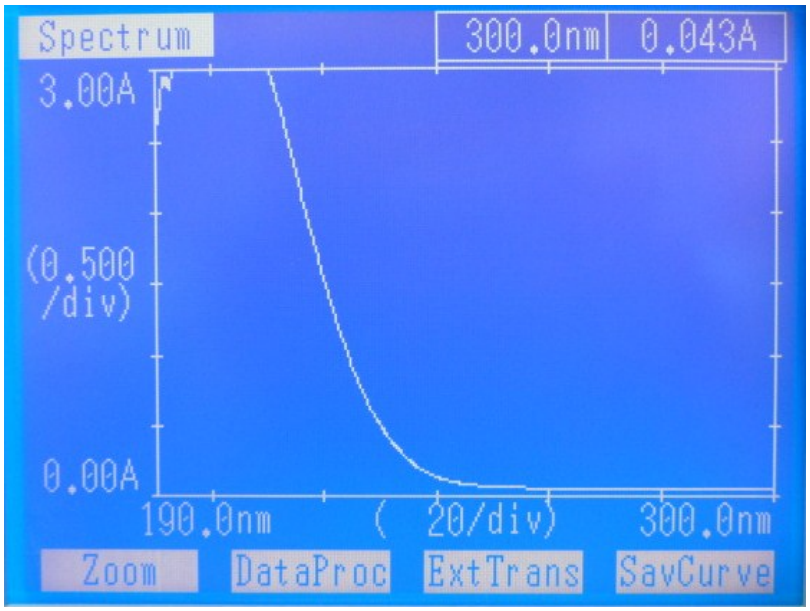

Figure A.1: UV-spectrophotometer wave length scan for chitosan solution.

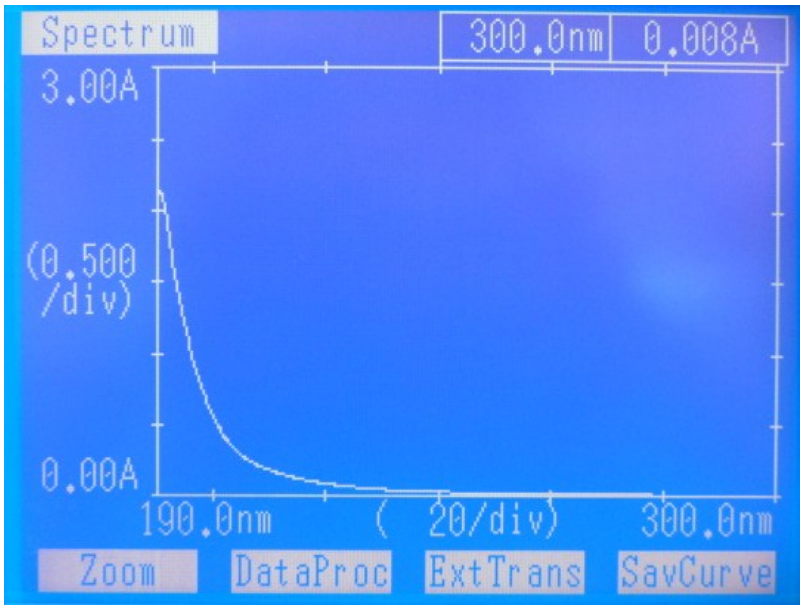

Figure A.2: UV-spectrophotometer wave length scan for TPP solution.

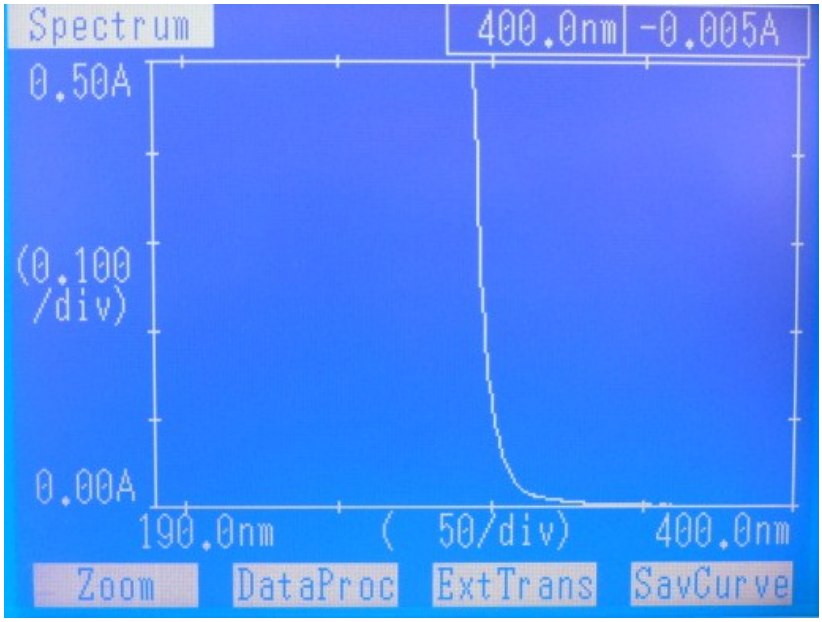

Figure A.3: UV-spectrophotometer wave length scan for Ad solution.

APPENDIX B: STANDARD CURVE- SUPERNATANT

UV-spectrophotometry was used to compute the concentration of adenosine in supernatant. The standard curve, UV absorbance against adenosine concentration, was acquired setting the UV wave length to 280 nm. A new standard curve was created for each entrapment/association experiment. Goof linear correlation was accomplished for each standard curve in the range of 0.00499 to 0.0373 mg/ml. An example of a regression equation established from one of the standard curves, Figure B.1, is: $y= 40.603 x + 0.1221$ ($R^2= 0.997$). The adenosine entrapment and association efficiency was then calculated based on the concentration of adenosine obtained.

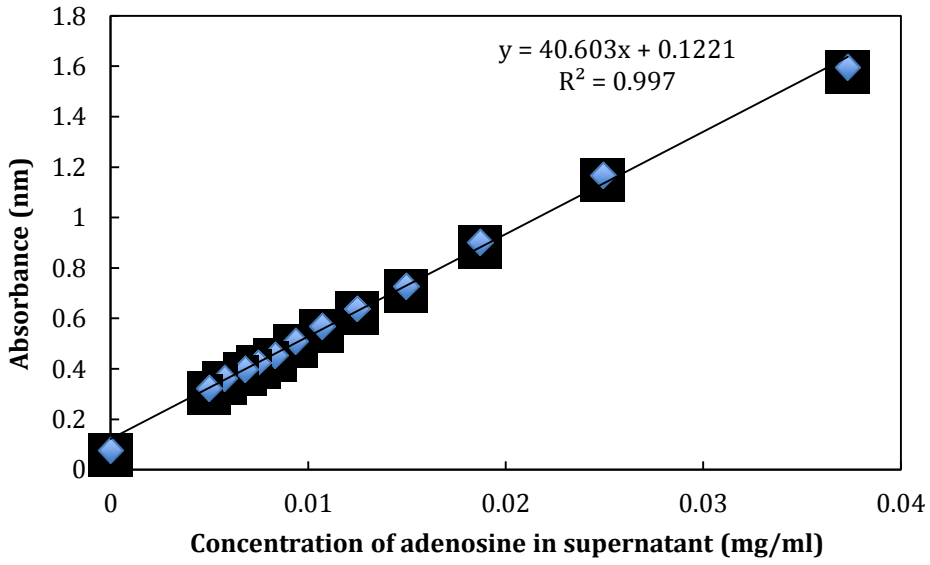

Figure B.1: Standard curve for adenosine in supernatant.

APPENDIX C: STANDARD CURVE- PBS

UV-spectrophotometry was also used to compute the concentration of adenosine in PBS solution. The standard curve, UV absorbance against adenosine concentration, was acquired setting the UV wave length to 280 nm. For each fresh batch of PBS solution a new standard curve was created. A good linear correlation was accomplished in the range of 0.00107 to 0.00624 mg/ml for all standard curves. An example of regression equation for one of the curves (Figure C.2) is: y= 39.2 x + 0.0537 (R^2= 0.9998). The amount of adenosine released was then calculated based on the concentration of adenosine obtained.

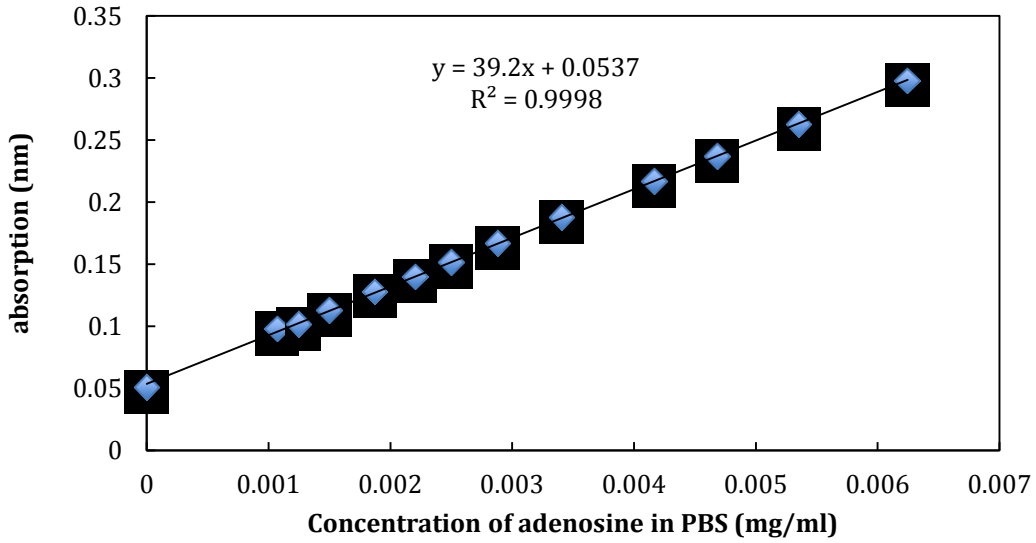

Figure C.1: Standard curve for adenosine in PBS.

APPENDIX D: LIQUID QUANTATIVE NMR DATA

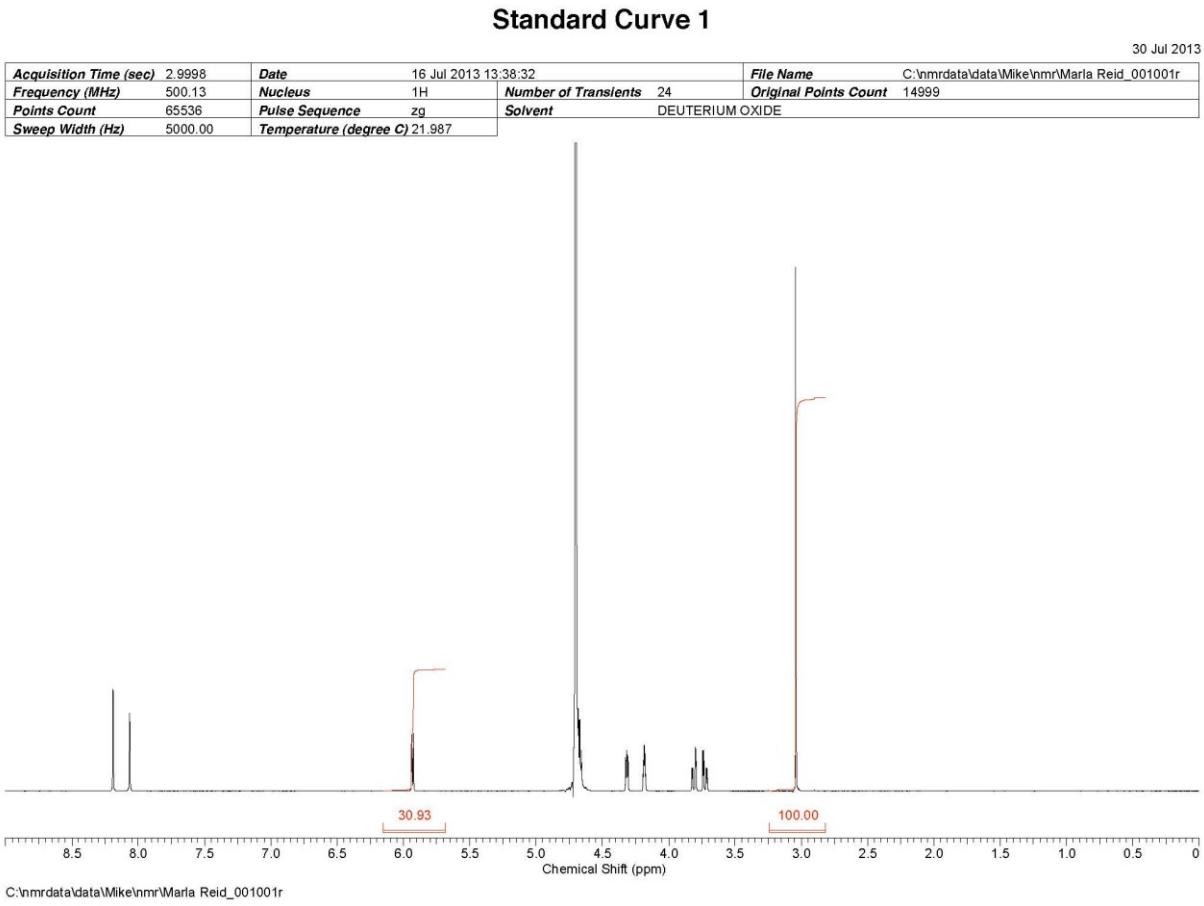

Figure D.1: Proton qNMR spectra for 10 mmol/l initial Ad loading in supernatant.

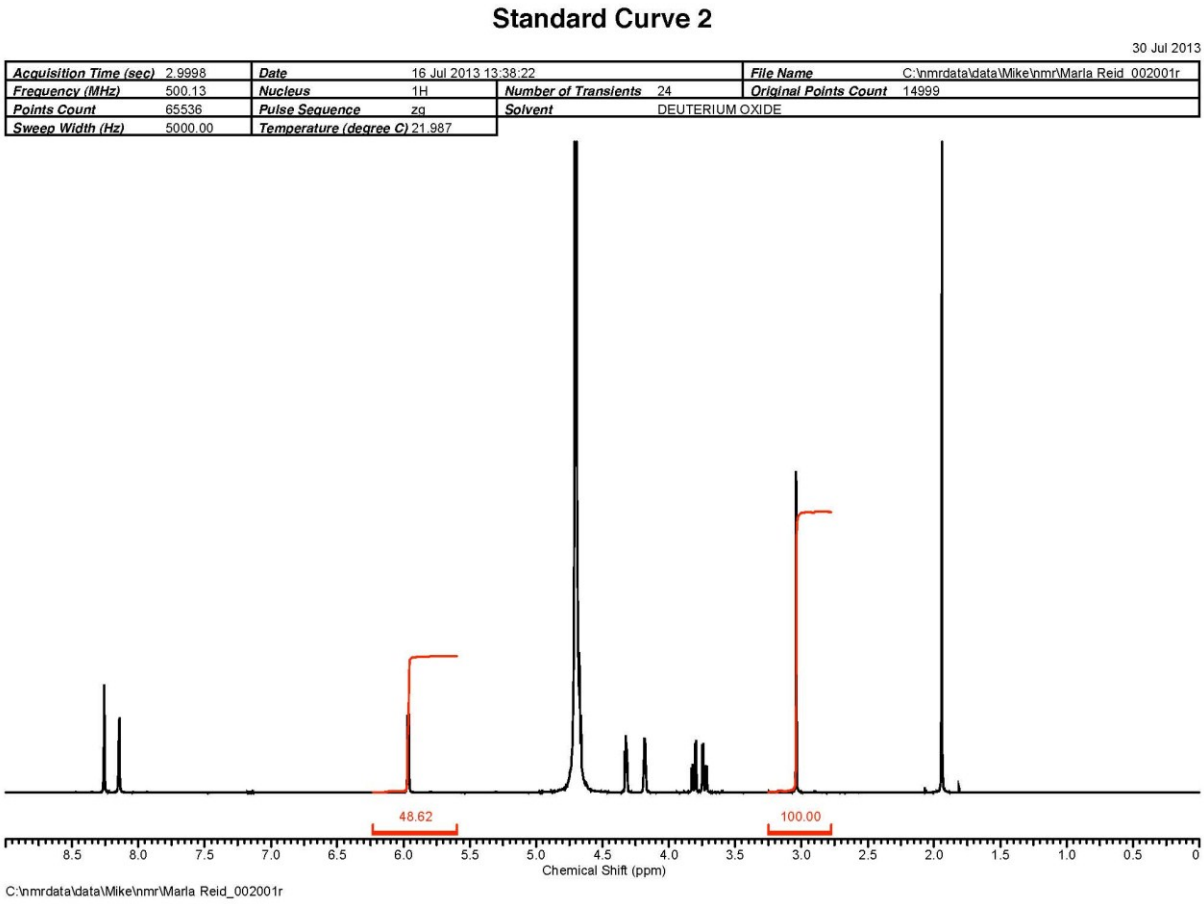

Figure D.2: Proton qNMR spectra for 6.7 mmol/l initial Ad loading in supernatant.

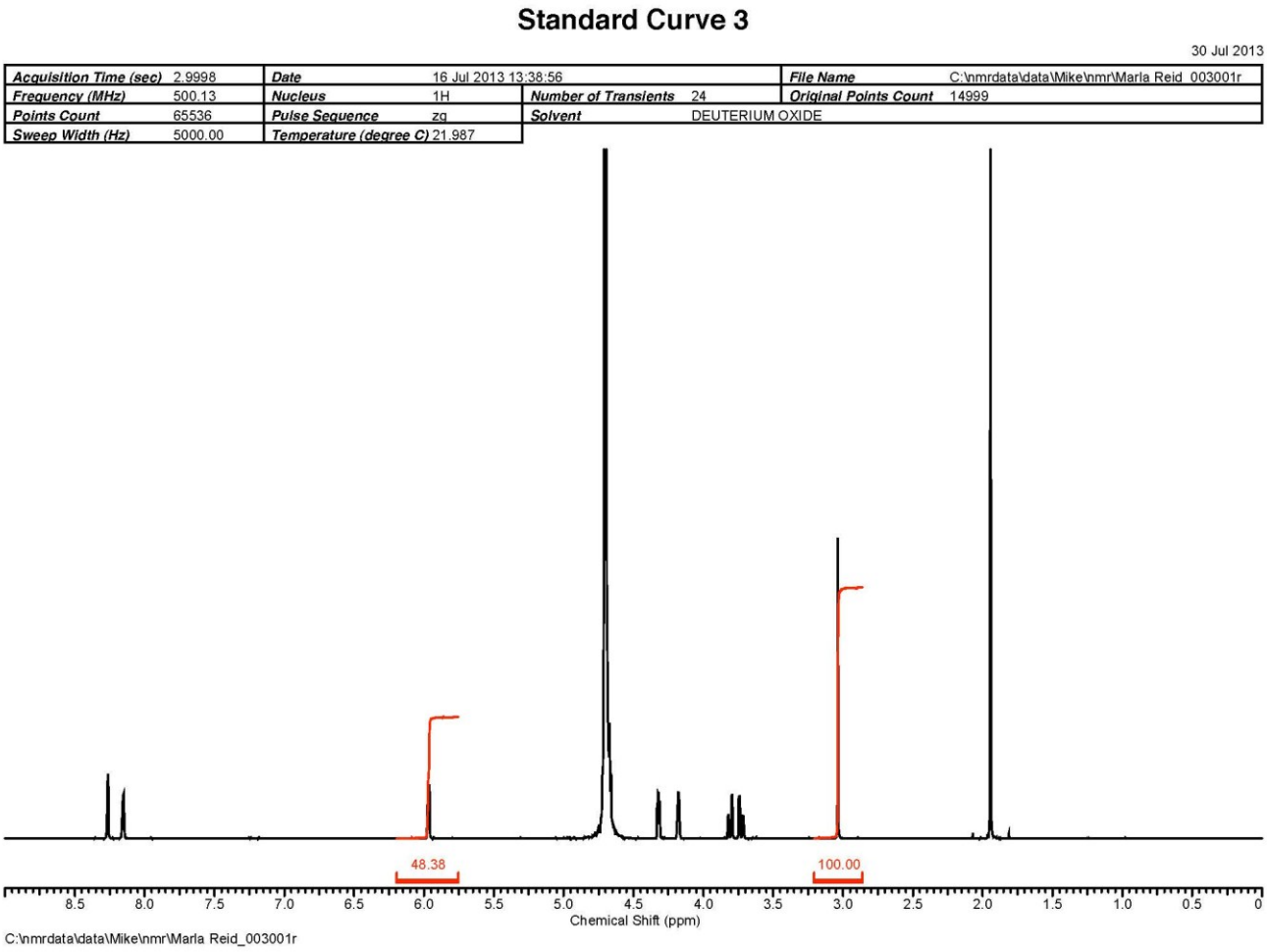

Figure D.3: Proton qNMR spectra for 5.6 mmol/l initial Ad loading in supernatant.

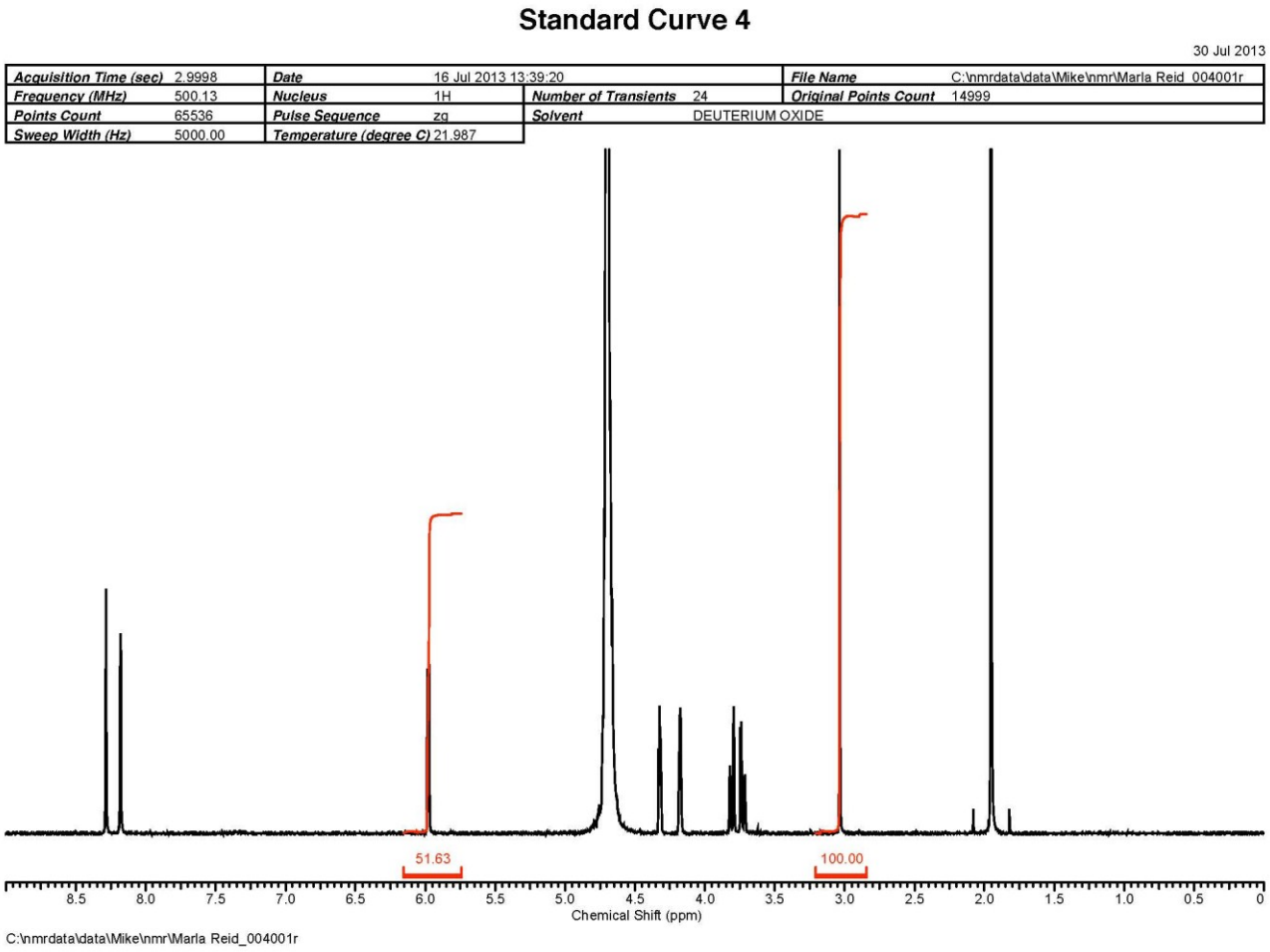

Figure D.4: Proton qNMR spectra for 2.8 mmol/l initial Ad loading in supernatant.

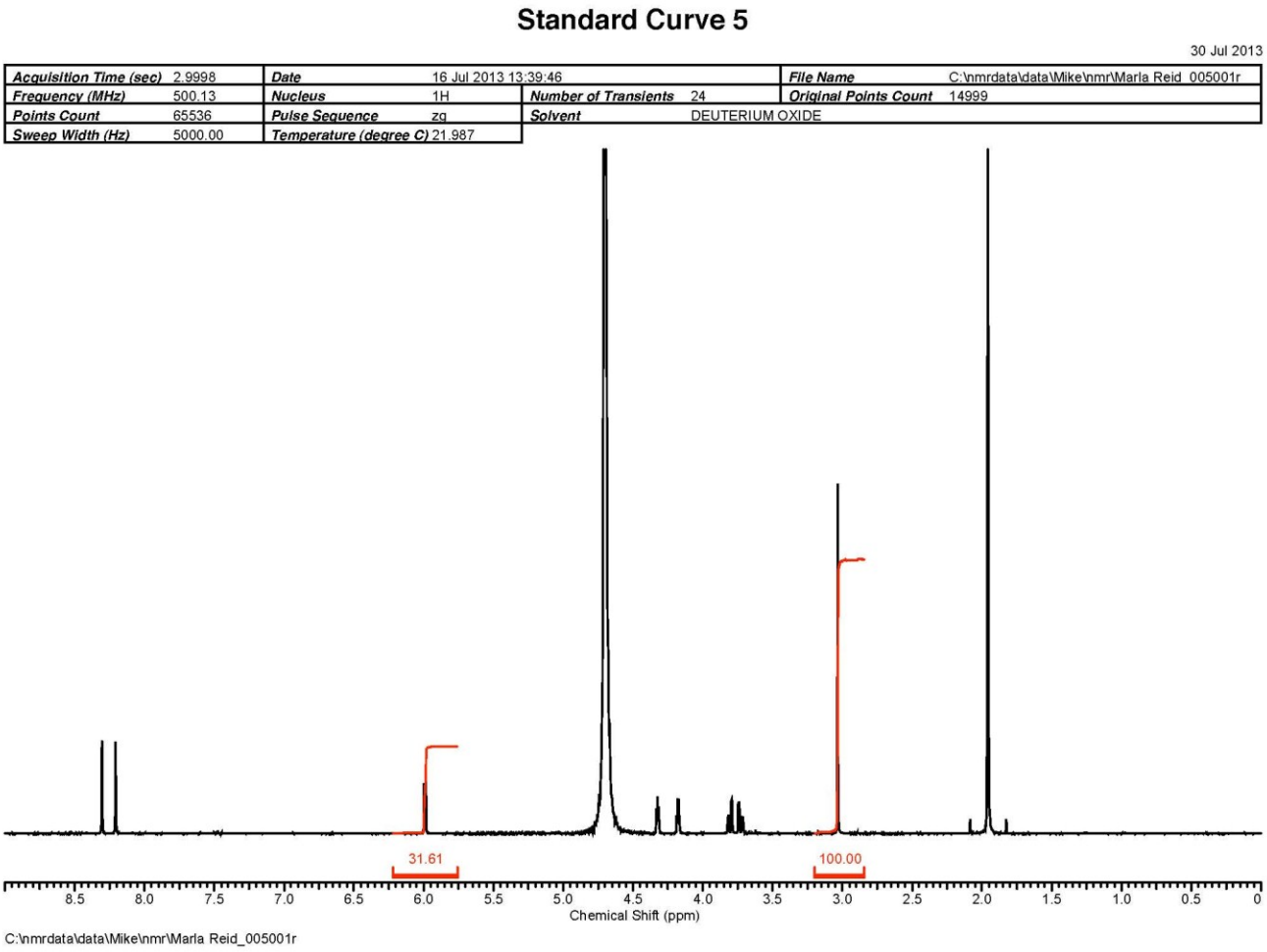

Figure D.5: Proton qNMR spectra for 1 mmol/l initial Ad loading in supernatant.

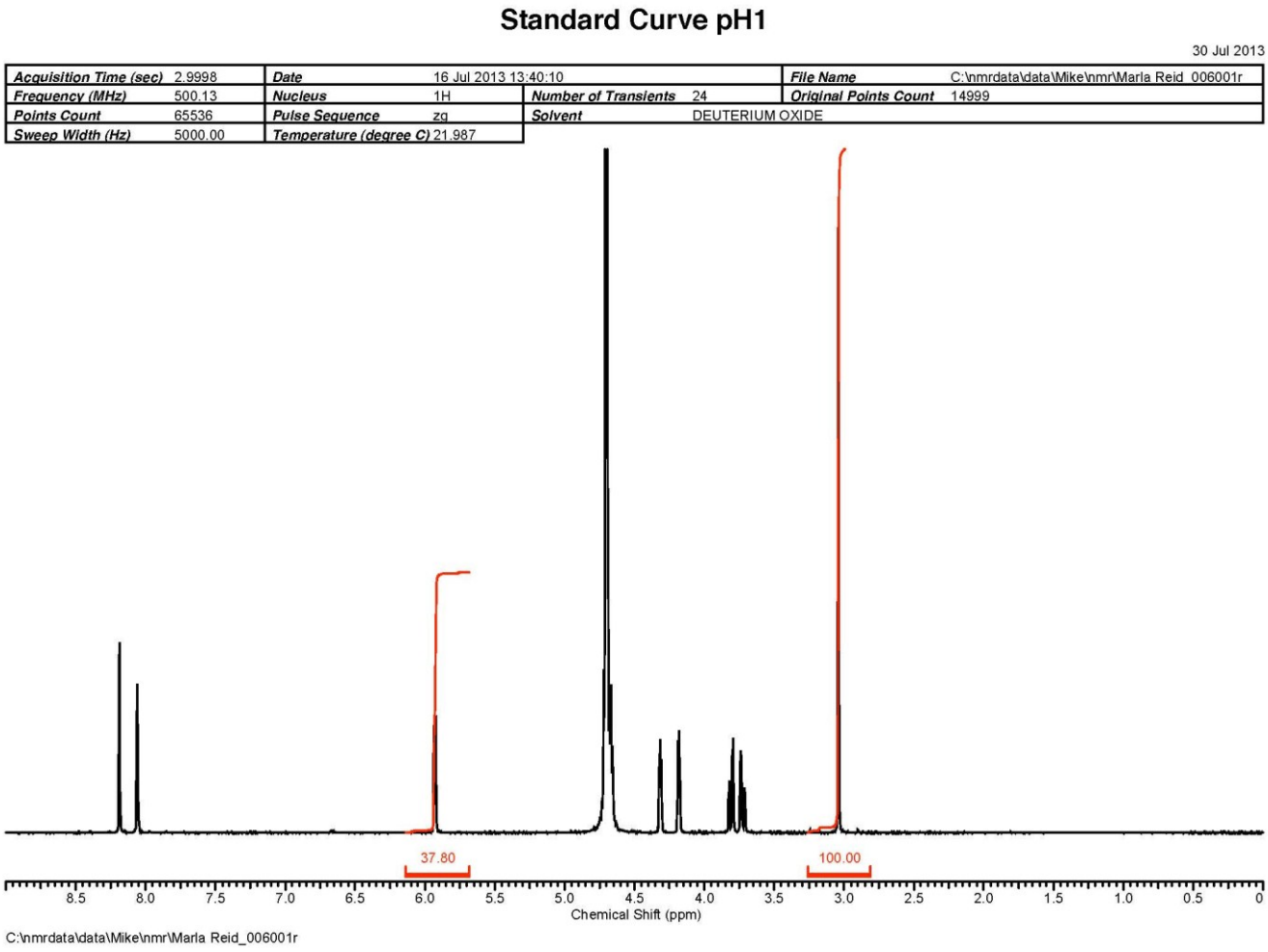

Figure D.6: Proton qNMR spectra for 10 mmol/l initial Ad loading in supernatant with pH change.

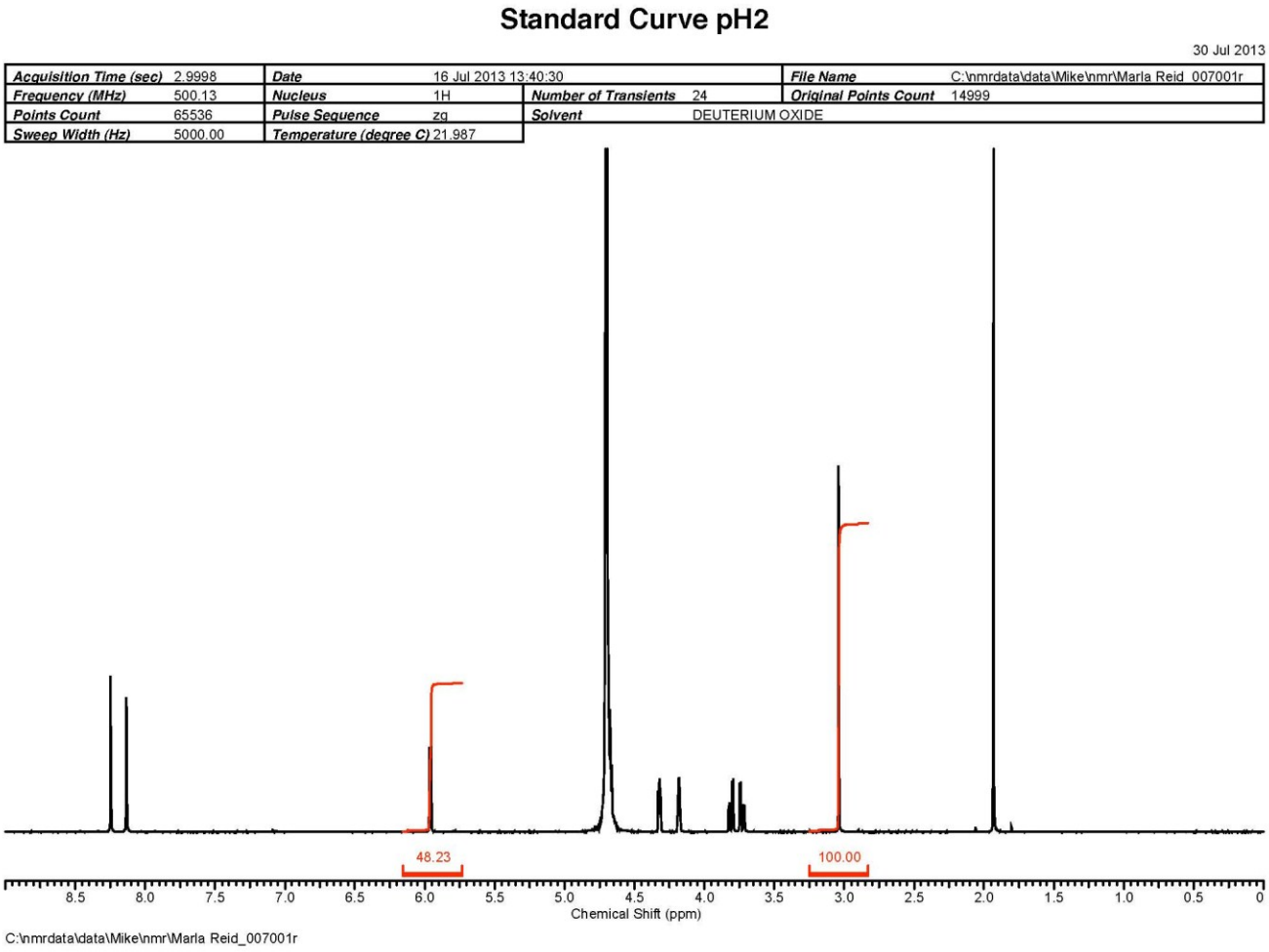

Figure D.7: Proton qNMR spectra for 6.7 mmol/l initial Ad loading in supernatant with pH change.

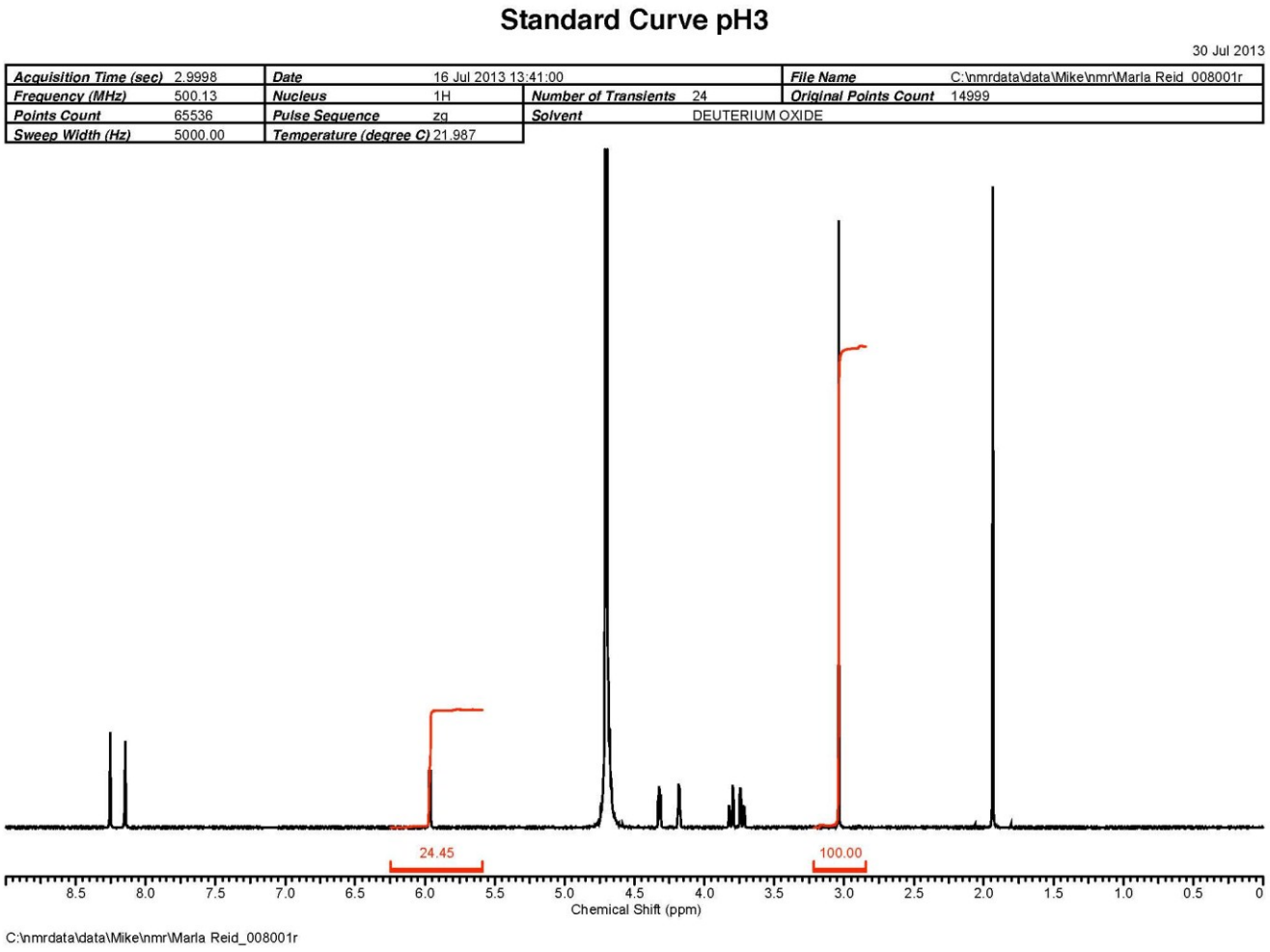

Figure D.8: Proton qNMR spectra for 5.6 mmol/l initial Ad loading in supernatant with pH change.

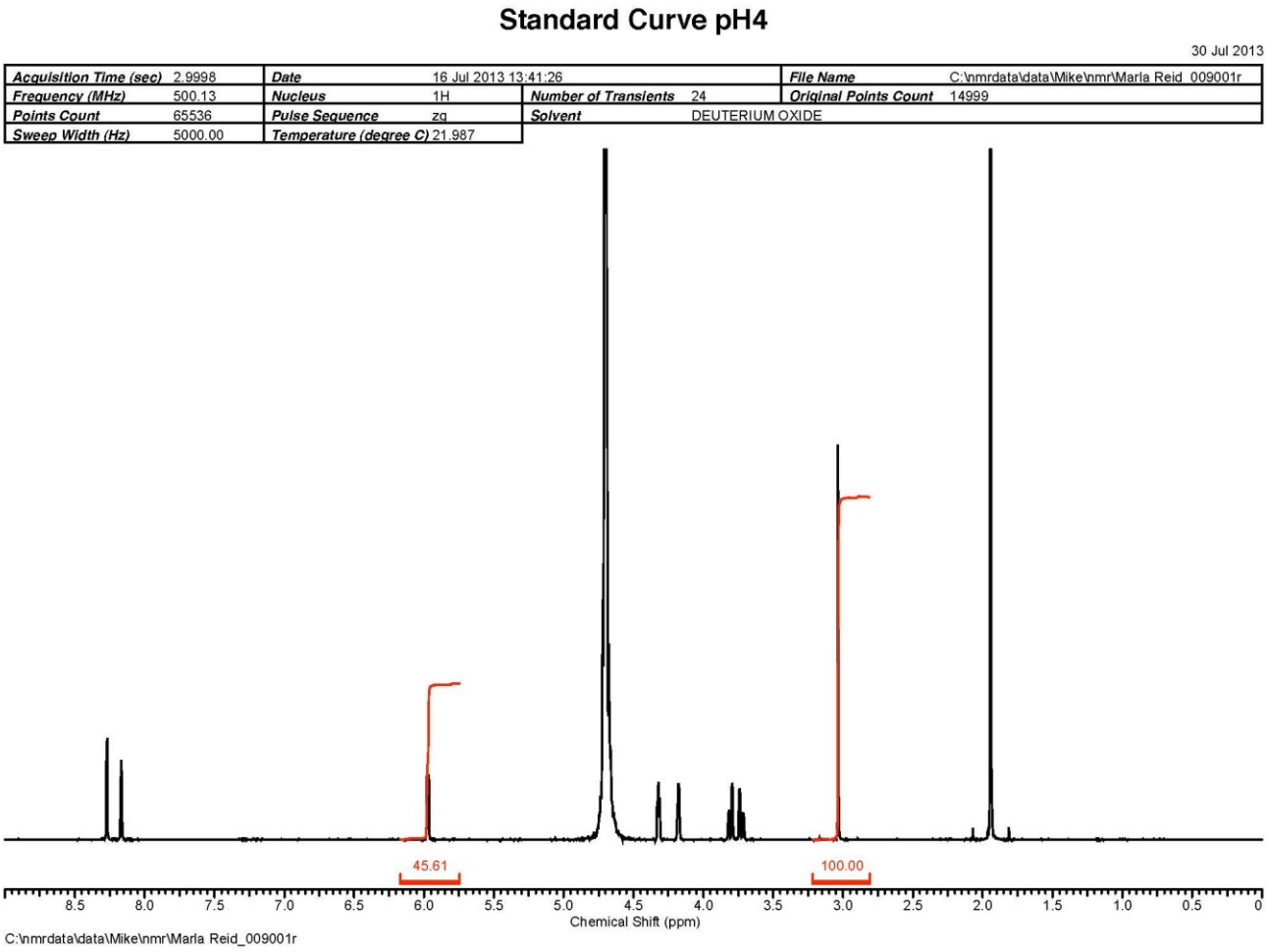

Figure D.9: Proton qNMR spectra for 2.8 mmol/l initial Ad loading in supernatant with pH change.

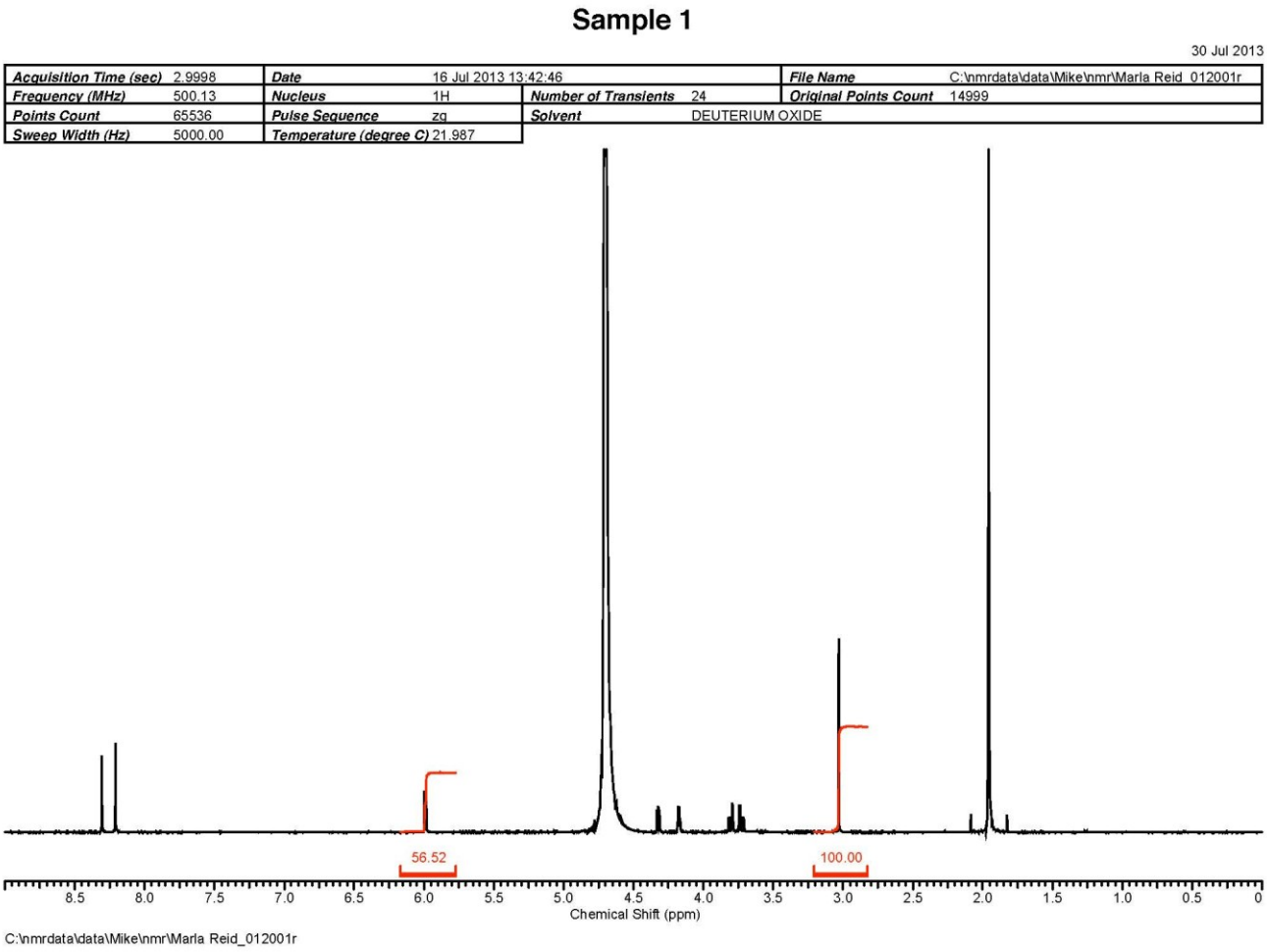

Figure D.10: Proton qNMR spectra- supernatant from adenosine loaded chitosan nanoparticles.

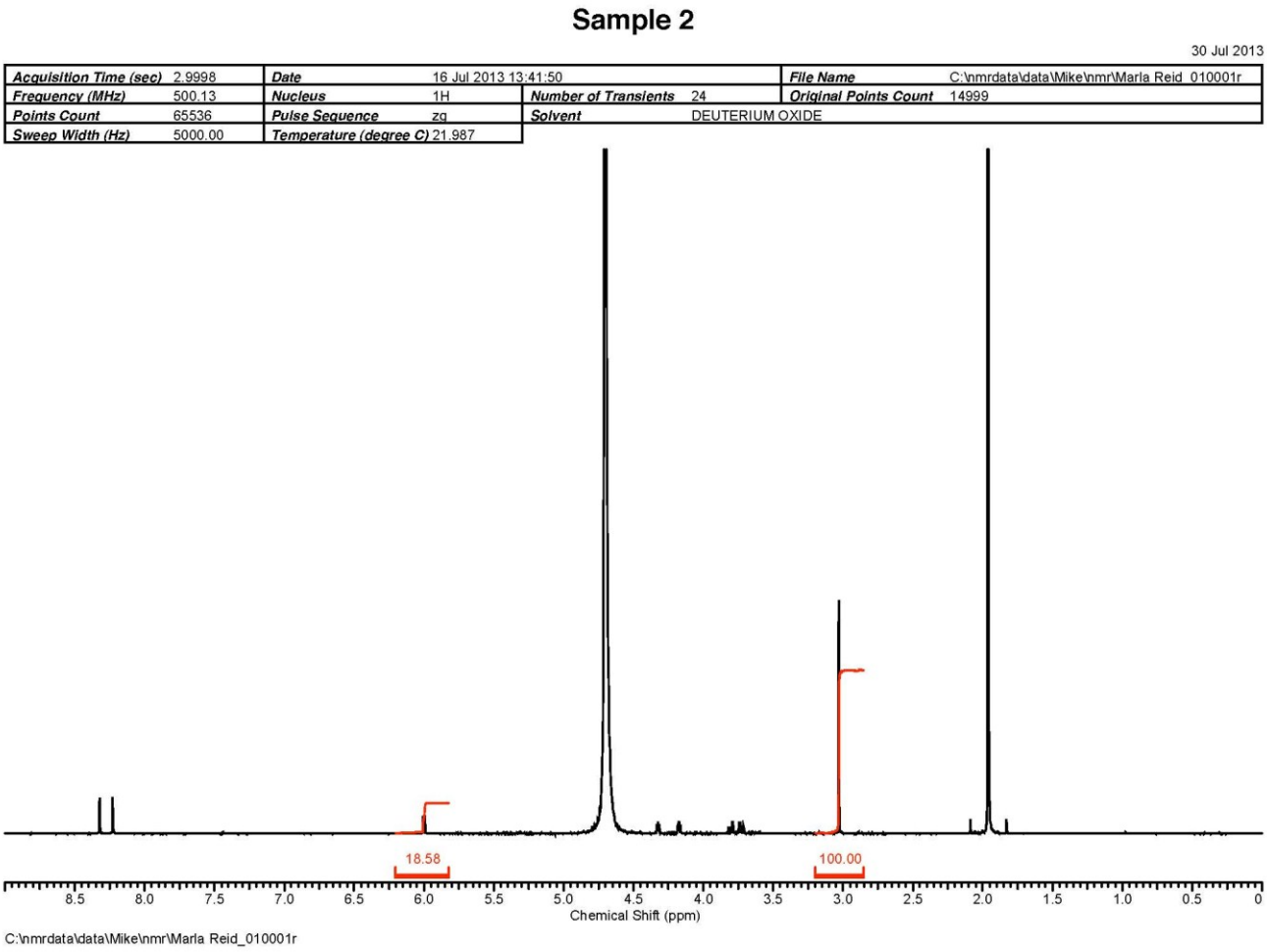

Figure D.11: Proton qNMR spectra- supernatant from adenosine loaded chitosan nanoparticles.

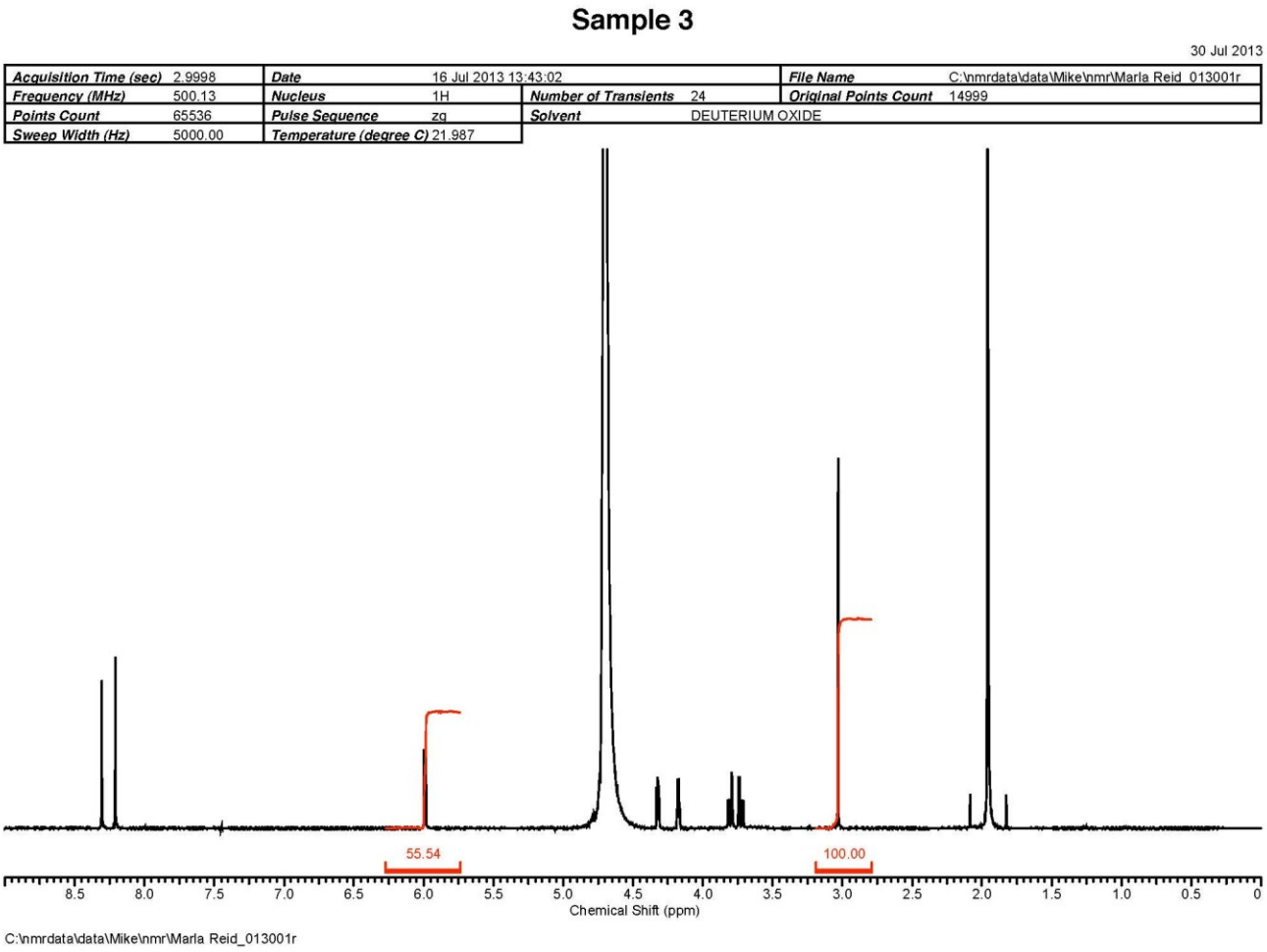

Figure D.12: Proton qNMR spectra- supernatant from adenosine loaded chitosan nanoparticles.

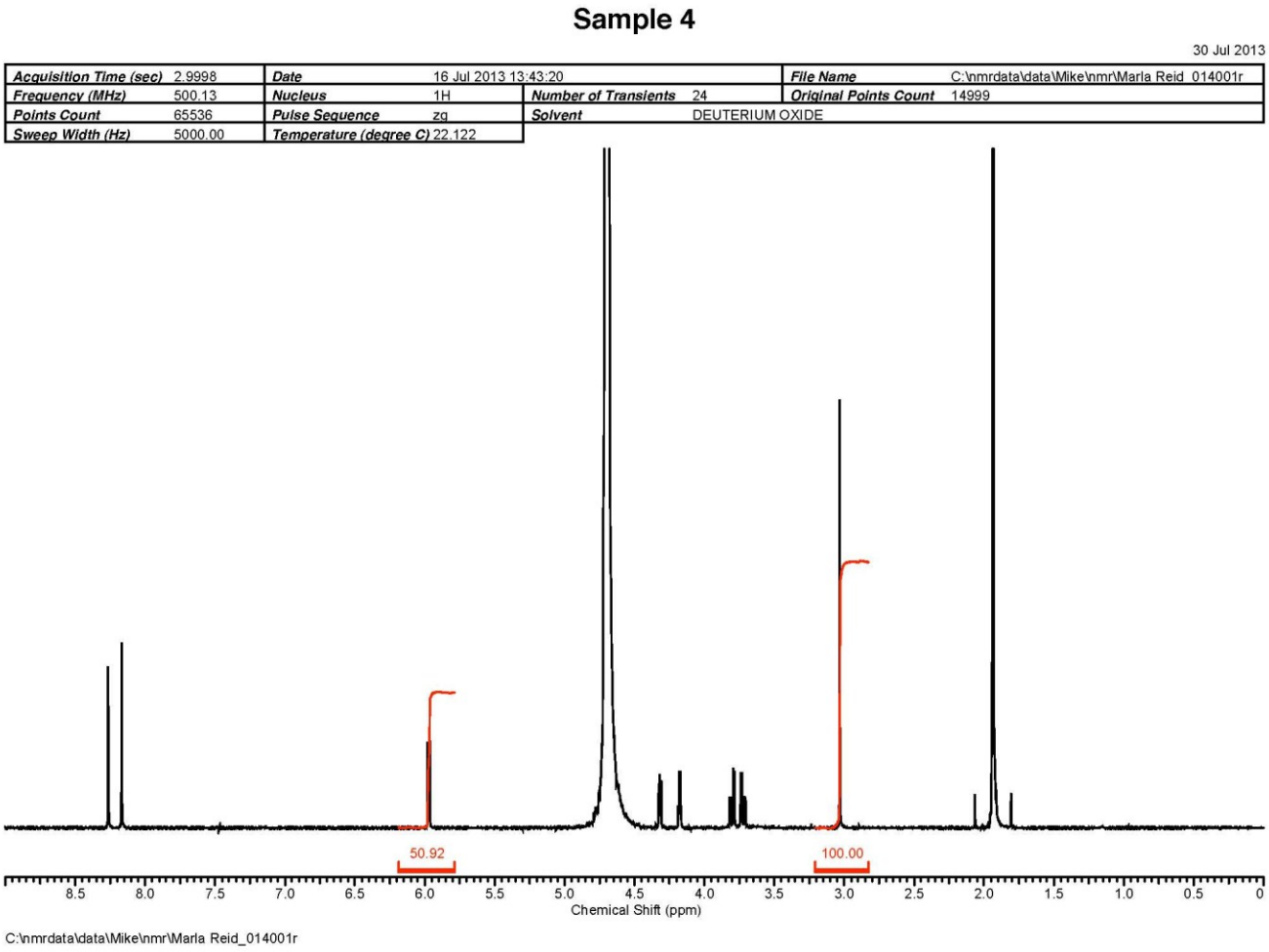

Figure D.13: Proton qNMR spectra- supernatant from adenosine loaded chitosan nanoparticles with pH change.

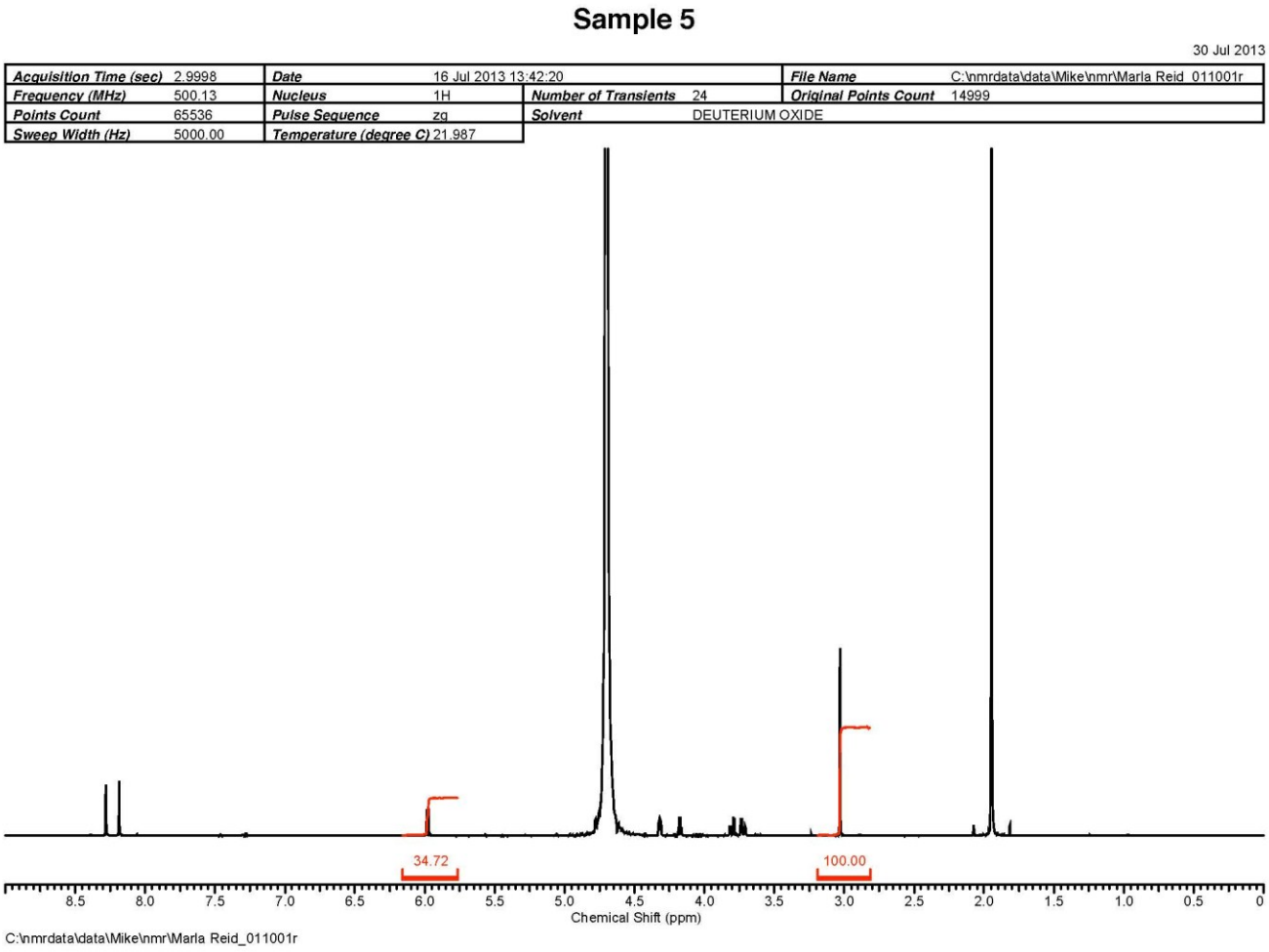

Figure D.14: Proton qNMR spectra- supernatant from adenosine loaded chitosan nanoparticles with pH change.

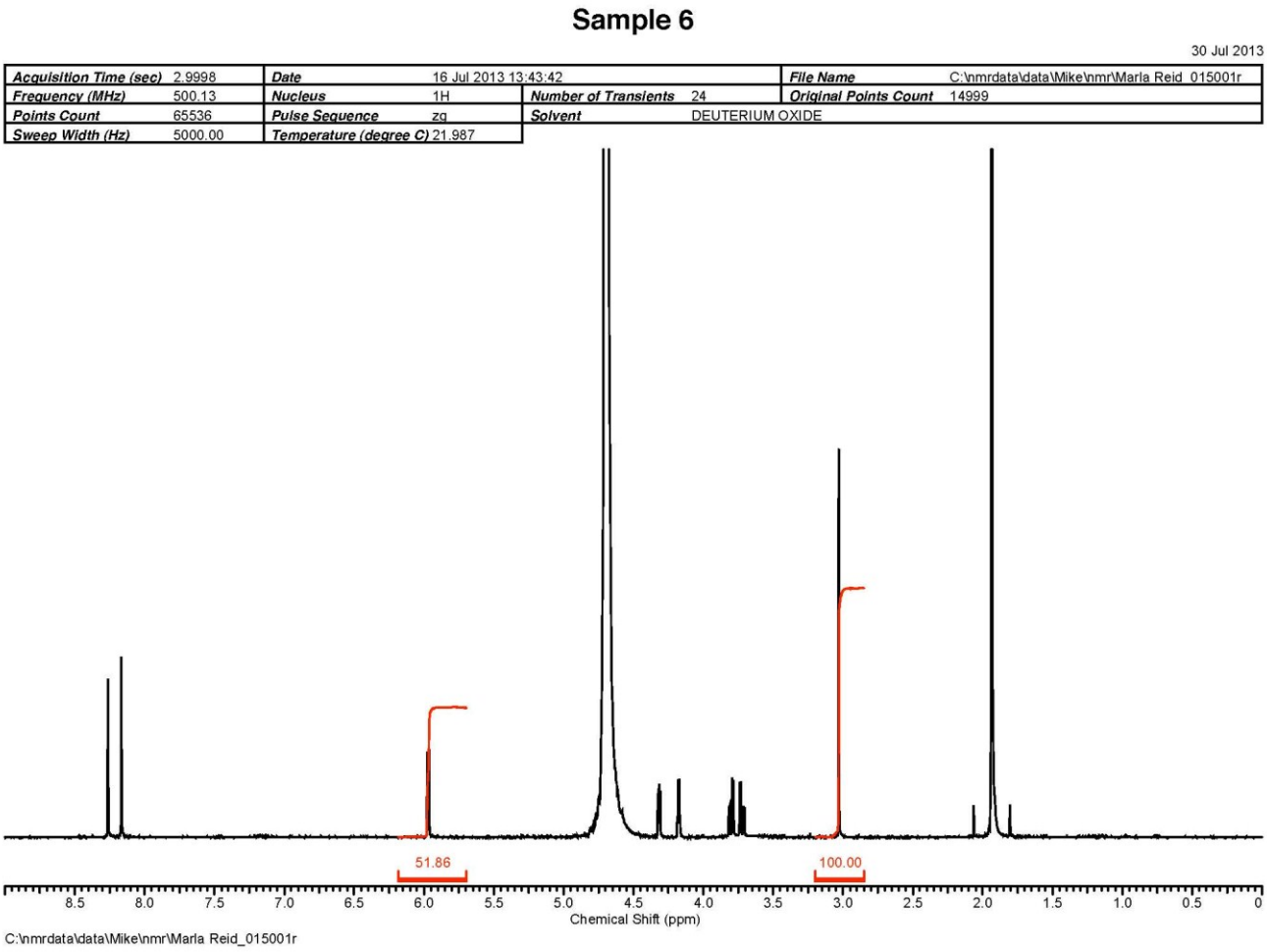

Figure D.15: Proton qNMR spectra- supernatant from adenosine loaded chitosan nanoparticles with pH change.

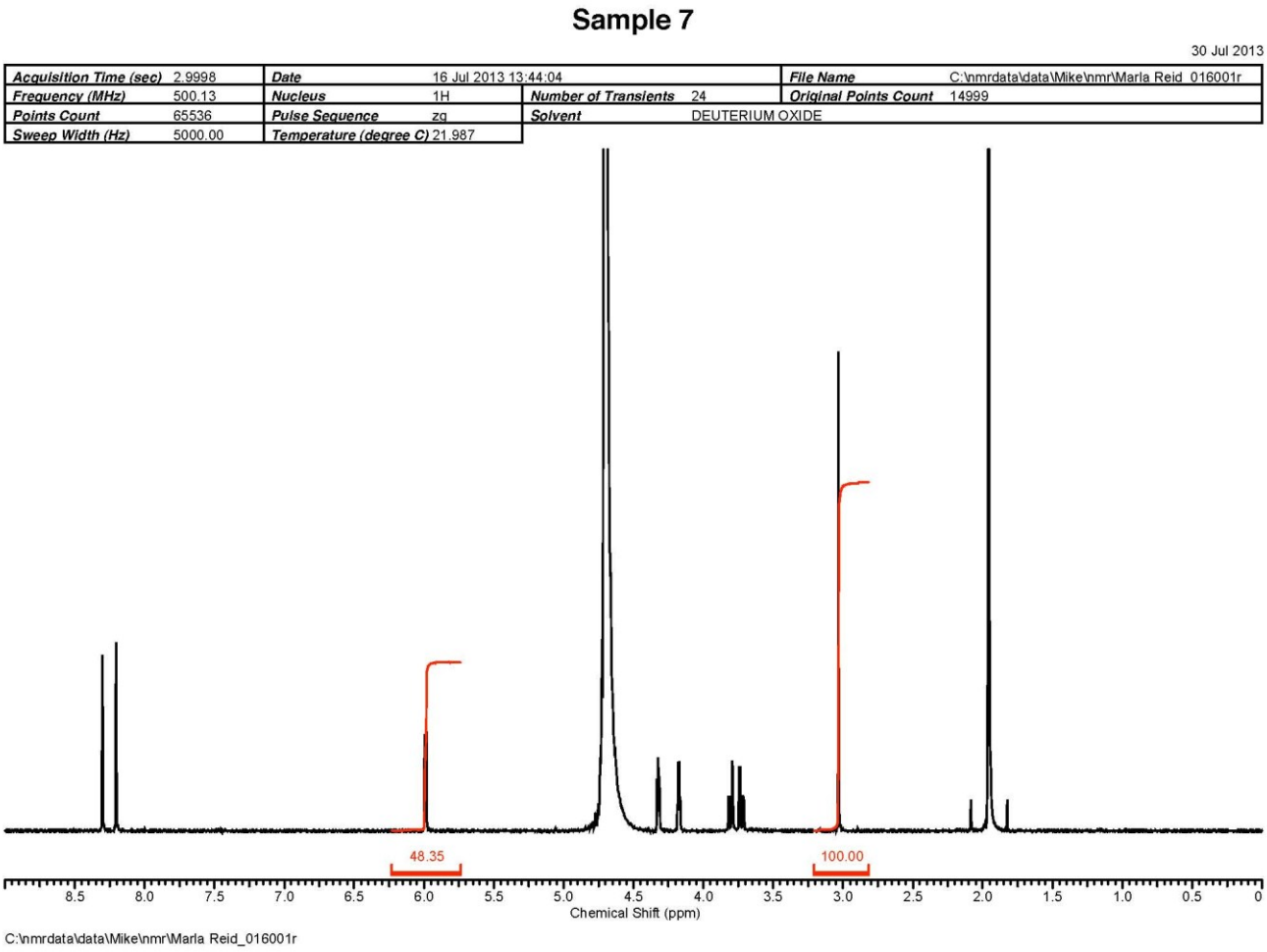

Figure D.16: Proton qNMR spectra- supernatant from adenosine loaded chitosan nanoparticles with pH change.

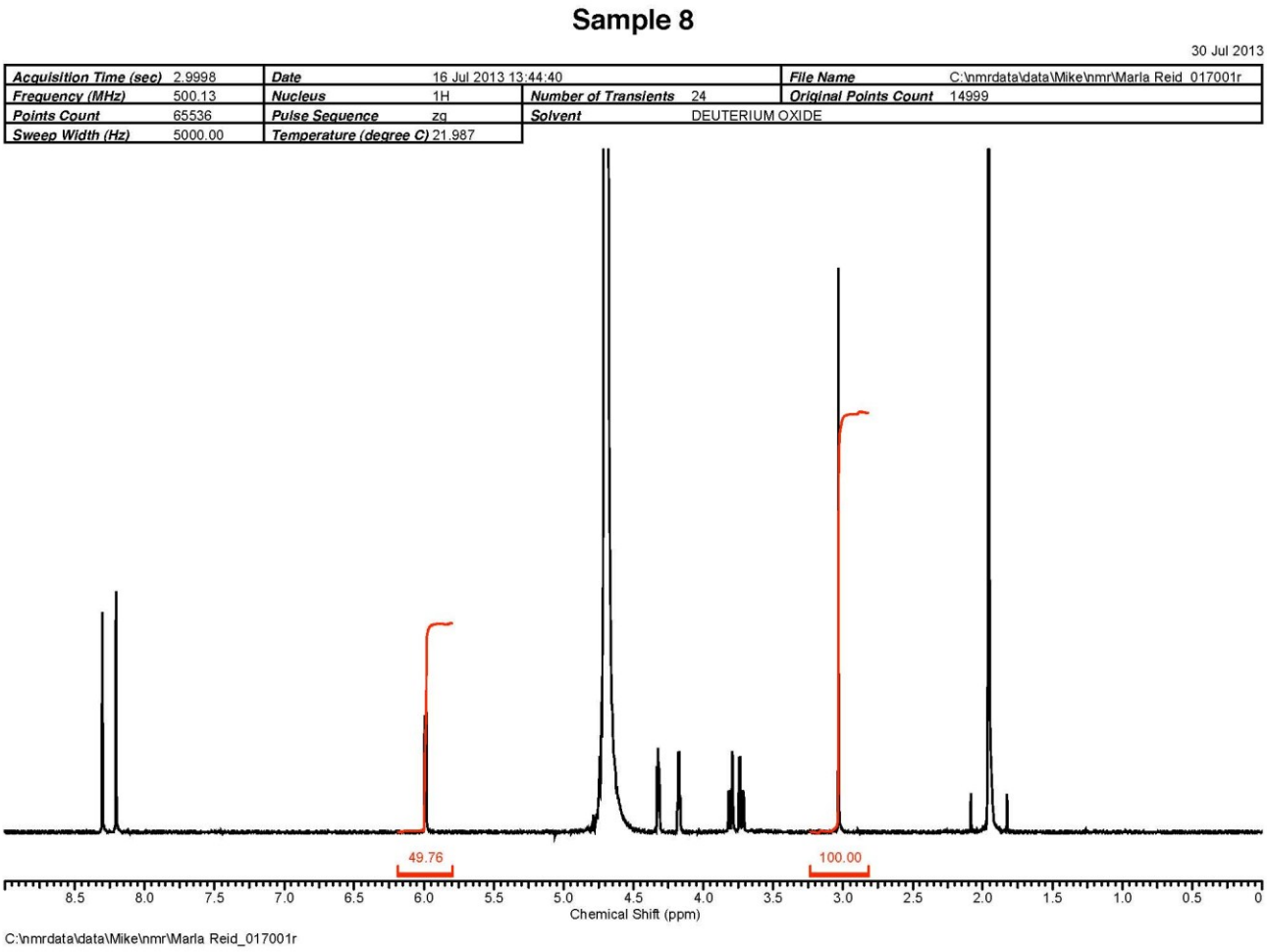

Figure D.17: Proton qNMR spectra- supernatant from adenosine loaded chitosan nanoparticles with pH change.

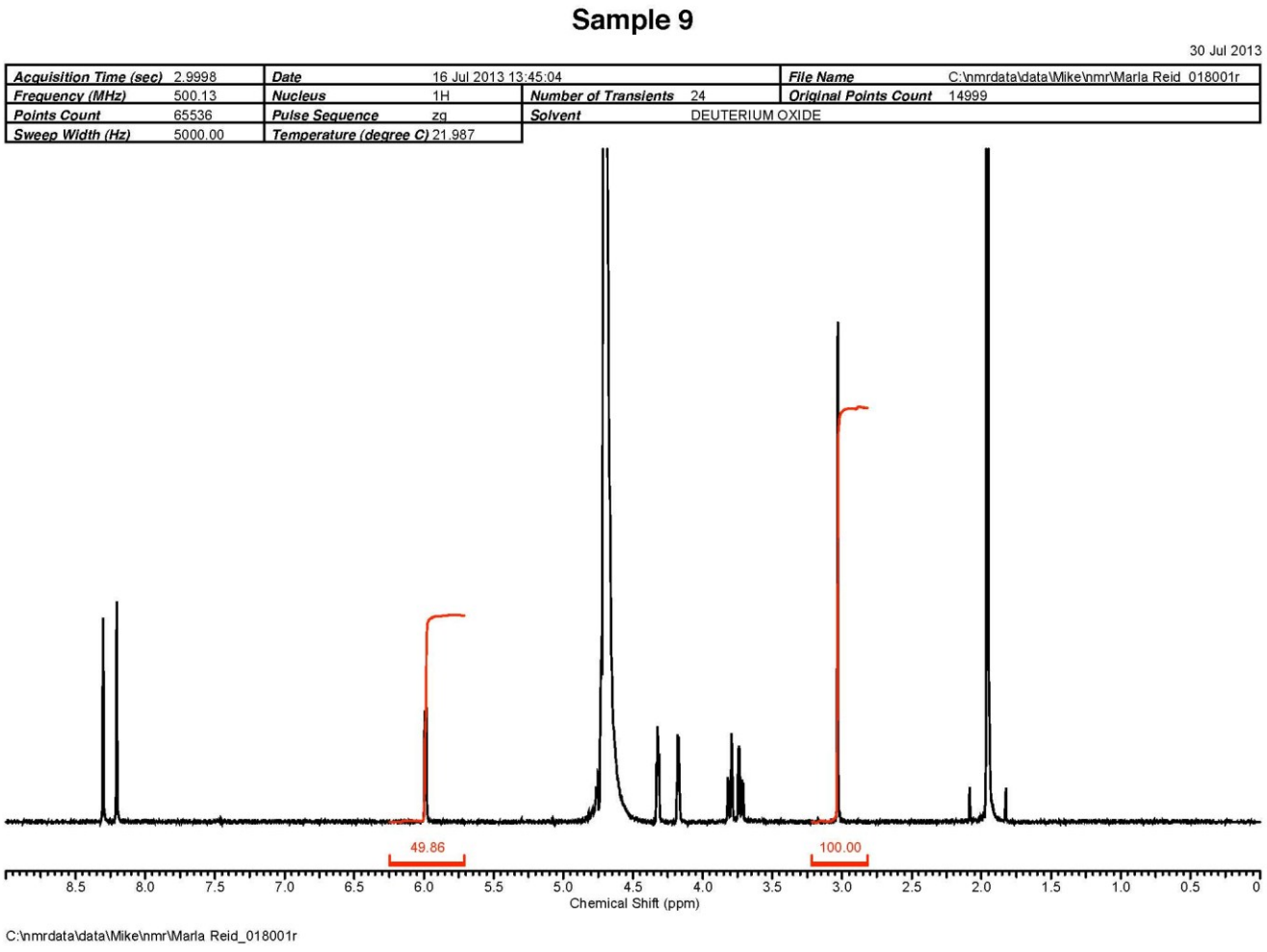

Figure D.18: Proton qNMR spectra- supernatant from adenosine loaded chitosan nanoparticles with pH change.

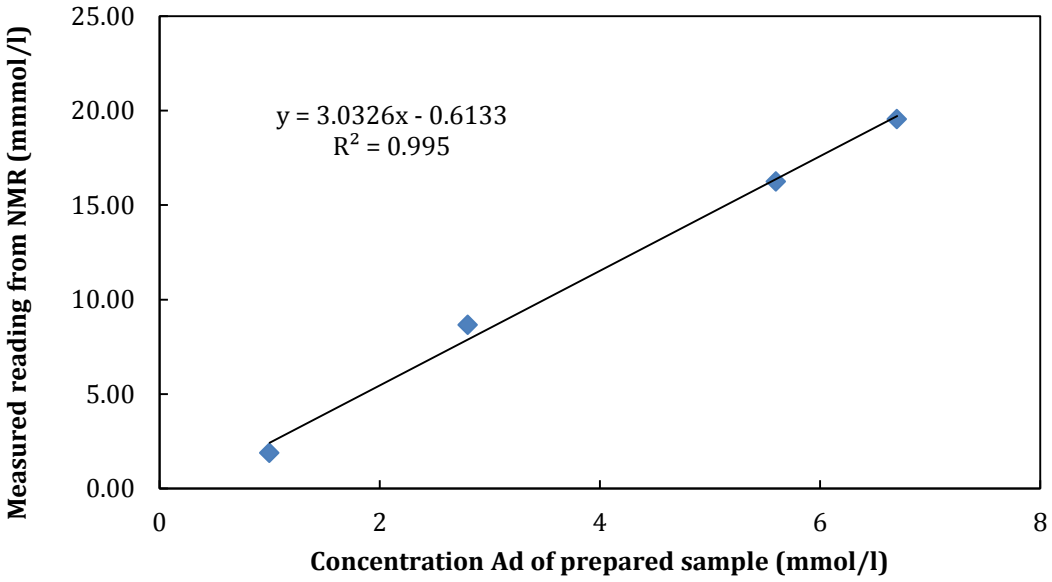

Figure D.19: Standard curve for adenosine in supernatant- found using NMR data.

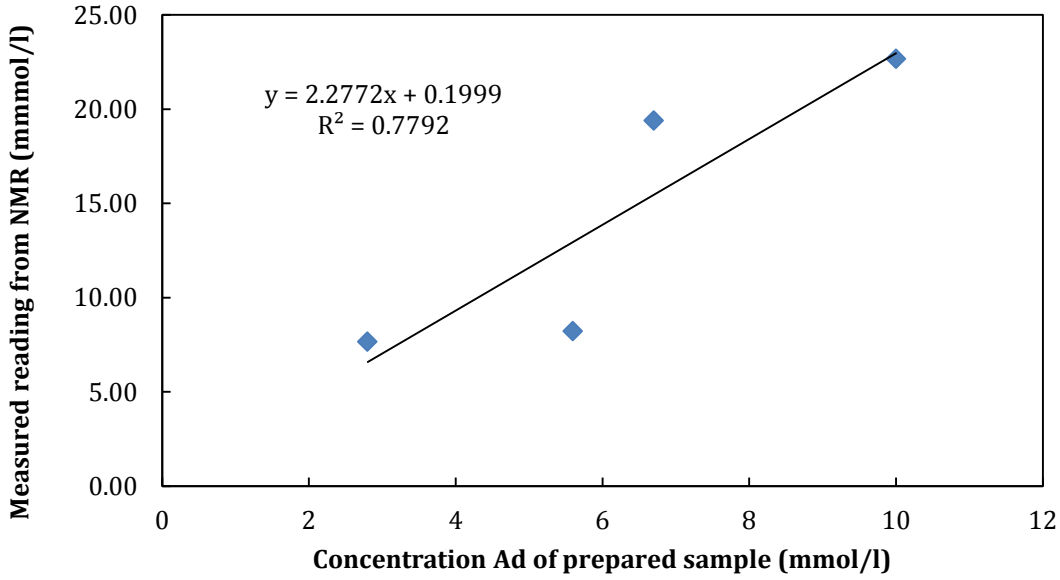

Figure D.20: Standard curve for adenosine in supernatant with pH change to 4.20- found using NMR data.

APPENDIX E: CHITOSAN PRECIPITATION- PH TEST

An experiment was conducted to observe the effect pH has on the precipitation of chitosan in solution. To alter the pH, NaOH was added drop wise to 50 ml of chitosan (1mg/mL) solution and the results were visually observed and recorded in Table E.1. Chitosan solution can be altered to 4.2 before observable precipitate is formed.

Table E.1: Observations from pH change of chitosan.

pH of chitosan solution	Observations
3.35	starting pH, no changes made
4	no change in solution appearance
4.2	no change in solution appearance
4.7	visible particles form
4.9	more visible particles form, solution more viscous
5.5	larger particles form (could be aggregation)
6.5	solution becomes cloudy from particles in suspension
10	lots of large particles in suspension, solution very cloudy

APPENDIX F: RAW DATA

Table F.1: Raw data for entrapment efficiency for 16% initial Ad loading entrapped nanoparticles.

mass of Ad loaded (mg)	Abs	Concentration (mg/ml) from standard curve	Diluent Volume (ml)	Supernatant Volume (mL)	Total Volume (ml)	Mass of Ad in supernatant and diluent solution (mg)	Concentration of Ad in 0.5 mL sample of supernatant (mg/mL)	mass of Ad in total supernatant sample in centrifuge test tube(mg)	Mass of Ad entrapped	Efficiency (%)
2.25	0.29	0.0031	3	0.5	3.5	0.0110	0.0219	0.66	1.59	70.75
2.25	0.28	0.0030	3	0.5	3.5	0.0105	0.0209	0.63	1.62	72.13
2.25	0.3	0.0032	3	0.5	3.5	0.0112	0.0225	0.67	1.58	70.02
2.25	0.29	0.0029	3	0.5	3.5	0.0103	0.0206	0.62	1.63	72.49
2.25	0.28	0.0032	3	0.5	3.5	0.0113	0.0225	0.68	1.57	69.94
2.25	0.27	0.0030	3	0.5	3.5	0.0105	0.0211	0.63	1.62	71.88
2.25	0.24	0.0035	3	0.5	3.5	0.0123	0.0246	0.74	1.51	67.14
2.25	0.26	0.0034	3	0.5	3.5	0.0119	0.0238	0.71	1.54	68.27
2.25	0.38	0.0053	3	0.5	3.5	0.0186	0.0372	1.12	1.13	50.42
2.25	0.28	0.0033	3	0.5	3.5	0.0115	0.0230	0.69	1.56	69.32
2.25	0.28	0.0031	3	0.5	3.5	0.0107	0.0214	0.64	1.61	71.50
2.25	0.32	0.0031	3	0.5	3.5	0.0108	0.0217	0.65	1.60	71.09
2.25	0.31	0.0030	3	0.5	3.5	0.0104	0.0207	0.62	1.63	72.40
2.25	0.19	0.0020	3	0.5	3.5	0.0072	0.0143	0.43	1.82	80.91
2.25	0.17	0.0017	3	0.5	3.5	0.0060	0.0120	0.36	1.89	83.98
2.25	0.19	0.0021	3	0.5	3.5	0.0072	0.0144	0.43	1.82	80.78
2.25	0.2	0.0023	3	0.5	3.5	0.0081	0.0163	0.49	1.76	78.32
2.25	0.21	0.0022	3	0.5	3.5	0.0077	0.0154	0.46	1.79	79.45
2.25	0.2	0.0021	3	0.5	3.5	0.0074	0.0149	0.45	1.80	80.14
2.25	0.3	0.0039	5	0.5	3.5	0.0135	0.0270	0.81	1.44	63.98

Table F.2: Raw data for entrapment efficiency for 39% initial Ad loading entrapped nanoparticles.

Mass of Ad loaded (mg)	Abs	Concentration (mg/ml) from standard curve	Diluent Volume (ml)	Supernatant Volume (mL)	Total Volume (ml)	Mass of Ad in supernatant and diluent solution (mg)	Concentration of Ad in 0.5 mL sample of supernatant (mg/mL)	Mass of Ad in total supernatant sample in centrifuge test tube (mg)	Mass of Ad entrapped	Efficiency (%)
22.5	0.77	0.0134	5	0.5	5.5	0.0739	0.1477	4.43	18.07	80.31
22.5	0.77	0.0135	5	0.5	5.5	0.0743	0.1487	4.46	18.04	80.18
22.5	0.72	0.0131	5	0.5	5.5	0.0720	0.1440	4.32	18.18	80.80
22.5	0.7	0.0128	5	0.5	5.5	0.0705	0.1410	4.23	18.27	81.19
22.5	0.77	0.0151	5	0.5	5.5	0.0832	0.1664	4.99	17.51	77.81
22.5	0.73	0.0142	5	0.5	5.5	0.0780	0.1560	4.68	17.82	79.20
22.5	0.7	0.0120	5	0.5	5.5	0.0658	0.1316	3.95	18.55	82.45
22.5	0.71	0.0122	5	0.5	5.5	0.0669	0.1338	4.01	18.49	82.17
22.5	0.72	0.0133	5	0.5	5.5	0.0734	0.1468	4.40	18.10	80.43
22.5	0.76	0.0141	5	0.5	5.5	0.0777	0.1555	4.66	17.84	79.27
22.5	0.72	0.0141	5	0.5	5.5	0.0775	0.1550	4.65	17.85	79.34
22.5	0.76	0.0150	5	0.5	5.5	0.0825	0.1649	4.95	17.55	78.01
22.5	0.82	0.0159	5	0.5	5.5	0.0872	0.1744	5.23	17.27	76.75
22.5	0.81	0.0155	5	0.5	5.5	0.0855	0.1710	5.13	17.37	77.20
22.5	0.73	0.0150	5	0.5	5.5	0.0824	0.1647	4.94	17.56	78.04
22.5	0.77	0.0152	5	0.5	5.5	0.0835	0.1671	5.01	17.49	77.72
22.5	0.76	0.0149	5	0.5	5.5	0.0818	0.1636	4.91	17.59	78.19
22.5	0.73	0.0143	5	0.5	5.5	0.0789	0.1577	4.73	17.77	78.97
22.5	0.78	0.0153	5	0.5	5.5	0.0843	0.1687	5.06	17.44	77.51
22.5	0.72	0.0149	5	0.5	5.5	0.0819	0.1639	4.92	17.58	78.15
22.5	0.7	0.0144	5	0.5	5.5	0.0790	0.1580	4.74	17.76	78.93
22.5	0.71	0.0146	5	0.5	5.5	0.0804	0.1608	4.82	17.68	78.56
22.5	0.74	0.0141	5	0.5	5.5	0.0776	0.1552	4.66	17.84	79.30
22.5	0.69	0.0131	5	0.5	5.5	0.0720	0.1439	4.32	18.18	80.81
22.5	0.71	0.0134	5	0.5	5.5	0.0738	0.1475	4.43	18.07	80.33
22.5	0.75	0.0135	5	0.5	5.5	0.0743	0.1486	4.46	18.04	80.19
22.5	0.8	0.0147	5	0.5	5.5	0.0808	0.1616	4.85	17.65	78.45
22.5	0.75	0.0135	5	0.5	5.5	0.0743	0.1486	4.46	18.04	80.19
22.5	0.79	0.0152	5	0.5	5.5	0.0836	0.1672	5.02	17.48	77.71
22.5	0.8	0.0154	5	0.5	5.5	0.0848	0.1695	5.09	17.41	77.39
22.5	0.79	0.0152	5	0.5	5.5	0.0839	0.1677	5.03	17.47	77.64
22.5	0.71	0.0135	5	0.5	5.5	0.0743	0.1485	4.46	18.04	80.19
22.5	0.7	0.0133	5	0.5	5.5	0.0731	0.1462	4.39	18.11	80.50
22.5	0.72	0.0150	5	0.5	5.5	0.0826	0.1653	4.96	17.54	77.96
22.5	0.72	0.0149	5	0.5	5.5	0.0817	0.1634	4.90	17.60	78.22

22.5	0.63	0.0126	5	0.5	5.5	0.0693	0.1387	4.16	18.34	81.51
22.5	0.75	0.0145	5	0.5	5.5	0.0800	0.1600	4.80	17.70	78.66
22.5	0.75	0.0144	5	0.5	5.5	0.0790	0.1579	4.74	17.76	78.94
22.5	0.78	0.0166	5	0.5	5.5	0.0911	0.1822	5.47	17.03	75.70
22.5	0.77	0.0165	5	0.5	5.5	0.0907	0.1814	5.44	17.06	75.81
22.5	0.66	0.0132	5	0.5	5.5	0.0725	0.1450	4.35	18.15	80.67
22.5	0.69	0.0139	5	0.5	5.5	0.0766	0.1532	4.60		79.57

Table F.3: Raw data for entrapment efficiency for 56% initial Ad loading entrapped nanoparticles.

Mass of Ad loaded (mg)	Abs	Concentration (mg/ml) from standard curve	Diluent Volume (ml)	Supernatant Volume (mL)	Total Volume (ml)	Mass of Ad in supernatant and diluent solution (mg)	Concentration of Ad in 0.5 mL sample of supernatant (mg/mL)	Mass of Ad in total supernatant sample in centrifuge test tube (mg)	Mass of Ad entrapped	Efficiency (%)
45	1.25	0.0257	6	0.5	6.5	0.1668	0.3336	10.01	34.99	77.76
45	1.23	0.0251	6	0.5	6.5	0.1629	0.3258	9.77	35.23	78.28
45	1.21	0.0251	6	0.5	6.5	0.1634	0.3268	9.80	35.20	78.21
45	1.22	0.0253	6	0.5	6.5	0.1646	0.3292	9.88	35.12	78.05
45	1.22	0.0265	6	0.5	6.5	0.1720	0.3441	10.32	34.68	77.06
45	1.2	0.0260	6	0.5	6.5	0.1690	0.3380	10.14	34.86	77.47
45	1.37	0.0292	6	0.5	6.5	0.1895	0.3790	11.37	33.63	74.74
45	1.25	0.0260	6	0.5	6.5	0.1691	0.3382	10.15	34.85	77.45
45	1.18	0.0266	6	0.5	6.5	0.1730	0.3459	10.38	34.62	76.94
45	1.31	0.0275	6	0.5	6.5	0.1789	0.3579	10.74	34.26	76.14
45	1.31	0.0274	6	0.5	6.5	0.1779	0.3558	10.67	34.33	76.28
45	1.11	0.0188	6	0.5	6.5	0.1221	0.2442	7.33	37.67	83.72
45	1.35	0.0236	6	0.5	6.5	0.1533	0.3065	9.20	35.80	79.57
45	1.16	0.0259	6	0.5	6.5	0.1686	0.3373	10.12	34.88	77.51
45	1.2	0.0270	6	0.5	6.5	0.1755	0.3510	10.53	34.47	76.60
45	1.24	0.0253	6	0.5	6.5	0.1641	0.3283	9.85	35.15	78.12
45	1.31	0.0266	6	0.5	6.5	0.1731	0.3462	10.39	34.61	76.92
45	1.05	0.0210	6	0.5	6.5	0.1367	0.2734	8.20	36.80	81.77
45	1.12	0.0225	6	0.5	6.5	0.1461	0.2923	8.77	36.23	80.52
45	1.21	0.0271	6	0.5	6.5	0.1761	0.3522	10.56	34.44	76.52

Table F.4: Raw data for association efficiency for 39% initial Ad loading entrapped nanoparticles.

Mass of Ad loaded (mg)	Abs	Concentration (mg/ml) from standard curve	Diluent Volume (ml)	Supernatant Volume (mL)	Total Volume (ml)	Mass of Ad in supernatant and diluent solution (mg)	Concentration of Ad in 0.5 mL sample of supernatant (mg/mL)	Mass of Ad in total supernatant sample in centrifuge test tube (mg)	Mass of Ad entrapped	Efficiency (%)
22.5	0.304	0.0034	5	0.5	5.5	0.0185	0.0369	1.11	8.79	88.82
22.5	0.369	0.0055	5	0.5	5.5	0.0304	0.0607	1.82	8.08	81.59
22.5	0.351	0.0051	5	0.5	5.5	0.0281	0.0561	1.68	8.22	82.99
22.5	0.315	0.0053	5	0.5	5.5	0.0289	0.0578	1.73	8.17	82.48

Table F.5: Raw release data of Ad from 39% initial Ad loading associated nanoparticles in PBS, pH 7.4.

Time (hour)	Time (min)	Trial 1 Mass of Ad released (mg)	Trial 2 Mass of Ad released (mg)	Trial 3 Mass of Ad released (mg)	Trial 4 Mass of Ad released (mg)	Average mass of Ad released	Percent released (%)
0.3	15	0.1603	0.1729	0.1487	0.1592	0.1603	0.85
0.6	35	0.1719	0.1866	0.1455	0.2088	0.1782	0.94
1.1	65	0.2130	0.1940	0.1782	0.2109	0.1990	1.05
2.1	125	0.2172	0.1993	0.2162	0.2278	0.2151	1.14
3.6	215	0.2352	0.2299	0.1750	0.1539	0.1985	1.05
5.6	335	0.2067	0.1750	0.3037	0.2520	0.2344	1.24
9.6	575	0.2288	0.2415	0.2489	0.1814	0.2251	1.19
20.4	1225	0.2257	0.1761	0.2489	0.1814	0.2080	1.10
22.4	1345	0.2341	0.2267	0.2837	0.2552	0.2499	1.32
24.4	1465	0.2426	0.2246	0.2478	0.1961	0.2278	1.21
37.5	2250	0.2687	0.1904	0.1699	0.2097	0.2097	1.11
45.7	2740	0.2246	0.2477	0.2806	0.2509	0.2509	1.33
61.5	3690	0.1934	0.2256	0.2856	0.2349	0.2349	1.24
67.5	4050	0.2487	0.2627	0.2557	0.2557	0.2557	1.35
73.7	4420	0.2647	0.2687	0.2667	0.2667	0.2667	1.41
87.3	5240	0.2326	0.2115	0.2221	0.2221	0.2221	1.18
96.0	5760	0.2517	0.2105	0.2311	0.2311	0.2311	1.22
111.0	6660	0.2216	0.2115	0.2165	0.2165	0.2165	1.15
120.0	7200	0.2266	0.2025	0.2145	0.2145	0.2145	1.14

Table F.6: Raw release data of Ad from 16% initial Ad loading entrapped nanoparticles in PBS, pH 7.4.

Time (hour)	Time (min)	Trial 1 Mass of Ad released (mg)	Trial 2 Mass of Ad released (mg)	Trial 3 Mass of Ad released (mg)	Average mass of Ad released (mg)	Percent release (%)
0.3	290	0.0544	0.0552	0.0548	0.0548	3.37
0.6	840	0.0546	0.0564	0.0555	0.0555	3.41
1.1	980	0.0537	0.0575	0.0556	0.0556	3.42
2.1	1340	0.0518	0.0575	0.0547	0.0547	3.36
3.6	2015	0.0564	0.0575	0.0570	0.0570	3.50
5.6	2735	0.0936	0.0575	0.0755	0.0755	4.65
9.6	3250	0.1023	0.0782	0.0903	0.0903	5.55
20.4	4195	0.1147	0.0903	0.1025	0.1025	6.30
22.4	4425	0.1147	0.1883	0.1515	0.1515	9.32
24.4	4645	0.1438	0.2382	0.1910	0.1910	11.75
37.5	5630	0.1837	0.3262	0.2550	0.2550	15.68
45.7	5760	0.2173	0.3343	0.2758	0.2758	16.96
61.5	6200	0.2155	0.4039	0.3097	0.3097	19.05
67.5	7054	0.2193	0.4057	0.3125	0.3125	19.22
73.7	7660	0.2264	0.4099	0.3181	0.3181	19.56
87.3	8865	0.2193	0.3623	0.2908	0.2908	17.89
96.0	10040	0.2736	0.3374	0.3055	0.3055	18.79
111.0	11450	0.2985	0.3326	0.3155	0.3155	19.41
120.0	12800	0.3486	0.3362	0.3424	0.3424	21.06

Table F.7: Raw release data of Ad from 39% initial Ad loading entrapped nanoparticles in PBS, pH 7.4.

Time (hour)	Time (min)	Trial 1 Mass of Ad released (mg)	Trial 2 Mass of Ad released (mg)	Trial 3 Mass of Ad released (mg)	Average mass of Ad released (mg)	Percent release (%)
0.3	290	0.0552	0.0790	0.0671	0.0671	0.38
0.6	840	0.0805	0.0805	0.0805	0.0805	0.45
1.1	980	0.0820	0.0790	0.0805	0.0805	0.45
2.1	1340	0.0810	0.0800	0.0805	0.0805	0.45
3.6	2015	0.0810	0.0800	0.0805	0.0805	0.45
5.6	2735	0.0820	0.0860	0.0840	0.0840	0.47
	2865	0.0820	0.0870	0.0845	0.0845	0.47
9.6	3250	0.1010	0.0980	0.0995	0.0995	0.56
20.4	4195	0.1040	0.1120	0.1080	0.1080	0.61
22.4	4425	0.1040	0.1100	0.1070	0.1070	0.60
24.4	4645	0.1060	0.1140	0.1100	0.1100	0.62
37.5	5630	0.1010	0.1080	0.1045	0.1045	0.59
45.7	5760	0.1100	0.1140	0.1120	0.1120	0.63
61.5	6200	0.0990	0.1060	0.1025	0.1025	0.57
67.5	7054	0.1040	0.1060	0.1050	0.1050	0.59
73.7	7660	0.1090	0.1100	0.1095	0.1095	0.61
87.3	8865	0.1150	0.1190	0.1170	0.1170	0.66
96.0	10040	0.1180	0.1200	0.1190	0.1190	0.67
111.0	11450	0.1160	0.1170	0.1165	0.1165	0.65
120.0	12800	0.1220	0.1210	0.1215	0.1215	0.68

Table F.8: Raw release data of Ad from 56% initial Ad loading entrapped nanoparticles in PBS, pH 7.4.

Time (hour)	Time (min)	Trial 1 Mass of Ad released (mg)	Trial 2 Mass of Ad released (mg)	Trial 3 Mass of Ad released (mg)	Average mass of Ad released (mg)	Percent release (%)
0.3	290	0.1100	0.0695	0.0897	0.0897	0.26
0.6	840	0.1100	0.1598	0.1349	0.1349	0.38
1.1	980	0.1143	0.1559	0.1351	0.1351	0.39
2.1	1340	0.1143	0.1680	0.1411	0.1411	0.40
3.6	2015	0.1559	0.1701	0.1630	0.1630	0.46
5.6	2735	0.1581	0.3440	0.2511	0.2511	0.72
9.6	3250	0.1680	0.4253	0.2966	0.2966	0.85
20.4	4195	0.1745	0.4239	0.2992	0.2992	0.85
22.4	4425	0.1756	0.4334	0.3045	0.3045	0.87
24.4	4645	0.1712	0.4437	0.3075	0.3075	0.88
37.5	5630	0.2238	0.4360	0.3299	0.3299	0.94
45.7	5760	0.2259	0.3906	0.3083	0.3083	0.88
61.5	6200	0.2533	0.3635	0.3084	0.3084	0.88
67.5	7054	0.2424	0.3675	0.3049	0.3049	0.87
73.7	7660	0.2533	0.3576	0.3054	0.3054	0.87
87.3	8865	0.2631	0.3576	0.3104	0.3104	0.88
96.0	10040	0.2588	0.3599	0.3094	0.3094	0.88
111.0	11450	0.2631	0.3706	0.3169	0.3169	0.90
120.0	12800	0.2708	0.3706	0.3207	0.3207	0.91

Table F.9: Raw data for stability of Ad over time, Trial 1.

Day	1			
Initial concentration of Ad (mg/ml)	Absorbency (nm)	Concentration of Ad calculated from standard curve (mg/ml)	Percent Ad degraded (%)	Percent Ad remaining (%)
0.00075	0.878	0.001023	36.33822	63.66178
0.0015	0.968	0.001431	4.62371	95.37629
0.003	1.305	0.002959	1.373963	98.62604
0.0045	1.632	0.004442	1.298387	98.70161
0.0075	2.261	0.007294	2.749437	97.25056
0.0105	2.834	0.009892	5.789732	94.21027

Table F.10: Raw data for stability of Ad over time, Trial 2.

Day	2			
Initial concentration of Ad (mg/ml)	Absorbency (nm)	Concentration of Ad calculated from standard curve (mg/ml)	Percent Ad degraded (%)	Percent Ad remaining (%)
0.00075	0.859	0.000936	24.85074	75.14926
0.0015	0.961	0.001399	6.739824	93.26018
0.003	1.302	0.002945	1.827416	98.17258
0.0045	1.658	0.004559	1.321564	98.67844
0.0075	2.214	0.007081	5.591076	94.40892
0.0105	2.834	0.009892	5.789732	94.21027

Table F.11: Raw data for stability of Ad over time, Trial 2.

Day	3			
Initial concentration of Ad (mg/ml)	Absorbency (nm)	Concentration of Ad calculated from standard curve (mg/ml)	Percent Ad degraded (%)	Percent Ad remaining (%)
0.00075	0.855	0.000918	22.43232	77.56768
0.0015	0.953	0.001363	9.15824	90.84176
0.003	1.293	0.002904	3.187775	96.81223
0.0045	1.658	0.004559	1.321564	98.67844
0.0075	2.251	0.007248	3.354041	96.64596
0.0105	2.914	0.010255	2.334851	97.66515

Table F.12: Raw data for stability of Ad over time, Trial 3.

Day	4			
Initial concentration of Ad (mg/ml)	Absorbency (nm)	Concentration of Ad calculated from standard curve (mg/ml)	Percent Ad degraded (%)	Percent Ad remaining (%)
0.00075	0.88	0.001032	37.54742	62.45258
0.0015	0.979	0.001481	1.298387	98.70161
0.003	1.313	0.002995	0.164755	99.83525
0.0045	1.681	0.004664	3.639213	96.36079
0.0075	2.27	0.007335	2.205293	97.79471
0.0105	2.834	0.009892	5.789732	94.21027

Table F.13: Raw data for stability of Ad over time, Trial 4.

Day	5			
Initial concentration of Ad (mg/ml)	Absorbency (nm)	Concentration of Ad calculated from standard curve (mg/ml)	Percent Ad degraded (%)	Percent Ad remaining (%)
0.00075	0.856	0.000923	23.03693	76.96307
0.0015	0.962	0.001403	6.437522	93.56248
0.003	1.297	0.002923	2.583171	97.41683
0.0045	1.694	0.004723	4.949188	95.05081
0.0075	2.23	0.007153	4.62371	95.37629
0.0105	2.9	0.010191	2.939455	97.06054

Table F.14: Raw data for stability of Ad over time, Trial 5.

Day	6			
Initial concentration of Ad (mg/ml)	Absorbency (nm)	Concentration of Ad calculated from standard curve (mg/ml)	Percent Ad degraded (%)	Percent Ad remaining (%)
0.00075	0.857	0.000927	23.64153	76.35847
0.0015	0.969	0.001435	4.321408	95.67859
0.003	1.288	0.002882	3.94353	96.05647
0.0045	1.696	0.004732	5.150723	94.84928
0.0075	2.214	0.007081	5.591076	94.40892
0.0105	2.96	0.010463	0.348295	99.6517

Table F.15: Raw data for stability of Ad over time, Trial 6.

Day	7			
Initial concentration of Ad (mg/ml)	Absorbency (nm)	Concentration of Ad calculated from standard curve (mg/ml)	Percent Ad degraded (%)	Percent Ad remaining (%)
0.00075	0.857	0.000927	23.64153	76.35847
0.0015	0.969	0.001435	4.321408	95.67859
0.003	1.288	0.002882	3.94353	96.05647
0.0045	1.696	0.004732	5.150723	94.84928
0.0075	2.214	0.007081	5.591076	94.40892
0.0105	2.96	0.010463	0.348295	99.6517

Table F.16: Raw data for stability of Ad over time, Trial 7.

Day	11			
Initial concentration of Ad (mg/ml)	Absorbency (nm)	Concentration of Ad calculated from standard curve (mg/ml)	Percent Ad degraded (%)	Percent Ad remaining (%)
0.00075	0.897	0.001109	47.82569	52.17431
0.0015	1.017	0.001653	10.18909	89.81091
0.003	1.358	0.003199	6.637041	93.36296
0.0045	1.765	0.005045	12.10367	87.89633
0.0075	2.2	0.007017	6.437522	93.56248
0.0105	2.767	0.009588	8.683194	91.31681

Table F.17: Raw data for stability of Ad over time, Trial 8.

Day	14			
Initial concentration of Ad (mg/ml)	Absorbency (nm)	Concentration of Ad calculated from standard curve (mg/ml)	Percent Ad degraded (%)	Percent Ad remaining (%)
0.00075	0.89	0.001077	43.59346	56.40654
0.0015	1.005	0.001598	6.561466	93.43853
0.003	1.346	0.003145	4.823229	95.17677
0.0045	1.715	0.004818	7.065302	92.9347
0.0075	2.189	0.006967	7.102586	92.89741
0.0105	2.834	0.009892	5.789732	94.21027

Table F.18: Raw data for calculated results for standard curve of adenosine in supernatant using qNMR.

mass of Ad initially loaded	conc. Standard (mg/ml)	Ad: area under peak	standard: area under peak	conc. Ad (mmol/l)	Conc. Ad (mg/ml)	conc. Ad (g/ml)	initial loading conc. Ad (g/ml)	%error
10	10	30.93	100	18.56	4.96	0.0050	0.00267	46.16
6.7	6.7	48.62	100	19.55	5.22	0.0052	0.00179	65.75
5.6	5.6	48.38	100	16.26	4.34	0.0043	0.00150	65.59
2.8	2.8	51.63	100	8.67	2.32	0.0023	0.00075	67.73
1	1	31.61	100	1.90	0.51	0.0005	0.00027	47.32

Table F.19: Raw data for calculated results for standard curve of adenosine in supernatant using qNMR with pH change of chitosan solution.

mass of Ad initially loaded	conc. Standard (mg/ml)	Ad: area under peak	standard: area under peak	conc. Ad (mmol/l)	Conc. Ad (mg/ml)	conc. Ad (g/ml)	initial loading conc. Ad (g/ml)	%error
10	10	37.8	100	22.68	6.06	0.00606	0.00267	55.95
6.7	6.7	48.23	100	19.39	5.18	0.00518	0.001789	65.47
5.6	5.6	24.48	100	8.23	2.20	0.00220	0.001495	31.99
2.8	2.8	45.61	100	7.66	2.05	0.00205	0.000748	63.47

Table F.20: Raw data for calculated results from supernatant of chitosan nanoparticles with various amounts of adenosine loaded.

mass of Ad initially loaded	Initial added Conc. (mmol/l)	conc. Standard (mg/ml)	Ad: area under peak	standard: area under peak	conc. Ad (mmol/l)	Conc. Ad (mg/ml)	conc. Ad (g/ml)	initial loading conc. Ad (g/ml)	%error
45	4.32	4.32	56.52	100	14.66	3.92	0.00392	0.00432	9.37
45	4.3	4.32	18.56	100	4.81	1.29	0.00129	0.00432	70.24
45	4.3	4.32	55.54	100	14.40	3.85	0.00385	0.00432	10.94
45*	4.3	4.32	50.92	100	13.20	3.53	0.00353	0.00432	18.35
45*	4.3	4.32	34.72	100	9.00	2.41	0.00241	0.00432	44.33
45*	4.3	4.32	51.86	100	13.45	3.59	0.00359	0.00432	16.85
90	8.6	8.64	48.35	100	25.07	6.70	0.00670	0.00432	55.05
90	8.6	8.64	49.76	100	25.80	6.90	0.00690	0.00432	59.57
90	8.6	8.64	49.86	100	25.86	6.91	0.00691	0.00432	59.90

* pH of chitosan was changed from 3.35 to 4.20

Table F.21: Raw data for entrapment efficiency for initial Ad loading entrapped nanoparticles.

Concentration of adenosine loaded (g/ml)	NMR reading from spectras (g/ml)	NMR reading converted by standard curve solution (g/ml)	Entrapment Efficiency (%)
0.004322	0.003916	0.001305	69.79
0.004322	0.001286	0.000429	90.08
0.004322	0.003849	0.001283	70.31

Table F.22: Raw data for entrapment efficiency for initial Ad loading entrapped nanoparticles, with chitosan pH to 4.2.

Concentration of adenosine loaded (g/ml)	NMR reading from spectras (g/ml)	NMR reading converted by standard curve solution (g/ml)	Entrapment Efficiency (%)
0.004322	0.003528	0.001550	64.14
0.004322	0.002406	0.001057	75.55
0.004322	0.003594	0.001578	63.48